Chapter 5

Lattice Boltzmann Method

5.1 Pseudo-kinetic computational methods

Understanding the flow properties of complex fluids in complex topologies is of importance to technological applications and it presents a relevant theoretical challenge too. Recently, new computational methods, called *pseudo-kinetic*, have been proposed which have several advantages over traditional computational methods. Notable examples include the Lattice Gas Cellular Automata, the Lattice Boltzmann Method, the Discrete Velocity Models (DVM), the Gas-Kinetic Scheme (GKS), the Smoothed Particle Hydrodynamics (SPH) and the dissipative particle dynamics (DPD). In structure, all these algorithms look much like molecular dynamics (MD), where atomic particles move according to Newton's laws. However, these tools realize a mesoscopic description of the fluid, and do not represent individual atoms or particles, but loosely deal with clusters of particles. This idea allows for much larger time steps so that physical behavior on time scales many orders of magnitude greater than that possible with MD, may be studied.

This chapter is organized as follows: a short historical background and a brief description of the Lattice Boltzmann Method are reported; some non-equilibrium statistical mechanics and how to design a lattice Boltzmann model are discussed;

finally, the innovative contents of this work, concerning the proposed lattice Boltzmann model for binary mixtures and the developed parallel code, are discussed. The introductory part of this chapter must be considered exemplifying and not exhaustive (see for example the review article [103]).

5.1.1 Basic idea

Among the pseudo-kinetic algorithms, the Lattice Boltzmann Method (LBM) seems very promising in terms of easiness to account for different phenomena (multi-physics aptitude) and effectiveness to deal with distributed computational domains (parallel computing aptitude). The models based on LBM are quite different from an accurate microscopic description on the one hand, and from a macroscopic description, i.e. Navier-Stokes equations in the continuum hydrodynamic limit, on the other hand. The key point is that, even though the actual microscopic dynamics greatly depends on the nature of the considered fluid (compares gases and liquids), it can lead to the same form of macroscopic equations. In other words, the macroscopic description is generally quite insensitive to the underlying exact interactions among particles.

For this reason, it is possible to design a very idealized microscopic description which, however, allows us to recover the desired macroscopic equations. In addition to real gases or real liquids one may consider artificial micro-worlds of particles "living" on lattices with interactions that conserve mass and momentum [102]. The micro-dynamics of such *artificial micro-worlds* should be very simple in order to run it efficiently on a computer. Consider, for example, a square lattice with four cells at each node such that one cell is associated with each link to the next neighbor node. These cells may be empty or occupied by at most one particle with unit mass. Thus

each cell has only two possible states and therefore is called a cellular automaton. Velocity and thereby also momentum can be assigned to each particle by the vector connecting the node to its next neighbor node along the link where the particle is located. These vectors are called *lattice velocities*. The microscopic interaction is strictly local in that it involves only particles at a single node. The particles exchange momentum while conserving mass and momentum summed up over each node. After this collision each particle streams along its associated link to its next neighbor node. The micro-dynamics consists on a repetition of *collisions* and *streaming*. Macroscopic values of mass and momentum density are calculated by coarse graining (calculation of mean values over large spatial regions with hundreds to thousands of nodes) [102].

The streaming is simply determined by the considered lattice because particles move according to the allowed directions. On the other hand, the interaction among different particles at a given node strongly affects the macroscopic hydrodynamics of the model. Essentially, the interaction is based on a great number of collisions but they cannot be directly taken into account within a mesoscopic framework because the allowed directions are very few. For this reason, some local collisional rules are needed which simulate the long-term effect due to collisions, i.e. the trend towards local equilibrium. The easiest strategy consists in introducing a simplified collisional operator which tries to force the actual particle population towards the equilibrium configuration. The effectiveness of the simplified collisional operator to perform the previous task, i.e. how fast the collisional operator is to fill the gap between actual and equilibrium configuration, is usually given by a proper set of *relaxation time constants*. The relaxation time constants determine the microscopic dynamics towards the local equilibrium and the macroscopic transport coefficients at the same time. Once the mesoscopic model has been defined, the relaxation time constants are the practical

tunable parameters which can be set in order to recover the desired dynamics, both microscopic and macroscopic.

5.1.2 Top-down versus bottom-up tuning strategy

In the previous section, the basic idea of mesoscopic models based on LBM has been discussed. The fundamental role of the relaxation time constants emerged, but how to select them has not been discussed. The algorithm for selecting the mesoscopic relaxation time constants is called *mesoscopic tuning strategy*. Since mesoscopic modeling is somewhere located between the microscopic and the macroscopic description, it does not exactly coincide with any of them. However, it seems reasonable in principle to reformulate the information coming from both microscopic and macroscopic description in a mesoscopic fashion. This yields two alternatives:

- the *top-down approach*, which means that the mesoscopic relaxation time constants are tuned in order to recover the macroscopic transport coefficients and the mesoscopic algorithm works as a numerical tool for solving the macroscopic equations;

- the *bottom-up approach*, which means that the mesoscopic relaxation time constants are tuned by roughly averaging the results due to accurate microscopic descriptions for the considered fluid and the mesoscopic algorithm brings the residual information to macroscopic level.

Both the previous approaches are somehow present in the researches on LBM. The LBM lies at the crossroad between two distinct lines of thought: one that views it as an appealing method to compete with numerical fluid mechanics (*top-down approach*) and the other that sees it as a sort of "telescope" of molecular dynamics (*bottom-up*

approach). This dual nature of LBM is a potential source of richness and of some confusion too [104].

This work deals with the first approach and the LBM will be essentially used as an alternative numerical scheme in order to solve the Navier-Stokes equations. In the following sections, the development of a pseudo-kinetic model for the gaseous mixtures allows us to appreciate that elementary considerations at mesoscopic level can unexpectedly affect the macroscopic dynamics. The bottom-up approach is much more promising because it seems to offer the challenge to widen the physical description of the investigated phenomena. For example, recently the first rigorous step in deriving turbulence models from kinetic theory based on LBM has been proposed [101]. Because LBM is still in rapid development it is not possible to give an actual and complete picture of the whole field. In the following, a short historical background and some basic concepts are reported.

5.2 Short historical background

5.2.1 Lattice Gas Cellular Automata

When outlining the historical origins of LBM, it is quite usual to introduce the lattice gas cellular automata as their ideal forerunners [102]. Let us take an additional step back in order to consider the Cellular Automata (CA). This is worth it because it allows us to understand that the original starting point of some mesoscopic modeling comes from the tools used to investigate complexity, i.e. self-organization naturally emerging from a great number of simple interacting objects. It is interesting that one of the first monograph written by Wolfram about this subject was called “Cellular Automata and Complexity” [105].

Around 1950 CA were introduced by Stanislas Ulam, John von Neumann, and

Konrad Zuse. John von Neumann proposed a self-reproducing cellular automaton [106] in 1966 which at the same time realized universal Turing machine. Zuse published his ideas concerning the application of cellular automata to physical problems in a monograph [107] in 1970. Some of his formulations already resemble to more recent automata proposed four years later by Hardy et al. [108]. In 1970 John Horton Conway introduced the game "Life", a two-dimensional CA with simple update rules but complex dynamics. Martin Gardner made CA very popular by a series of papers on "Life" in Scientific American.

The first Lattice-Gas Cellular Automata (LGCA), i.e. a special kind of CA for the simulation of fluid flow and other physical problems, was proposed in 1973 by Hardy, Pomeau and de Pazzis [108]. Its name HPP is derived from the initials of the three authors. Although the HPP model conserves mass and momentum it does not yield the desired Navier-Stokes equation in the macroscopic limit.

In 1983 Stephen Wolfram revived the interest in CA by a series of papers [109–111]. The one-dimensional arrays of cells considered by Wolfram expressed complex patterns when initialized randomly and updated by simple deterministic rules depending on the state of the cell and a few of its neighbors.

In 1986 Frisch, Hasslacher and Pomeau discovered that a CA over a lattice with hexagonal symmetry, i.e. with a somewhat higher symmetry than for the HPP model, leads to the Navier-Stokes equation in the macroscopic limit. The theoretical foundations of LGCA were given soon after by Wolfram [113] and Frisch et al. [114].

Despite the amount of work was done, the main drawback of LGCA remained the statistical noise, i.e. strong oscillations limited the applications of the new tool. In order to solve this problem, the Lattice Boltzmann Method (LBM) was proposed. Shortly it became apparent that all other anomalies plaguing LGCA could also be

naturally disposed of by the LBM. As a result LBM rapidly evolved into a self standing research subject bearing an increasingly fainter relation to its LGCA ancestor [104].

5.2.2 Models based on Lattice Boltzmann Method

The basic idea which made it possible to formulate the Lattice Boltzmann Method (LBM) is very simple: just replace the Boolean occupation numbers, involved in the previous LGCA, with the corresponding ensemble-averaged populations. In this way, the link between artificial micro-world and the usual kinetic theory became stronger [102].

Initially, LBM had already been used at the cradle of LGCA by Frisch et al. [114] to calculate the viscosity of LGCA. At this stage LBM was simply an analysis tool. Then, LBM as an independent numerical method for hydrodynamic simulations was introduced by McNamara and Zanetti in 1988 [115]. The main motivation for the transition from LGCA to LBM was the desire to get rid of the statistical noise. The Boolean fields were replaced by continuous distributions over the previous lattices. It is worth to point out that, at the beginning, Fermi-Dirac distributions were used as equilibrium functions, instead of the Maxwellian distribution functions later introduced.

The collisional operator for LBM was initially based on the collisions of certain LGCA and only later on it was substituted by the BGK, from the initials of Bhatnagar, Gross and Krook who proposed it first in 1954 [125], collisional operator by Koelman [116], Qian et al. [117] and others. The last paper (1992) marks the beginning of the "modern" research period in this field. These lattice BGK models mark a new level of abstraction: collisions are no more defined explicitly, but on the other hand the link with the continuous kinetic theory is considered an important feature,

which cannot be renounced. The connection between the models based on LBM and the continuous Boltzmann equation are discussed in various papers [116, 118]. Substantial progress can be made in the aforementioned subject once a better understanding of this connection is attained. Furthermore, the connection between LBM models and the continuous Boltzmann equation can directly show the relationship between LBM and other newly developed pseudo-kinetic methods [119]. In the following, some concepts from non-equilibrium statistical mechanics will be discussed.

5.3 Some non-equilibrium statistical mechanics

5.3.1 The Boltzmann equation

Let us consider a dilute gas made of point-like, structureless, N particles interacting via a short-range two-body potential. Under such conditions, intermolecular interactions can be described solely in terms of localized binary collisions with particles spending most of their lifespan on free trajectories. Since we are interested in an enormous number of particles, we deal with the problem of characterizing the system as a whole by means of physical observables which can be defined at macroscopic scale in the fluid continuum approach.

Anyway, a detailed microscopic description is practically impossible and, from a certain point of view, it is not needed because the growth of uncertainty for a system made of so many particles is such as to prevent any deterministic prediction of the state of the system [104, 121]. For this reason, the idea of considering the system as a whole by introducing the fluid approach seems reasonable. However it could be not so easy to define the concept of fluid because various time scales exist. Qualitatively, the fluid motion is controlled by the following time scales, which identify a corresponding sequence of dynamical stages [120].

- *Initial stage.* At the beginning of the initial stage the system can be characterized by any kind of initial condition and for this reason it is impossible to produce a simplified description of it. All the coordinates and the microscopic velocities of the particles should be known in order to properly characterize the system: from the statistical point of view, these information are collected by the multi-body distribution function. During this stage, the collisions reduce the discrepancies among different particles and the system starts to reveal a coherent behavior emerging from its components.

- *Kinetic stage.* During this stage, the coherent behavior of the system dominates and the peculiar behavior of the single particle is no more relevant. The multi-body distribution function relaxed to the single-particle distribution function, which gives the probability to find a particle in a given state without distinguishing it from all other particles is enough to characterize the system.

- *Fluid stage.* During this stage, the single-particle distribution function can be described in terms of lower order moments, i.e. macroscopic quantities, and their gradients. The single-particle distribution function is so regular to be determinated by macroscopic quantities because each particle is affected by an average effect due to all neighboring particles. In this case, the description can be simplified by reformulating the governing equations in terms of macroscopic quantities only.

Let us introduce the single-particle distribution function $f(\mathbf{x}, \mathbf{v}, t)$, where $\mathbf{x}$ is the generic coordinate and $\mathbf{v}$ is the generic microscopic velocity. The function $f(\mathbf{x}, \mathbf{v}, t)$ is defined such that $f(\mathbf{x}, \mathbf{v}, t)d\mathbf{x}d\mathbf{v}$ is the probability to find a particle at time t positioned between $\mathbf{x}$ and $\mathbf{x} + d\mathbf{x}$ with velocity in the range defined by $\mathbf{v}$ and $\mathbf{v} + d\mathbf{v}$.

The Boltzmann equation essentially describes the evolution of $f(\mathbf{x}, \mathbf{v}, t)$ in terms of elementary interactions, i.e. collisions, which are treated as if they proceed instantly. The Boltzmann equation deals with the kinetic and the fluid stage making it possible to understand the existing link between kinetic and hydrodynamic description.

The Boltzmann equation has been derived as a result of a systematic approximation starting from the elementary laws of mechanics not before 1946. Boltzmann derived the equation which bears his name by a different reasoning already in 1872 by a heuristic approach. It can be derived by applying some approximations: only two-particle collisions are considered; the velocities of the two colliding particles are uncorrelated before collision (*molecular chaos* hypothesis) and finally external forces do not influence the local collision dynamics. The Boltzmann equation is an integro-differential equation for the single particle distribution function and it can be expressed as:

$$\frac{\partial f}{\partial t} + \mathbf{v} \cdot \nabla f + \mathbf{g} \cdot \nabla_{\mathbf{v}} f = Q(f, f), \tag{5.1}$$

where $\mathbf{g}$ is the acceleration due to an external force field and the quadratic expression $Q(f, f)$ is the collision integral. The collision integral describes the time rate of change of the single particle distribution function due to collisions and it has the following expression:

$$Q(f, f) = \int d\mathbf{v} \int \Xi(\Omega) |\mathbf{v} - \mathbf{v}_{\odot}| [f(\check{\mathbf{v}}) f(\check{\mathbf{v}}_{\odot}) - f(\mathbf{v}) f(\mathbf{v}_{\odot})] \, d\Omega, \tag{5.2}$$

where $d\Omega$ is the solid angle the particles are scattered into and $\Xi(\Omega)$ is the differential collisional cross section for the two-particle collision in the center of mass of the reference frame. The generic collision transforms the velocities from $[\mathbf{v}, \mathbf{v}_{\odot}]$ (incoming configuration before collision) into $[\check{\mathbf{v}}, \check{\mathbf{v}}_{\odot}]$ (outgoing configuration after collision), where $\mathbf{v}$ is the microscopic velocity for the generic *test particle* and $\mathbf{v}_{\odot}$ is the microscopic velocity for the generic *field particle*, which is one of the dummy variables

in the previous integral. The differential collisional cross section can be calculated by means of the laws of mechanics and the analytical expression for the interacting potential.

The single-particle distribution function allows us to calculate the macroscopic quantities which are involved in the hydrodynamic description. A detailed description of the link between kinetic description and hydrodynamics is beyond the purposes of the present work but a lot of literature exists on this topic [121,122]. In the following, some concepts will be discussed in order to derive the conservation equations.

The fluid density ρ, the macroscopic velocity $\mathbf{u}$ and the specific internal energy e can be found from the distribution function f as follows:

$$\rho(\mathbf{x},t) = \int m\, f(\mathbf{x},\mathbf{v},t)\, d\mathbf{v}, \tag{5.3}$$

$$\rho(\mathbf{x},t)\, \mathbf{u}(\mathbf{x},t) = \int m\, \mathbf{v}\, f(\mathbf{x},\mathbf{v},t)\, d\mathbf{v}, \tag{5.4}$$

$$\rho(\mathbf{x},t)\, e(\mathbf{x},t) = \int m\, (\mathbf{v}-\mathbf{u})^2/2\, f(\mathbf{x},\mathbf{v},t)\, d\mathbf{v}, \tag{5.5}$$

where m is the particle mass. Any solution of the Boltzmann equation requires that an expression is found for the collisional operator. Even without knowing the form of $Q(f,f)$ several properties can be deduced. In particular, let us define *collisional invariant* any quantity defined such that:

$$\int \Psi(\mathbf{v})\, Q(f,f)\, d\mathbf{v} = 0. \tag{5.6}$$

Since the collision conserves mass, momentum and energy, it is easy to check that $\Psi(\mathbf{v}) = m,\ m\, v_i,\ m\, \mathbf{v}^2/2$ are collisional invariant (v_i is the generic component of the microscopic velocity along the i coordinate). Multiplying the Boltzmann equation by a generic collisional invariant and integrating over the test particle velocity

components, it is possible to recover the following expression:

$$\int \Psi(\mathbf{v}) \left(\frac{\partial f}{\partial t} + \mathbf{v} \cdot \nabla f + \mathbf{g} \cdot \nabla_{\mathbf{v}} f \right) d\mathbf{v} = \int \Psi(\mathbf{v})\, Q(f, f)\, d\mathbf{v} = 0. \tag{5.7}$$

Let us introduce the notation $\langle\langle o \rangle\rangle$ to indicate the weighted average with respect to the single-particle distribution function, namely

$$\langle\langle \Psi \rangle\rangle = \int \Psi(\mathbf{v}) f(\mathbf{x}, \mathbf{v}, t)\, d\mathbf{v}. \tag{5.8}$$

Integrating by parts Eq. (5.7), the following expression,

$$\frac{\partial \langle\langle \Psi \rangle\rangle}{\partial t} + \nabla \cdot \langle\langle \Psi\, \mathbf{v} \rangle\rangle = \mathbf{g} \cdot \langle\langle \nabla_{\mathbf{v}} \Psi \rangle\rangle\,, \tag{5.9}$$

is recovered which involves the averaged quantities. Some simplifying considerations must be taken into account. First of all, $\lim_{\mathbf{v}\to\infty}(\Psi\, f) = 0$ because the probability to find particles with infinite velocity is zero. Moreover the microscopic velocity $\mathbf{v}$ commutes with ∇ and with $\partial/\partial t$ because $\mathbf{x}$, $\mathbf{v}$ and t are independent variables in the phase space.

Equation (5.9) can be explicitly rewritten for each collisional invariant, namely

$$\frac{\partial \rho}{\partial t} + \nabla \cdot (\rho\, \mathbf{u}) = 0, \tag{5.10}$$

$$\frac{\partial}{\partial t}(\rho\, \mathbf{u}) + \nabla \cdot \left(\int m \mathbf{v} \otimes \mathbf{v} f\, d\mathbf{v} \right) = \rho\, \mathbf{g}, \tag{5.11}$$

$$\frac{\partial}{\partial t} \left(\frac{1}{2} \int m \mathbf{v}^2 f\, d\mathbf{v} \right) + \nabla \cdot \left(\frac{1}{2} \int m \mathbf{v}^2\, \mathbf{v} f\, d\mathbf{v} \right) = \rho\, \mathbf{u} \cdot \mathbf{g}. \tag{5.12}$$

Equation (5.10) is simply the continuity equation. In the remaining equations some additional terms emerge which must be properly discussed. Let us define peculiar velocity $\mathbf{v}''$, or kinetic fluctuation, the difference between the microscopic velocity and the hydraulic macroscopic velocity, i.e. $\mathbf{v}'' = \mathbf{v} - \mathbf{u}$. The unknown integral in Eq. (5.11) can be expressed as a function of the peculiar velocity, namely

$$\int m(\mathbf{u} + \mathbf{v}'') \otimes (\mathbf{u} + \mathbf{v}'') f\, d\mathbf{v}'' = -\mathbf{S} + \rho\, \mathbf{u} \otimes \mathbf{u}, \tag{5.13}$$

where $\mathbf{S}$ is the stress tensor, which has the following expression:

$$\mathbf{S} = -\int m\mathbf{v}'' \otimes \mathbf{v}'' f \, d\mathbf{v}''. \tag{5.14}$$

Taking into account the previous definition, the Eq. (5.11) can be reformulated in the following way:

$$\frac{\partial}{\partial t}(\rho \, \mathbf{u}) + \nabla \cdot (\rho \, \mathbf{u} \otimes \mathbf{u}) = \nabla \cdot \mathbf{S} + \rho \, \mathbf{g}, \tag{5.15}$$

The previous equation is the usual equation for momentum conservation in the macroscopic hydrodynamic formulation.

In a similar way, we can proceed for both integrals involved in Eq. (5.12):

$$\frac{1}{2}\int m(\mathbf{u} + \mathbf{v}'')^2(\mathbf{u} + \mathbf{v}'') f \, d\mathbf{v}'' = \frac{1}{2}\,\rho \mathbf{u}^2 \, \mathbf{u} - \mathbf{S}\,\mathbf{u} + \rho \, e \, \mathbf{u} + \mathbf{q} \tag{5.16}$$

$$\frac{1}{2}\int m(\mathbf{u} + \mathbf{v}'')^2 f \, d\mathbf{v}'' = \rho \, e + \frac{1}{2}\,\rho \, \mathbf{u}^2, \tag{5.17}$$

where $\mathbf{q}$ is the heat flux defined as:

$$\mathbf{q} = \frac{1}{2}\int m(\mathbf{v}'')^2 \mathbf{v}'' f \, d\mathbf{v}''. \tag{5.18}$$

Taking into account the previous definition, the Eq. (5.12) can be reformulated in the following way:

$$\frac{\partial}{\partial t}(\rho \, e^t) + \nabla \cdot (\rho \, \mathbf{u} \, e^t) = \nabla \cdot (\mathbf{S}\,\mathbf{u}) - \nabla \cdot \mathbf{q} + \rho \, \mathbf{u} \cdot \mathbf{g}, \tag{5.19}$$

where e^t is the total internal energy defined as $e^t = e + \rho \, \mathbf{u}^2/2$. The previous equation is the usual equation for energy conservation in the macroscopic hydrodynamic formulation.

5.3.2 Maxwellian distribution function

In this section some particular single-particle distribution functions will be discussed. Let us search for a particular solution f^e of the Boltzmann equation such that

$Q(f^e, f^e) = 0$. Recalling the expression of the collisional operator, given by Eq. (5.2), this is possible if and only if:

$$f^e(\check{\mathbf{v}}) f^e(\check{\mathbf{v}}_\odot) = f^e(\mathbf{v}) f^e(\mathbf{v}_\odot). \tag{5.20}$$

Let us divide the previous expression by a constant f_0 with the same physical dimensions of a single-particle distribution function and let us apply the logarithm:

$$\ln\left[f^e(\check{\mathbf{v}})/f_0\right] + \ln\left[f^e(\check{\mathbf{v}}_\odot)/f_0\right] = \ln\left[f^e(\check{\mathbf{v}})/f_0\right] + \ln\left[f^e(\check{\mathbf{v}}_\odot)/f_0\right]. \tag{5.21}$$

This means that $\ln\left[f^e/f_0\right]$ must be a collisional invariant. Since a linear combination of collisional invariants is also a collisional invariant, the most general expression is:

$$\ln\left[f^e/f_0\right] = a + \mathbf{b}\cdot\mathbf{v} + c\,\mathbf{v}^2, \tag{5.22}$$

where a, $\mathbf{b}$ and c are $D+2$ interpolation coefficients (D is the number of coordinates). Taking into account the definitions given by Eqs. (5.3), it is possible to express the unknown interpolation coefficients by means of the macroscopic moments, namely

$$f^e = \frac{\rho/m}{(2\pi\, e)^{D/2}} \exp\left[-\frac{(\mathbf{v}-\mathbf{u})^2}{2\, e}\right], \tag{5.23}$$

where f^e is the *Maxwellian distribution function*. The condition $Q(f^e, f^e) = 0$ defines the *local equilibrium* for the system of particles. If the system is in local equilibrium, then the single-particle distribution function is Maxwellian. This does not mean that the macroscopic velocity and the internal energy are constant in space and time. If this was the case, then the system would be in *global equilibrium* and each term of the streaming operator, i.e. the left hand side of the Boltzmann equation (5.1), would be annihilated. Instead local equilibrium simply prescribes that the collisions among particles do not affect the substantial time derivative of the distribution function but the local time derivative can compensate the advection term due to spatial gradients of macroscopic quantities.

Equation (5.23) gives the opportunity to calculate the stress tensor and the heat flux for a system in local equilibrium. The stress tensor becomes:

$$\mathbf{S}_e = -\int m\mathbf{v}'' \otimes \mathbf{v}'' f^e \, d\mathbf{v}'' = -\rho\, e\, \mathbf{I}, \tag{5.24}$$

where $\mathbf{I}$ is the identity matrix, while the heat flux becomes:

$$\mathbf{q}_e = \frac{1}{2}\int m(\mathbf{v}'')^2 \mathbf{v}'' f^e \, d\mathbf{v}'' = 0. \tag{5.25}$$

Introducing a macroscopic quantity called *pressure* defined such that $p = \rho\, e$ and substituting the previous expressions in the equation for momentum conservation, given by Eq. (5.15), and in the equation for internal energy conservation, given by Eq. (5.19), the Euler system of equations for ideal gases ($p = \rho\, e$) is recovered.

5.3.3 Chapman-Enskog asymptotic analysis

When the system is not in local equilibrium ($f \neq f^e$), during the fluid stage the stress tensor and the heat flux are related to the macroscopic moments by means of more complicated correlations in comparison with those discussed in the previous section and given by Eqs. (5.24, 5.25). In this case, the specific role of collisions emerges and the collision integral must be properly analyzed in order to point out the link between the kinetic interaction potential and the macroscopic transport phenomena [121, 122].

In fact, by applying certain models of the microscopic collision processes one can obtain explicit formulas for the transport coefficients, which are involved in the expressions for the stress tensor and the heat flux. The derivation of a closed system of macroscopic equations, including the transport coefficients, from the Boltzmann equation and the microscopic collision models runs under the name of Chapman-Enskog asymptotic analysis. This method has been developed by Chapman and

Enskog between 1910 and 1920 [121]. Therefore, it seems appropriate to discuss a few interesting features before beginning with the formal derivations and to restrict the calculation to a simple collision model, which will be considered in the next section. The Chapman-Enskog asymptotic analysis is a particular case of multi-scale singular perturbation technique [123].

The expansion parameter of Chapman-Enskog is essentially the Knudsen number Kn, i.e. the ratio between the mean free length (the mean distance between two successive collisions) and the characteristic spatial scale of the system (for example, radius of an obstacle in a flow or channel diameter). When the Knudsen number is of the order of 10^{-3} or larger the gas in the considered system cannot be described by means of the usual continuous approach and when it is of the order of 1 or larger the gas cannot be described as a fluid.

Let us consider the following formal expansion of the single-particle distribution function

$$f = \sum_{\xi=0}^{\infty} K^{\xi} f^{(\xi)}, \tag{5.26}$$

and similar expansions for time and space derivatives:

$$\frac{\partial}{\partial t} = \sum_{\xi=1}^{\infty} K^{\xi} \frac{\partial}{\partial t^{(\xi)}}, \tag{5.27}$$

$$\frac{\partial}{\partial x_i} = \sum_{\xi=1}^{\infty} K^{\xi} \frac{\partial}{\partial x_i^{(\xi)}}, \tag{5.28}$$

where x_i is the generic coordinate and K is a small parameter such that $K \propto Kn$. The previous expansion for f involves a contraction of the description of the system temporal development [102, 124]. Whereas the distribution function f of the Boltzmann equation is explicitly dependent on time, space and velocity, the distribution functions $f^{(\xi)}$ of the Chapman-Enskog expansion depend only implicitly on time via local density, macroscopic velocity and internal energy, i.e. the $f^{(\xi)}$ are not the most

general solutions of the Boltzmann equation. It can be shown [121] that arbitrary initial distributions relax very fast toward this special kind of distribution. However it is well known that the Chapman-Enskog expansion can yield solutions which are simply nonexistent when equations other than the Navier-Stokes system are considered [121]. Since, in this case, we limit our interest to the transport coefficients involved in the Navier-Stokes system, the Chapman-Enskog expansion will be considered.

Equation (5.26) defines a power series expansion in the parameter K, supposed small for the considered application. This formal parameter in the expansion allows one to keep track of the relative orders of magnitude of the various terms and it can be considered essentially as a label [102]. When expansions of different quantities are combined, however, the powers of K have to be related such that the terms of leading order yield a meaningful balance.

The Chapman-Enskog asymptotic analysis assumes that the spatial derivative on the left hand side of the Boltzmann equation (5.1) has the same order of the leading term in the time derivative, namely

$$\frac{\partial}{\partial x_i} \approx K \frac{\partial}{\partial x_i^{(1)}}. \tag{5.29}$$

Actually, in space only one macroscopic scale will be considered because different macroscopic processes like advection and diffusion can be distinguished by their time scales but act on similar spatial scales [102].

Some expansion must be introduced for the microscopic velocity derivative too. In this case, it is more difficult to identify the proper scale because microscopic velocity is removed by the contraction of the description of temporal development. However, it seems reasonable to assume that the velocity derivative on the left hand side of the Boltzmann equation (5.1) has the same order of the spatial derivative because it takes into account the effects due to the external force field $\mathbf{g}$, which, at macroscopic

level, has the same order of diffusion and advection phenomena. This yields

$$\frac{\partial}{\partial v_i} \approx K \frac{\partial}{\partial v_i^{(1)}}, \tag{5.30}$$

where v_i is the generic component of the microscopic velocity.

In the next sections, the Chapman-Enskog asymptotic analysis will be extensively applied in order to deduce the macroscopic equations from kinetic models or mesoscopic lattice Boltzmann models. In particular, for lattice Boltzmann models, the Chapman-Enskog analysis is an important tool (though not unique) which allows us to exactly define what macroscopic equations the numerical code is solving, even though they are not explicitly implemented.

5.3.4 Model equations and the BGK model

One of the major problems when dealing with the Boltzmann equation is the complicated nature of the collision integral. Therefore it is not surprising that alternative, simpler expressions have been proposed. The idea behind this replacement is that the large amount of detail of two-body interactions is not likely to significantly influence the values of many experimentally measured quantities [121]. A simplified collisional operator identifies a *model equation*.

In order to construct a model equation, the simplified collisional operator must satisfy some constraints. First of all it must conserve the collisional invariants, i.e. Eq. (5.6) must hold for the model equation too. Since the properties of the collisional operator affects directly those of the corresponding macroscopic equations, conserving the collisional invariants is very important and it must be guaranteed by the discretized lattice Boltzmann models too. Secondly, the simplified collisional operator must ensure that the system evolves towards the local equilibrium condition and

then towards the global equilibrium condition.

Both constraints are fulfilled by the most widely known model equation usually called the BGK model. It was proposed by Bhatnagar, Gross and Krook in 1954 [125] and independently at about the same time by Welander in 1954 [126]. The simplest way to ensure a correct relaxation towards equilibrium is to imagine that each collision changes the distribution function f by an amount proportional to the difference of f from a local Maxwellian f^e:

$$J(f) = -\frac{1}{\tau}(f - f^e), \tag{5.31}$$

where τ is called *relaxation time constant*. At any space point and time instant the Maxwellian distribution function $f^e(\mathbf{x}, \mathbf{v}, t)$ must have exactly the same density, macroscopic velocity and internal energy of the fluid as given by the distribution function $f(\mathbf{x}, \mathbf{v}, t)$.

Sometimes the BGK operator is called linearized operator but this expression can be misleading. In fact, the BGK operator is explicitly linear in f but f^e implicitly depends on f because it is a function of local density, velocity and internal energy, which all are statistical moments of the distribution function f. For this reason, if one substitutes the BGK operator in the Boltzmann equation (5.1), i.e. $Q(f, f) \to J(f)$, the final result is a strongly non-linear differential equation. This model equation is no more integral because $J(f)$ depends on local information only and the collisional operator is no more a quadratic form.

From some points of view, the BGK model equation cannot be rigorously defined a kinetic equation, if kinetic equation means coming from a fully developed coherent microscopic description within non-equilibrium statistical mechanics. In fact, the BGK model shares with the Boltzmann equation a pseudo-kinetic fashion because it is defined with respect to single-particle distribution functions and it reproduces

the fundamental outlines of the kinetic description, i.e. conservation of the collisional invariants and relaxation towards equilibrium. However, how to calculate the relaxation time constant τ exclusively by means of a kinetic description is not evident. The usual practice is to tune the relaxation time constant in order to match the desired macroscopic transport coefficients. This will be clear after performing the Chapman-Enskog expansion of the BGK model. What it is important to point out here is that the previous tuning strategy holds for any kind of fluid which can be described by the macroscopic equations coming from BGK model. There is no need to restrict the applications to rarefied ideal gases only, as it is usually done by the Boltzmann equation. For this reason, the BGK model can be defined a *mesoscopic* model and the previous tuning strategy is coherent with the top-down approach previously discussed at the beginning of this chapter.

Substituting the previous expansions given by Eqs. (5.26, 5.29, 5.30) in the BGK model, a coupled hierarchy system of equations in the powers of K is obtained. The first elements of this system are:

$$f^{(0)} = f^{e}, \tag{5.32}$$

$$\frac{\partial f^{(0)}}{\partial t^{(1)}} + \mathbf{v} \cdot \nabla^{(1)} f^{(0)} + \mathbf{g} \cdot \nabla^{(1)}_{\mathbf{v}} f^{(0)} = -\frac{1}{\tau} f^{(1)}, \tag{5.33}$$

$$\frac{\partial f^{(0)}}{\partial t^{(2)}} + \frac{\partial f^{(1)}}{\partial t^{(1)}} + \mathbf{v} \cdot \nabla^{(1)} f^{(1)} + \mathbf{g} \cdot \nabla^{(1)}_{\mathbf{v}} f^{(1)} = -\frac{1}{\tau} f^{(2)}. \tag{5.34}$$

The effects of the external force field in the Eq. (5.34), which involve the terms $O(K^2)$, can be neglected. This practice is based on the fact that the non-equilibrium distribution function does not differ too much from the equilibrium distribution with regard to the microscopic velocity during the fluid stage. Moreover Eq. (5.33) can be simplified by means of the first order of the expansion given by Eq. (5.32):

$$\nabla^{(1)}_{\mathbf{v}} f^{(0)} \approx -\frac{f^{e}}{e} \left(\mathbf{v} - \mathbf{u} \right), \tag{5.35}$$

where the velocity scale index has been omitted $\mathbf{v}^{(1)} \rightarrow \mathbf{v}$ because it is the dummy variable in the next integrals. Finally, the system of equations becomes:

$$\frac{\partial f^e}{\partial t^{(1)}} + \mathbf{v} \cdot \nabla^{(1)} f^e - \frac{f^e}{e}\, \mathbf{g} \cdot (\mathbf{v} - \mathbf{u}) = -\frac{1}{\tau}\, f^{(1)}, \tag{5.36}$$

$$\frac{\partial f^e}{\partial t^{(2)}} + \frac{\partial f^{(1)}}{\partial t^{(1)}} + \mathbf{v} \cdot \nabla^{(1)} f^{(1)} = -\frac{1}{\tau}\, f^{(2)}. \tag{5.37}$$

Equation (5.36) states that the lowest order deviation $f^{(1)}$ from a local Maxwellian distribution f^e is proportional to the gradients in space and time of f^e. The calculation of $f^{(1)}$ is much more complicated when the collision integral is not approximated [121].

In order to recover the macroscopic equations for the moments of the velocity distribution function, the previous equations must be multiplied by the generic collisional invariant $\Psi(\mathbf{v}) = m,\ m\, v_i,\ m\, \mathbf{v}^2/2$ and then the integration over the microscopic velocity must be performed. Since the previous equations are coupled, this procedure will be useful only if the integral equations will be decoupled. Multiplying the BGK operator given by Eq. (5.31) by the generic collisional invariant $\Psi(\mathbf{v})$ and integrating over the microscopic velocity yields

$$\int \Psi(\mathbf{v})\, [f - f^e_\sigma]\, d\mathbf{v} = \int \Psi(\mathbf{v}) \sum_{\xi=1}^{\infty} K^\xi\, f^{(\xi)}\, d\mathbf{v} = 0, \tag{5.38}$$

where the property given by Eq. (5.6) has been applied. Since the previous relation must be satisfied for any small value of the parameter K, finally we obtain:

$$\int \Psi(\mathbf{v})\, f^{(\xi)}\, d\mathbf{v} = 0, \tag{5.39}$$

for $\xi \geq 1$. The previous equation demonstrates that in the single-fluid BGK model the higher-order terms due to the expansion of the distribution function, i.e. $f^{(\xi)}$ for $\xi \geq 1$, do not affect the moments of the collisional invariants. This fundamental property ensures that for single-fluid BGK model the integral equations are decoupled.

Multiplying Eq. (5.36) by the collisional invariants and integrating with regard to the microscopic velocity, the following equations are recovered:

$$\frac{\partial \rho}{\partial t^{(1)}} + \nabla^{(1)} \cdot (\rho\, \mathbf{u}) = 0, \tag{5.40}$$

$$\frac{\partial}{\partial t^{(1)}}(\rho\, \mathbf{u}) + \nabla^{(1)} \cdot (\rho\, \mathbf{u} \otimes \mathbf{u}) = -\nabla^{(1)}(\rho\, e) + \rho\, \mathbf{g}, \tag{5.41}$$

$$\frac{\partial}{\partial t^{(1)}}(\rho\, e^t) + \nabla^{(1)} \cdot (\rho\, \mathbf{u}\, e^t) = -\nabla^{(1)} \cdot (\rho\, e\, \mathbf{u}) + \rho\, \mathbf{u} \cdot \mathbf{g}, \tag{5.42}$$

where $e^t = e + \rho \mathbf{u}^2/2$ is the specific total energy. Introducing again the pressure defined such that $p = \rho\, e$, the previous equations become identical to the Euler system of equations for ideal gases. The result previously obtained by assuming $f = f^e$ is recovered.

Multiplying the Eq. (5.37) by the collisional invariants and integrating with regard to the microscopic velocity, the following equations are recovered:

$$\frac{\partial \rho}{\partial t^{(2)}} = 0, \tag{5.43}$$

$$\frac{\partial}{\partial t^{(2)}}(\rho\, \mathbf{u}) = \nabla^{(1)} \cdot \left[\mathbf{S}_\nu + O(|\mathbf{u}|^3)\right], \tag{5.44}$$

$$\frac{\partial}{\partial t^{(2)}}(\rho\, e^t) = \nabla^{(1)} \cdot \left[-\mathbf{q}_\lambda + \mathbf{S}_\nu\, \mathbf{u} + O(|\mathbf{u}|^3)\right], \tag{5.45}$$

where $\mathbf{S}_\nu$ is the viscous part of the stress tensor, due to the BGK model, defined as

$$\mathbf{S}_\nu = \mathbf{S} - \mathbf{S}_e = \mathbf{S} + \rho\, e\, \mathbf{I} = -\rho\, e\, \tau\, \nabla^{(1)} \cdot \mathbf{u}\, \mathbf{I} + \rho\, e\, \tau\, \left[\nabla^{(1)}\mathbf{u} + \nabla^{(1)}\mathbf{u}^T\right], \tag{5.46}$$

and $\mathbf{q}_\lambda$ is the heat flux, due to the BGK model, defined as

$$\mathbf{q}_\lambda = \mathbf{q} - \mathbf{q}_e = -2\, \rho\, e\, \tau\, \nabla^{(1)} e. \tag{5.47}$$

The first-order perturbation does not produce any effect on the continuity equation, while introduces some diffusion terms in both momentum and energy equation which are essentially due to microscopic collisions.

Since we are interested in the low Mach number limit, the terms which involve higher powers of the velocities $O(|\mathbf{u}|^3)$ can be neglected. Summing the simplified forms of Eqs. (5.43, 5.44, 5.45) with the Eqs. (5.40, 5.41, 5.42), the final system of equations is obtained:

$$\frac{\partial \rho}{\partial t} + \nabla \cdot (\rho\, \mathbf{u}) = 0, \tag{5.48}$$

$$\frac{\partial}{\partial t}(\rho\, \mathbf{u}) + \nabla \cdot (\rho\, \mathbf{u} \otimes \mathbf{u}) = -\nabla(\rho\, e) + \nabla \cdot \mathbf{S}_\nu + \rho\, \mathbf{g}, \tag{5.49}$$

$$\frac{\partial}{\partial t}(\rho\, e^t) + \nabla \cdot (\rho\, \mathbf{u}\, e^t) = -\nabla \cdot (\rho\, e\, \mathbf{u}) + \nabla \cdot [-\mathbf{q}_\lambda + \mathbf{S}_\mu\, \mathbf{u}] + \rho\, \mathbf{u} \cdot \mathbf{g}, \tag{5.50}$$

where the viscous part of the stress tensor can be simplified because in the low Mach number limit the velocity field is essentially divergence free, namely

$$\mathbf{S}_\nu = \rho\, e\, \tau\, \left(\nabla \mathbf{u} + \nabla \mathbf{u}^T\right), \tag{5.51}$$

and the heat flux is $\mathbf{q}_\lambda = -2\, \rho\, e\, \tau\, \nabla e$. Assuming the ideal gas law as constitutive equation ($p = \rho\, e$), a kinematic viscosity $\nu = e\, \tau$ and a thermal diffusivity $\iota = 2\, e\, \tau$, the previous system of equation exactly recovers the Navier-Stokes system of equations. It is interesting to point out that a consequence of the BGK model is a fixed Prandtl number $Pr = \nu/\iota = 1/2$.

The single-fluid continuous BGK model is the starting point for the development of the lattice Boltzmann models discussed in the next section. The drawback about the fixed Prandtl number suggests from the beginning that a limited number of mesoscopic parameters (only τ in this case) can sometimes be insufficient to independently match the desired macroscopic transport coefficients (ν and ι in this case).

5.4 Design of lattice Boltzmann models

Using the very rudimentary concepts of non-equilibrium statistical mechanics introduced in the previous section, how to design a lattice Boltzmann version of the

single-phase BGK model will be investigated. It is shown that the lattice Boltzmann models are a special discretized form of the Boltzmann equation, eventually modified in order to include additional effects.

Nowadays it is well known that the lattice Boltzmann models can be derived from continuous kinetic models and they are completely independent of LGCA, if historical reasons are neglected. More detailed derivations analyzing this relationship can be found in literature [119, 127, 128]. Here the goal is to outline the most important features.

- A set of discretized microscopic velocities is needed and it must possess a sufficient *symmetry* in order to ensure isotropy of certain tensors involved in the macroscopic equations. A proper degree of symmetry can allow us to consider a few number of velocities and this makes the calculations feasible. This is probably the condition that historically created more difficulties [102].

- The Chapman-Enskog asymptotic analysis allows us to investigate only the dynamics of the lower-order moments, which usually must satisfy some constraints in order to recover the desired macroscopic hydrodynamics. However higher-order *spurious moments* or *ghost moments* always exist and they can affect the stability and the reliability of the numerical results.

5.4.1 Discretization according to Lattice Boltzmann Method

First of all, let us start with the discretization of time. The BGK equation can be formally rewritten in the form of an ordinary differential equation:

$$\frac{D\,f}{D\,t} = -\frac{1}{\tau}\,(f - f^e) - \mathbf{g}\cdot\nabla_{\mathbf{v}} f, \tag{5.52}$$

where $D/D\,t = \partial/\partial\,t + \mathbf{v}\cdot\nabla$ is the time derivative along the characteristic line

defined by the microscopic velocity $\mathbf{v}$. If we expand the substantial derivative along the characteristic line in its Taylor expansion

$$\frac{D\,f}{D\,t} = \frac{f(\mathbf{x}+\mathbf{v}\,\delta t, \mathbf{v}, t+\,\delta t) - f(\mathbf{x},\mathbf{v},t)}{\delta t} - \frac{\delta t}{2}\,\frac{D}{D\,t}\frac{D\,f}{D\,t} + O(\delta t^2), \tag{5.53}$$

and, further, neglect the terms of order $O(\delta t)$, then the following expression yields:

$$f(\mathbf{x}+\mathbf{v}\,\delta t, \mathbf{v}, \delta t) - f(\mathbf{x},\mathbf{v},t) = -\frac{\delta t}{\tau}\,[f(\mathbf{x},\mathbf{v},t) - f^e(\mathbf{x},\mathbf{v},t)] - \delta t\,\mathbf{g}\cdot\nabla_{\mathbf{v}} f. \tag{5.54}$$

Recalling the approximation previously discussed for the term which takes into account the effects due to the external force field $\nabla_{\mathbf{v}} f \approx -(\mathbf{v}-\mathbf{u})\,f^e/e$, the previous equation can be simplified:

$$f(\mathbf{x}+\mathbf{v}\,\delta t, \mathbf{v}, t+\delta t) - f(\mathbf{x},\mathbf{v},t) = -\frac{\delta t}{\tau}\,[f(\mathbf{x},\mathbf{v},t) - f^e(\mathbf{x},\mathbf{v},t)] + \frac{\delta t\,f^e}{e}\,(\mathbf{v}-\mathbf{u})\cdot\mathbf{g}. \tag{5.55}$$

Therefore, the previous equation, which is the evolution equation of the distribution function f with discrete time, is accurate to the first order in δt. Terms of order $O(\delta t^2)$ have been reported in the expansion given by Eq. (5.53) because they will be considered when discussing the discrete lattice effects. Since the previous discretization has been performed along the characteristic line defined by the velocity $\mathbf{v}$, then time and spatial discretization are not independent one another and this should be taken into account for velocity discretization too.

In order to numerically evaluate the hydrodynamic moments involved in the Maxwellian distribution function f^e, appropriate discretization in the velocity projection of the phase space must be accomplished. The discrete ordinate method (DOM) is commonly utilized for solving the integro-differential equations involved for modeling the rarefied gas flows [129] and it will be adopted for solving simpler differential equations in this case. According to this method, a set of discrete microscopic velocities $\mathbf{v}_\lambda$ must be defined and the velocity distribution function will be exclusively

evaluated for the selected velocities. This set of microscopic velocities is called *lattice* and this justifies why the technique is called Lattice Boltzmann Method. With appropriate discretization, integration in velocity projection (with weight function given by the equilibrium distribution function f^e) can be approximated by quadrature formula up to a certain degree of accuracy. In LBM, the equilibrium distribution function is obtained by a truncated small velocity expansion or low-Mach-number approximation, namely

$$f^e \approx \frac{\rho}{m\,(2\pi e)^{D/2}} \exp\left[-\frac{\mathbf{v}^2}{2\,e}\right]\left[1+\frac{\mathbf{v}\cdot\mathbf{u}}{e}+\frac{(\mathbf{v}\cdot\mathbf{u})^2}{2\,e^2}-\frac{\mathbf{u}^2}{2\,e}\right]. \tag{5.56}$$

The previous expansion simplifies the calculation of the moments because it requires simpler quadrature formulas. Essentially the low-Mach-number approximation allows us to substitute the original exponential function with a simpler polynomial, which describes small deviations of the distribution function from the state at rest [127].

In deriving the Navier-Stokes equations from the Boltzmann equation via the Chapman-Enskog analysis, discussed in the previous section, the first two orders of approximations of the distribution function, i.e. f^e and $f^{(1)}$ must be considered [119]. Therefore, given the equilibrium distribution function f^e by Eq. (5.56), the quadrature used to evaluate the hydrodynamic moments must be able to exactly compute the generic moment Γ_ψ with respect to f^e:

$$\Gamma_\psi = \frac{\rho}{m\,(2\pi e)^{D/2}} \int \psi(\mathbf{v})\left[1+\frac{\mathbf{v}\cdot\mathbf{u}}{e}+\frac{(\mathbf{v}\cdot\mathbf{u})^2}{2\,e^2}-\frac{\mathbf{u}^2}{2\,e}\right]\exp\left[-\frac{\mathbf{v}^2}{2\,e}\right] d\mathbf{v}, \tag{5.57}$$

where $\psi(\mathbf{v})$ depends on the considered macroscopic equation and it can be equal to

$$\psi(\mathbf{v}) = \begin{cases} m & m\,v_i & m\,v_i\,v_j & \text{in Eq. (5.10)} \\ m\,v_i & m\,v_i\,v_j & m\,v_i\,v_j\,v_k & \text{in Eq. (5.11)} \\ m\,v_i^2 & m\,v_i^2\,v_j & m\,v_i^2\,v_j\,v_k & \text{in Eq. (5.12)} \end{cases}.$$

It is worth to point out that $\psi(\mathbf{v}) = m,\, m\,v_i,\, m\,v_i^2$ are naturally involved in the definitions of the collisional invariants, while the other terms derive from non-linear

streaming. In particular, the macroscopic equations require to calculate the streaming of the corresponding collisional invariants with a weight function given by f^e and by $f^{(1)}$, which involves an additional recursive streaming with a weight function given by f^e and depicted by Eq. (5.36). For this reason, the Chapman-Enskog analysis forces to consider moments two-order higher than corresponding collisional invariants. Let us introduce the dimensionless velocity $\mathbf{v}^* = \mathbf{v}/\sqrt{2\,e}$ and $\mathbf{u}^* = \mathbf{u}/\sqrt{2\,e}$, namely

$$\Gamma_\psi = \frac{\rho}{m\,\pi^{D/2}} \int \psi(\mathbf{v}^*)\, \left[1 + 2\,\mathbf{v}^* \cdot \mathbf{u}^* + 2\,(\mathbf{v}^* \cdot \mathbf{u}^*)^2 - (\mathbf{u}^*)^2\right] \exp\left[-(\mathbf{v}^*)^2\right]\, d\mathbf{v}^*. \tag{5.58}$$

The previous expression can be calculated numerically with Gaussian-type quadrature [130].

For the sake of simplicity but without losing generality, let us consider the two dimensional case. If the Cartesian coordinate system is used, then the generic argument $\psi(\mathbf{v})$ of the hydrodynamic moment Γ_ψ becomes:

$$\psi(\mathbf{v}) = m\, v_x^m\, v_y^n, \tag{5.59}$$

where $0 \leq m \leq 4$ and $0 \leq n \leq 4$. Naturally, the third-order Hermite formula is the optimal choice to evaluate Γ_ψ for the purpose of deriving the discretization of the phase space [119]. Introducing the third-order Hermite formula in Eq. (5.58) for the two dimensional case, the following results hold

$$\Gamma_\psi = \frac{\rho}{m} \sum_{i=1}^{3} \sum_{j=1}^{3} \frac{\zeta_i \zeta_j}{\pi}\, \psi(v_i^*, v_j^*)\, \left[1 + 2\,(v_i^*\, u_x^* + v_j^*\, u_y^*) + 2\,\left(v_i^*\, u_x^* + v_j^*\, u_y^*\right)^2 - (\mathbf{u}^*)^2\right], \tag{5.60}$$

where the three abscissas of the quadrature are

$$v_1^* = -\sqrt{3/2}\ \ ,\ \ v_2^* = 0\ \ ,\ \ v_3^* = +\sqrt{3/2}\,, \tag{5.61}$$

and the corresponding weight coefficients are

$$\zeta_1 = \sqrt{\pi}\,/6\ \ ,\ \ \zeta_2 = 2\,\sqrt{\pi}\,/3\ \ ,\ \ \zeta_3 = \sqrt{\pi}\,/6\,. \tag{5.62}$$

The generic integral given by Eq. (5.60) involves 3×3 terms, which can be rearranged by defining a set of 9 allowed velocities $\mathbf{v}^\lambda = \sqrt{2\,e}\,[v_i^*,\, v_j^*]^T$, namely

$$\mathbf{v}^\lambda = \begin{cases} c & [0,\, 0] & \lambda = 0 \\ c & [\cos(\lambda\,\pi/2 - \pi/2),\, \sin(\lambda\,\pi/2 - \pi/2)] & \lambda = 1,2,3,4 \\ \sqrt{2}\,c & [\cos(\lambda\,\pi/2 - 9\,\pi/4),\, \sin(\lambda\,\pi/2 - 9\,\pi/4)] & \lambda = 5,6,7,8 \end{cases}, \quad (5.63)$$

where $c = \sqrt{3\,e}$ is called the *lattice velocity*. It is worth to point out that the velocity discretization is coupled to that of the physical space such that a lattice structure is obtained, i.e. $c = \delta x/\delta t$. In a similar way, the weight coefficients can be rearranged too $\varsigma^\lambda = \zeta_i \zeta_j/\pi$ and they are, explicitly,

$$\varsigma^\lambda = \begin{cases} 4/9 & \lambda = 0 \\ 1/9 & \lambda = 1,2,3,4 \\ 1/36 & \lambda = 5,6,7,8 \end{cases}. \quad (5.64)$$

Finally, both previous rearrangements can be introduced in the generic moment Γ_ψ to yield:

$$\Gamma_\psi = \sum_{\lambda=0}^{8} \varsigma^\lambda\, \varphi^{e\,\lambda}\, \psi(\mathbf{v}^\lambda)/m, \quad (5.65)$$

where $\varphi^{e\,\lambda}$ is a two-dimensional second-order polynomial form called the *discretized equilibrium distribution function* and it is defined as

$$\varphi^{e\,\lambda} = \rho \left[1 + \frac{\mathbf{v}^\lambda \cdot \mathbf{u}}{e} + \frac{\left(\mathbf{v}^\lambda \cdot \mathbf{u}\right)^2}{2\,e^2} - \frac{\mathbf{u}^2}{2\,e}\right]. \quad (5.66)$$

It is easy to verify that $\varphi^{e\,\lambda} = f^{e\,\lambda}/Q^\lambda$, where

$$Q^\lambda = \frac{1}{m_\sigma\,(2\pi\,e)} \exp\left[-\frac{(\mathbf{v}^\lambda)^2}{2\,e}\right]. \quad (5.67)$$

The discrete kinetic equation (5.55) can be reformulated in terms of the new variables $\varphi^\lambda = f^\lambda/Q^\lambda$ and $\varphi^{e\,\lambda}$, namely

$$\varphi^\lambda(\mathbf{x}+\mathbf{v}\,\delta t, \mathbf{v}, t+\delta t) - \varphi^\lambda(\mathbf{x}, \mathbf{v}, t) = -\frac{\delta t}{\tau}\,\left[\varphi^\lambda(\mathbf{x}, \mathbf{v}, t) - \varphi^{e\,\lambda}(\mathbf{x}, \mathbf{v}, t)\right] + \frac{\delta t\,\varphi^{e\,\lambda}}{e}\,(\mathbf{v}^\lambda - \mathbf{u})\cdot\mathbf{g}. \quad (5.68)$$

Since only the terms up to the second-order in the macroscopic quantities have been considered in the approximation given by Eq. (5.56), the forcing term in Eq. (5.68)

can be simplified by neglecting higher order terms. It is well known that considering different-order approximations can lead to numerical inaccuracies. Since the acceleration due to the external force field can be considered of the first-order, the terms multiplying the acceleration must be of the first-order with regard to the macroscopic velocity [132]. For this reason, the equations for the discretized distribution functions become:

$$\varphi^{\lambda}(\mathbf{x}+\mathbf{v}\,\delta t,\mathbf{v},t+\delta t)-\varphi^{\lambda}(\mathbf{x},\mathbf{v},t)=-\frac{\delta t}{\tau}\left[\varphi^{\lambda}(\mathbf{x},\mathbf{v},t)-\varphi^{e\,\lambda}(\mathbf{x},\mathbf{v},t)\right]+\frac{\delta t}{\sqrt{e}}\,\mathbf{k}^{\lambda}\cdot\mathbf{g}, \quad (5.69)$$

where

$$\mathbf{k}^{\lambda}=\rho\left(\frac{\mathbf{v}^{\lambda}-\mathbf{u}}{\sqrt{e}}+\frac{\mathbf{v}^{\lambda}\cdot\mathbf{u}}{\sqrt{e^3}}\,\mathbf{v}^{\lambda}\right). \quad (5.70)$$

The lattice defined by Eq. (5.63) is labeled $D2Q9$ and it is a square lattice for two-dimensional computational domains ($D=2$) involving nine discrete velocities ($Q=9$). In the following, all the lattices will be labeled in a similar way by indicating the number of physical dimensions (D) and the number of microscopic discrete velocities (Q). This nomenclature was proposed by Qian, d'Humiéres and Lallemand, who first introduced this lattice and many others [117].

The discussed methodology aiming to define a particular set of allowed velocities and corresponding weight factors for performing the numerical calculation of the discrete moments is general and it can be applied to derive many lattices [119] for two-dimensional and three-dimensional simulations. Some examples of possible lattices are reported in Tab. 5.1. The $D2Q7$ is important for historical reasons because it is the direct descendant of the lattice gas cellular automata but it is less accurate than the previously derived $D2Q9$.

The derivation process is more complicate for three-dimensional domains. In this case, each point on a unit cubic lattice space has six nearest neighbors, $(\pm1,0,0)$, $(0,\pm1,0)$, and $(0,0,\pm1)$, twelve next nearest neighbors, $(\pm1,\pm1,0)$, $(\pm1,0,\pm1)$, and

Table 5.1: Some lattices and corresponding weight factors considered by the Lattice Boltzmann Method for two-dimensional ($D2Q7$ and $D2Q9$) and three-dimensional ($D3Q13$ and $D3Q19$) simulations. The notation $DdQq$ for the q velocity model in the d-dimensional space is adopted [117].

$D2Q7$	$\mathbf{v}^\lambda = \begin{cases} (0,\,0) & \lambda = 0 \\ (\pm c,\,0),(\pm c/2,\,\pm c\sqrt{3}/2) & \lambda = 1,2,3,4,5,6 \end{cases}$ $\varsigma^\lambda = \begin{cases} 1/2 & \lambda = 0 \\ 1/12 & \lambda = 1,2,3,4,5,6 \end{cases}$
$D2Q9$	$\mathbf{v}^\lambda = \begin{cases} (0,\,0) & \lambda = 0 \\ (\pm c,\,0),(0,\,\pm c) & \lambda = 1,2,3,4 \\ (\pm c,\,\pm c) & \lambda = 5,6,7,8 \end{cases}$ $\varsigma^\lambda = \begin{cases} 4/9 & \lambda = 0 \\ 1/9 & \lambda = 1,2,3,4 \\ 1/36 & \lambda = 5,6,7,8 \end{cases}$
$D3Q15$	$\mathbf{v}^\lambda = \begin{cases} (0,\,0,\,0) & \lambda = 0 \\ (\pm c,\,0,\,0),(0,\,\pm c,\,0),(0,\,0,\,\pm c) & \lambda = 1,2,...,6 \\ (\pm c,\,\pm c,\,\pm c) & \lambda = 7,8,...,14 \end{cases}$ $\varsigma^\lambda = \begin{cases} 2/9 & \lambda = 0 \\ 1/9 & \lambda = 1,2,...,6 \\ 1/72 & \lambda = 7,8,...,14 \end{cases}$
$D3Q19$	$\mathbf{v}^\lambda = \begin{cases} (0,\,0,\,0) & \lambda = 0 \\ (\pm c,\,0,\,0),(0,\,\pm c,\,0),(0,\,0,\,\pm c) & \lambda = 1,2,...,6 \\ (\pm c,\,\pm c,\,0),(\pm c,\,0,\,\pm c),(0,\,\pm c,\,\pm c) & \lambda = 7,8,...,18 \end{cases}$ $\varsigma^\lambda = \begin{cases} 1/3 & i = 0 \\ 1/18 & i = 1,2,...,6 \\ 1/36 & i = 7,8,...,18 \end{cases}$

$(0, \pm 1, \pm 1)$, and eight third nearest neighbors, $(\pm 1, \pm 1, \pm 1)$. Elementary discrete velocity sets for lattice Boltzmann models in three dimensions are constructed from the set of 26 vectors pointing from the origin to the above neighbours and the zero vector $(0, 0, 0)$. The 27 velocities are usually grouped into four subsets labeled by their squared modulus, 0, 1, 2, and 3. In Tab. 5.1 two lattices have been considered: the $D3Q15$ lattice and the $D3Q19$ lattice. Both these lattices were proposed at the beginning of the Lattice Boltzmann Method [117]. The $D3Q13$ lattice [131] only uses the subsets 0 and 2 and it is considered too simple in order to analyze complex fluid flow.

In conclusion, the Lattice Boltzmann Method has the following ingredients:

1. an *evolution equation*, in the form of Eq. (5.69) with discretized time and phase space involving a lattice structure and a momentum space reduced to a small set of discrete momenta;
2. an *equilibrium distribution function*, given by Eq. (5.66), which leads to the Navier-Stokes equations and involves the conservation constraints, which are the hydrodynamic collisional invariants;
3. a *lattice*, i.e. a set of allowed microscopic velocities, which is characterized by enough symmetry to accurately calculate the hydrodynamic moments.

5.4.2 Discrete lattice effects

Deriving the discrete Eqs. (5.69) of the lattice Boltzmann BGK model, it has been pointed out that, since only the first term of the Taylor expansion given by Eq. (5.53) was included, the numerical method is accurate only to the first order in δt. In this section, some tricks will be analyzed in order to increase the accuracy up to the second order in δt.

In order to analyze the second order errors of the numerical scheme, let us suppose to expand the normalized velocity distribution function φ^λ in terms of a small parameter K, as previously done in the Chapman-Enskog analysis for f. We can analogously proceed for the substantial derivative which involves the generic microscopic lattice velocity, by grouping together terms with the same order of magnitude:

$$\frac{D_\lambda^{(\xi)}}{D\,t^{(\xi)}} = \frac{\partial}{\partial\,t^{(\xi)}} + \mathbf{v}^\lambda \cdot \nabla^{(\xi)}. \tag{5.71}$$

Substituting the previous expansion in the BGK model, a coupled hierarchy system of equations in the powers of K is obtained and the first elements of this system are:

$$\frac{D_\lambda^{(1)}\,\varphi^{\lambda\,e}}{D\,t^{(1)}} = -\frac{1}{\tau}\,\varphi^{\lambda\,(1)} + \frac{1}{\sqrt{e}}\,\mathbf{k}^\lambda \cdot \mathbf{g}, \tag{5.72}$$

$$\frac{\partial\varphi^{\lambda\,e}}{\partial\,t^{(2)}} + \frac{D_\lambda^{(1)}\,\varphi^{\lambda\,(1)}}{D\,t^{(1)}} + \frac{\delta\,t}{2}\,\frac{D_\lambda^{(1)}}{D\,t^{(1)}}\,\frac{D_\lambda^{(1)}\,\varphi^{\lambda\,e}}{D\,t^{(1)}} = -\frac{1}{\tau}\,\varphi^{\lambda\,(2)}. \tag{5.73}$$

In order to analyze the discrete lattice effects, only the continuity and the momentum equation will be considered, but similar considerations hold for the energy equation too. Multiplying the Eqs. (5.72) and (5.73) by the collisional invariants and integrating over the microscopic velocity, the following equations are recovered:

$$\frac{\partial\rho}{\partial t} + \nabla\cdot(\rho\mathbf{u}) = -\frac{\delta\,t}{2}\,\nabla\cdot(\rho\,\mathbf{g})\,, \tag{5.74}$$

$$\begin{aligned}\frac{\partial\,(\rho\mathbf{u})}{\partial t} \;&+\; \nabla\cdot(\rho\mathbf{u}\otimes\mathbf{u}) = -\nabla\,(\rho\,e) + \rho\,\mathbf{g}\\ &+\; \nabla\cdot\left[d\,\rho\,e\,\tau\,\left(\nabla\mathbf{u} + \nabla\mathbf{u}^T\right)\right] - \frac{\delta\,t}{2}\,\frac{\partial}{\partial t}\,(\rho\,\mathbf{g})\\ &-\; \frac{\delta t}{2}\,\nabla\cdot(\rho\,\mathbf{u}\otimes\mathbf{g} + \rho\,\mathbf{g}\otimes\mathbf{u})\,,\end{aligned} \tag{5.75}$$

where $d = 1 - \delta t/(2\,\tau)$. The previous equations differ from continuity and momentum equations due to the original BGK model, given by Eqs. (5.10) and (5.11) respectively. Some additional terms proportional to δt arise and they reduce the accuracy of the numerical scheme to the first order only. These terms are called *discrete lattice effects*.

For increasing the accuracy of the numerical scheme, the spurious terms must be dropped out. In order to cancel the discrete lattice effects, let us introduce the following corrected velocities [132, 133]:

$$\rho\,\mathbf{u}^{\star} = \sum_{\lambda=0}^{8} \varsigma^{\lambda}\,\mathbf{v}^{\lambda}\,\varphi^{\lambda} + \rho\,\mathbf{g}\,\delta t/2. \tag{5.76}$$

Similarly the corrected equilibrium distribution function $\varphi^{e\,\lambda\star}$ and the corrected forcing term $\mathbf{k}^{\lambda\star}$ calculated by means of the corrected velocity $\mathbf{u}^{\star}$ can be obtained. Thanks to these quantities, the final lattice Boltzmann model can be formulated:

$$\varphi^{\lambda}(\mathbf{x}+\mathbf{v}\,\delta t,\mathbf{v},t+\,\delta t) - \varphi^{\lambda}(\mathbf{x},\mathbf{v},t) = -\frac{\delta t}{\tau}\,\left[\varphi^{\lambda}(\mathbf{x},\mathbf{v},t) - \varphi^{e\,\lambda\star}(\mathbf{x},\mathbf{v},t)\right] + \frac{\delta t\,d}{\sqrt{e}}\,\mathbf{k}^{\lambda\star}\cdot\mathbf{g}. \tag{5.77}$$

An additional factor d has been added to the forcing term too. The Chapman-Enskog analysis of the corrected model ensures that the continuity equation is correctly recovered while the momentum equation becomes

$$\frac{\partial\,(\rho\mathbf{u})}{\partial t} + \nabla\cdot(\rho\mathbf{u}\otimes\mathbf{u}) = -\nabla\,(\rho\,e) + \rho\,\mathbf{g} + \nabla\cdot\left[d\,\rho\,e\,\tau\,\left(\nabla\mathbf{u} + \nabla\mathbf{u}^{T}\right)\right]. \tag{5.78}$$

Essentially it is possible to achieve a second order accuracy by modifying the definition of the kinematic viscosity, i.e. $\nu = d\,\tau\,e$. Obviously since the kinematic viscosity must be positive, then $d > 0$ and this implies $\delta t < 2\,\tau$, i.e. a stability threshold exists because the numerical scheme remains explicit.

The previous numerical tricks allow us to produce a numerical scheme with second order accuracy by correcting an evolution equation which was originally first order accurate only.

5.4.3 Multi-Relaxation-Time models

In the previous sections, the advantages and the drawbacks of the simplest lattice Boltzmann models have been discussed. Essentially, the discretization of the velocity

space due to the lattice allows us to easily solve a pseudo-kinetic equation characterized by some relaxation time constants. Independently from the considered approach for tuning the relaxation time constants, the number of these parameters actually determines the complexity and the reliability of the mesoscopic model. Within the framework of the top-down tuning strategy, the number of relaxation time constants limits the number of the macroscopic transport coefficients which can be independently tuned.

In particular, the situation is quite critical for thermal models. Fully thermo-hydrodynamic lattice Boltzmann schemes represent a standing challenge to LBM research and despite several brilliant attempts a fully thermo-hydrodynamic lattice Boltzmann scheme working safely over a wide range of temperatures is still missing [104].

In order to increase the number of tunable parameters and consequently the number of macroscopic equations meaningfully solved, the following tools are quite promising:

- the *hybrid design*, which means that the additional scalar equations are solved by means of different numerical schemes and only the fluid flow is computed by the LBM;
- the *multi-relaxation-time collisional operator*, which allows us to consider the maximum number of relaxation time constants for a given lattice by controlling independently the relaxation behavior of each moment;
- the *multi-lattice design*, which essentially uses different lattices for solving different macroscopic equations without neglecting the physical coupling among them.

In this section the multi-relaxation-time (MRT) formulation will be discussed, while

the multi-lattice design will be analyzed in the next section and more extensively concerning (real or virtual) gaseous mixtures. The hybrid design is neglected because it does not add any information with regard to the LBM.

Before discussing how to increase the relaxation time constants, the pseudo-kinetic problem on the lattice must be reformulated. Henceforth the Dirac notations of "bra" $\langle\cdot|$ and "ket" $|\cdot\rangle$ vectors are used to denote the row and column vectors respectively. Let us introduce the following definitions:

$$\left\langle \varphi^{\dagger} \right| = \left[\varsigma^0 \, \varphi^0(\mathbf{x} + \mathbf{v}\,\delta t, \mathbf{v}, t + \delta t), \ldots \varsigma^8 \, \varphi^8(\mathbf{x} + \mathbf{v}\,\delta t, \mathbf{v}, t + \delta t) \right] , \tag{5.79}$$

$$\langle \varphi | = \left[\varsigma^0 \, \varphi^0(\mathbf{x}, \mathbf{v}, t), \ldots \varsigma^8 \, \varphi^8(\mathbf{x}, \mathbf{v}, t) \right] , \tag{5.80}$$

$$\langle \varphi^e | = \left[\varsigma^0 \, \varphi^{e\,0}(\mathbf{x}, \mathbf{v}, t), \ldots \varsigma^8 \, \varphi^{e\,8}(\mathbf{x}, \mathbf{v}, t) \right] . \tag{5.81}$$

Introducing the previous definitions in Eq. (5.69), neglecting the external force field, i.e. assuming $\mathbf{g} = 0$, and assembling all the equations for lattice components, the whole system of equations can be rewritten in matrix form in the following way:

$$\left|\varphi^{\dagger}\right\rangle - |\varphi\rangle = -\omega \, \mathbf{I} \, \left(|\varphi\rangle - |\varphi^e\rangle \right) , \tag{5.82}$$

where $\omega = \delta t / \tau$. The external force field has been dropped out because it is much easier to take it into account by means of equations recasted in the momentum space, as it will be clear later on. In order to increase the relaxation time constants, it is seems obvious to generalize the previous equation by means of the matrix $\mathbf{C}$ which is in principle full, namely

$$\left|\varphi^{\dagger}\right\rangle - |\varphi\rangle = -\mathbf{C} \, \left(|\varphi\rangle - |\varphi^e\rangle \right) . \tag{5.83}$$

In this way, the problem is to reasonably fill $\mathbf{C}$ by ensuring physically reliable results. In the previous sections, the *velocity representation* has been used and this simplified the understanding of the streaming step of the lattice Boltzmann algorithm, i.e. the

fact that the discretized distribution functions are moved according to the discrete lattice directions. However, it is well understood in the context of kinetic theory that various physical processes in fluids, such as viscous transport, can be approximately described by coupling or interaction among *modes* of the collisional operator, and these modes are directly related to the moments, that is the hydrodynamic modes are linear combinations of mass and momentum [134–136]. Thus the *moment representation* provides a convenient and effective tool for incorporating physics into the LBM. Because the physical significance of the moments is obvious (hydrodynamic quantities and their fluxes), the relaxation time constants of the moments are directly related to the various transport coefficients. This mechanism allows us to control each mode independently.

The multiple-relaxation-time (MRT) lattice Boltzmann method was developed for the first time by d'Humiéres [137]. This has been persistently investigated, and much progress has been made. Successes include formulation of optimal boundary conditions [138], thermal [139] and viscoelastic models [140] and improved numerical stability [134, 135]. In particular, it was shown that the MRT models are much more stable than their BGK counterparts, because the different relaxation times can be individually tuned to achieve optimal stability.

For the sake of simplicity but without losing generality, let us consider again the two-dimensional case and the $D2Q9$ lattice. Recalling Eq. (5.65), it easy to verify that the hydrodynamic modes in this case can be written as proper combinations of the following terms:

$$\Gamma_\psi = \sum_{\lambda=0}^{8} \varsigma^\lambda \, \varphi^{e\,\lambda} \, (v_x^\lambda)^m \, (v_y^\lambda)^n = c^{m+n} \sum_{\lambda=0}^{8} \varsigma^\lambda \, \varphi^{e\,\lambda} \, (e_x^\lambda)^m \, (e_y^\lambda)^n, \tag{5.84}$$

where $e_x^\lambda = v_x^\lambda / c$ and $e_y^\lambda = v_y^\lambda / c$ are the dimensionless components of the discrete lattice velocities. Some hydrodynamic modes are proportional to the collisional in-

variants, i.e. ρ, $\rho\,\mathbf{u}$ and $\rho\,e$. For these modes, the following definitions hold:

$$\rho = \sum_{\lambda=0}^{8} \varsigma^{\lambda}\,\varphi^{e\,\lambda}\,R_{1,\,\lambda+1}\,, \tag{5.85}$$

$$\rho\,u_x = c\sum_{\lambda=0}^{8} \varsigma^{\lambda}\,\varphi^{e\,\lambda}\,R_{2,\,\lambda+1}\,, \tag{5.86}$$

$$\rho\,u_y = c\sum_{\lambda=0}^{8} \varsigma^{\lambda}\,\varphi^{e\,\lambda}\,R_{3,\,\lambda+1}\,, \tag{5.87}$$

$$\rho\,(e+\mathbf{u}^2/2) = c^2/2\sum_{\lambda=0}^{8} \varsigma^{\lambda}\,\varphi^{e\,\lambda}\,R_{4,\,\lambda+1}\,, \tag{5.88}$$

where $R_{1,\,\lambda+1}=1$, $R_{2,\,\lambda+1}=e_x^{\lambda}$, $R_{3,\,\lambda+1}=e_y^{\lambda}$ and $R_{4,\,\lambda+1}=(e_x^{\lambda})^2+(e_y^{\lambda})^2$. The previous equations define the first four rows of the matrix $\mathbf{R}$, defined as

$$\mathbf{R}=\begin{bmatrix} \langle\varrho_R^0| \\ \langle\varrho_R^1| \\ \langle\varrho_R^2| \\ \langle\varrho_R^3| \\ \langle\varrho_R^4| \\ \langle\varrho_R^5| \\ \langle\varrho_R^6| \\ \langle\varrho_R^7| \\ \langle\varrho_R^8| \end{bmatrix} = \begin{bmatrix} 1 & 1 & 1 & 1 & 1 & 1 & 1 & 1 & 1 \\ 0 & 1 & 0 & -1 & 0 & 1 & -1 & -1 & 1 \\ 0 & 0 & 1 & 0 & -1 & 1 & 1 & -1 & -1 \\ 0 & 1 & 1 & 1 & 1 & 2 & 2 & 2 & 2 \\ 0 & 1 & -1 & 1 & -1 & 0 & 0 & 0 & 0 \\ 0 & 0 & 0 & 0 & 0 & 1 & -1 & 1 & -1 \\ 0 & 0 & 0 & 0 & 0 & 1 & -1 & -1 & 1 \\ 0 & 0 & 0 & 0 & 0 & 1 & 1 & -1 & -1 \\ 0 & 0 & 0 & 0 & 0 & 1 & 1 & 1 & 1 \end{bmatrix}. \tag{5.89}$$

Considering the terms involved in the Chapman-Enskog expansion, it is possible to define the hydrodynamic modes corresponding to the diagonal and off-diagonal component of the stress tensor, i.e. $R_{5,\,\lambda+1}=(e_x^{\lambda})^2-(e_y^{\lambda})^2$ and $R_{6,\,\lambda+1}=e_x^{\lambda}\,e_y^{\lambda}$, those corresponding to the x and y component of energy flux, i.e. $R_{7,\,\lambda+1}=e_x^{\lambda}\,(e_y^{\lambda})^2$ and $R_{8,\,\lambda+1}=(e_x^{\lambda})^2\,e_y^{\lambda}$, and finally that corresponding to higher-order energy transport, i.e. $R_{9,\,\lambda+1}=(e_x^{\lambda})^2\,(e_y^{\lambda})^2$. The matrix $\mathbf{R}$ can be considered as composed by as many rows $\left\langle\varrho_R^{\lambda}\right|$ as the number of allowed velocities. The first four rows are involved in the definitions of the collisional invariants, namely it is easy to verify that $\langle\varrho_R^0|\varphi\rangle=\rho$, $c\,\langle\varrho_R^1|\varphi\rangle=\rho\,u_x$, $c\,\langle\varrho_R^2|\varphi\rangle=\rho\,u_y$ and finally $c^2/2\,\langle\varrho_R^3|\varphi\rangle=\rho\,(e+\mathbf{u}^2/2)$. Even though the matrix $\mathbf{R}$ has been directly constructed by the definitions of the hydrodynamic modes, it is not a good choice as basis for defining the moment representation because

it is not orthogonal.

The matrix $\mathbf{R}$ can be orthogonalized by the usual Gram-Schmidt procedure. By means of this technique, the row vectors of the resulting matrix will be mutually orthogonal, but we will not require that they are normalized too because it is better to choose their norms in order to simplify algebraic manipulations. The Gram-Schmidt procedure yields:

$$\mathbf{M} = \begin{bmatrix} \langle \varrho_M^0 | \\ \langle \varrho_M^1 | \\ \langle \varrho_M^2 | \\ \langle \varrho_M^3 | \\ \langle \varrho_M^4 | \\ \langle \varrho_M^5 | \\ \langle \varrho_M^6 | \\ \langle \varrho_M^7 | \\ \langle \varrho_M^8 | \end{bmatrix} = \begin{bmatrix} 1 & 1 & 1 & 1 & 1 & 1 & 1 & 1 & 1 \\ 0 & 1 & 0 & -1 & 0 & 1 & -1 & -1 & 1 \\ 0 & 0 & 1 & 0 & -1 & 1 & 1 & -1 & -1 \\ -4 & -1 & -1 & -1 & -1 & 2 & 2 & 2 & 2 \\ 0 & 1 & -1 & 1 & -1 & 0 & 0 & 0 & 0 \\ 0 & 0 & 0 & 0 & 0 & 1 & -1 & 1 & -1 \\ 0 & -2 & 0 & 2 & 0 & 1 & -1 & -1 & 1 \\ 0 & 0 & -2 & 0 & 2 & 1 & 1 & -1 & -1 \\ 4 & -2 & -2 & -2 & -2 & 1 & 1 & 1 & 1 \end{bmatrix}. \tag{5.90}$$

It is worth to point out that the first three rows do not change, i.e. $\langle \varrho_M^0 | = \langle \varrho_R^0 |$, $\langle \varrho_M^1 | = \langle \varrho_R^1 |$ and $\langle \varrho_M^2 | = \langle \varrho_R^2 |$, because they were already orthogonal. The rows $\left\langle \varrho_M^\lambda \right|$ of the matrix $\mathbf{M}$ allow us to rigorously define the concept of hydrodynamic mode, namely $\eta^\lambda = \left\langle \varrho_M^\lambda | \varphi \right\rangle$ and consequently $\langle \eta | = [\eta^0, \eta^1, ... \eta^8]$. If the matrix $\mathbf{C}$ is chosen such that the generic vector $\left\langle \varrho_M^\lambda \right|$ is its generic eigenvector, the linear relaxation of the kinetic modes in the moment space naturally accomplishes the collision process. Then the collisional operator given by Eq. (5.83) of the MRT lattice Boltzmann model can be reformulated in the momentum space [134, 136]:

$$\left| \varphi^\dagger \right\rangle - |\varphi\rangle = -\mathbf{M}^{-1} \hat{\mathbf{C}} \left(|\eta\rangle - |\eta^e\rangle \right), \tag{5.91}$$

where the collision matrix $\hat{\mathbf{C}} = \mathbf{M}\,\mathbf{C}\,\mathbf{M}^{-1}$ is diagonal: $\hat{\mathbf{C}} = \mathrm{diag}\,(0, 0, 0, 0, \omega^4, ... \omega^8)$. The moments can be separated into two groups: the "hydrodynamic" (conserved) moments and the "kinetic" (non-conserved) moments. The first group consists of the moments locally conserved during the collision process, so that in general $\eta^\lambda = \eta^{e\,\lambda}$.

The second group consists of the moments not conserved during the collision process, so that $\eta^\lambda \neq \eta^{e\,\lambda}$. The equilibrium functions for the non-conserved moments can be easily calculated by means of the equilibrium distribution functions. Recalling that $|\eta^e\rangle = \mathbf{M}\,|\varphi^e\rangle$, the following expressions can be obtained $\eta^{e\,4} = \rho\,[(u_x/c)^2 - (u_y/c)^2]$, $\eta^{e\,5} = \rho\,u_x\,u_y/c^2$, $\eta^{e\,6} = -\rho\,u_x/c$, $\eta^{e\,7} = -\rho\,u_y/c$ and $\eta^{e\,8} = \rho\,[1-3\,(u_x/c)^2-3\,(u_y/c)^2]$. For conserved and non-conserved moments, equation (5.91) can be rewritten as

$$\left|\varphi^\dagger\right\rangle - |\varphi\rangle = -\sum_{\lambda=0}^{8} \frac{\omega^\lambda}{\left\langle \varrho_M^\lambda | \varrho_M^\lambda \right\rangle} \left(\eta^\lambda - \eta^{e\,\lambda}\right) \left|\varrho_M^\lambda\right\rangle, \tag{5.92}$$

where we have used the fact that $\mathbf{M}\,\mathbf{M}^T$ is a diagonal matrix with diagonal elements $\left\langle \varrho_M^\lambda | \varrho_M^\lambda \right\rangle$. The values of dimensionless relaxation frequencies for the conserved moments are set to zero, i.e. $\omega^\lambda = 0$ for $\lambda \leq 3$. In order to ensure a proper degree of symmetry for the stress tensor and the heat flux, then it must be that $\omega^5 = \omega^4$ and $\omega^7 = \omega^6$. The external force field, which has been previously dropped out, can be easily considered here by modifying the macroscopic velocity at each time step in order to ensure the desired acceleration. Obviously, in this case, the macroscopic velocity will not be a conserved invariant.

Finally the MRT model has three tunable dimensionless frequencies (ω^4, ω^6 and ω^8) instead of the usual single relaxation frequency for the BGK model (ω). This allows us to independently tune the kinematic viscosity ν by means of the parameter ω^4 and the thermal diffusivity ι by means of the parameter ω^6. The last frequency does not appreciably affect the hydrodynamics. This discussion proves that the MRT model can overcome the limit of the usual BGK model, i.e. the fixed Prandtl number.

5.4.4 Multi-Lattice models

In this section, an alternative strategy aimed at increasing the number of tunable parameters, known as multi-lattice approach, will be discussed. Essentially, this uses

different lattices for solving different macroscopic equations without neglecting the physical coupling among them.

In other words, the basic idea is to use a large set of discrete velocities with a distribution function for particle density and another for particle internal energy density [141]. This scheme effectively doubles the number of discrete velocities and the numerical accuracy of these schemes remains largely unknown [135]. Even though nowadays these schemes still present some drawbacks for the thermo-hydrodynamic simulations, they are characterized by an interesting feature: a more complicate set of macroscopic equations, including the energy equation, is solved by means of a *virtual* mixture of elementary particles. Obviously this way of describing the phenomena seems far from an actual kinetic description but it allows us to increase the number of equations meaningfully solved and to purposedly design a lattice in order to produce the desired effect. The idea that virtual particles can carry a specific quantum of information has been largely applied. For example, the concept of *field mediators* for simulating multi-phase mixtures in the LBM framework belongs to this approach [142].

Here a very simple example is reported, in order to understand to concept of virtual mixture [143]. Let us consider again the BGK model given by Eqs. (5.1) and (5.31):

$$\frac{D\,f}{Dt} = -\frac{1}{\tau}\,(f - f^e) - \mathbf{g}\cdot\nabla_{\mathbf{v}} f = -\frac{1}{\tau}\,(f - f^e) + \frac{f^e}{e}\,\mathbf{g}\cdot(\mathbf{v}-\mathbf{u}), \tag{5.93}$$

where the usual simplifying approximation for the external force field has been applied. Now let us introduce a new variable, the internal energy density distribution function:

$$f_\varepsilon = \frac{(\mathbf{v}-\mathbf{u})^2}{2}\,f. \tag{5.94}$$

The internal energy can be redefined according to the previous quantity:

$$\rho(\mathbf{x},t)\,e(\mathbf{x},t) = \int m\,(\mathbf{v}-\mathbf{u})^2/2\,f(\mathbf{x},\mathbf{v},t)\,d\mathbf{v} = \int m\,f_\varepsilon(\mathbf{x},\mathbf{v},t)\,d\mathbf{v}. \tag{5.95}$$

Instead of deriving the internal energy from the second moment of the density distribution function f, the previous definition is used and a specific evolution equation is derived, which involves a second relaxation time constant τ_ε, called *thermal relaxation time constant*. The substantial rate of change of the internal energy density distribution function is:

$$\begin{aligned}\frac{D\,f_\varepsilon}{Dt} &= \frac{(\mathbf{v}-\mathbf{u})^2}{2}\,\frac{D\,f}{Dt} - f\,(\mathbf{v}-\mathbf{u})\cdot\frac{D\,\mathbf{u}}{D\,t} = \\ &= \frac{(\mathbf{v}-\mathbf{u})^2}{2}\,\left[J(f) + \frac{f^e}{e}\,\mathbf{g}\cdot(\mathbf{v}-\mathbf{u})\right] - f\,(\mathbf{v}-\mathbf{u})\cdot\frac{D\,\mathbf{u}}{D\,t},\end{aligned} \tag{5.96}$$

where the BGK model has been applied. Hence a new collisional model is introduced:

$$\frac{(\mathbf{v}-\mathbf{u})^2}{2}\,J(f) = -\frac{1}{\tau_\varepsilon}\,(f_\varepsilon - f^e_\varepsilon), \tag{5.97}$$

where

$$f^e_\varepsilon = \frac{(\mathbf{v}-\mathbf{u})^2}{2}\,f^e. \tag{5.98}$$

Introducing the previous assumptions in Eq. (5.96) yields

$$\frac{D\,f_\varepsilon}{D\,t} = -\frac{1}{\tau_\varepsilon}\,(f_\varepsilon - f^e_\varepsilon) + \frac{f^e_\varepsilon}{e}\,\mathbf{g}\cdot(\mathbf{v}-\mathbf{u}) - f\,(\mathbf{v}-\mathbf{u})\cdot\frac{D\,\mathbf{u}}{D\,t}, \tag{5.99}$$

where the last term in the previous equation is the *heat dissipation term*. The heat dissipation term essentially takes into account the viscous heat dissipation and the compression work done by the pressure which are involved in the macroscopic internal energy equation [143].

For understanding the evolution equation for the internal energy density distribution function, the Chapman-Enskog analyis can be applied. Substituting the usual

expansions in Eq. (5.99), a coupled hierarchy system of equations in the powers of K is obtained. Its first elements are:

$$f_\varepsilon^{(0)} = f_\varepsilon^e, \tag{5.100}$$

$$\frac{D^{(1)} f_\varepsilon^{(0)}}{D\, t^{(1)}} = -\frac{1}{\tau_\varepsilon}\, f_\varepsilon^{(1)} + \frac{f^e}{e}\,(\mathbf{v}-\mathbf{u})\cdot\left[\frac{(\mathbf{v}-\mathbf{u})^2}{2}\,\mathbf{g} - e\,\frac{D^{(1)}\mathbf{u}}{D\, t^{(1)}}\right], \tag{5.101}$$

$$\frac{\partial f_\varepsilon^{(0)}}{\partial\, t^{(2)}} + \frac{D^{(1)} f_\varepsilon^{(1)}}{D\, t^{(1)}} = -\frac{1}{\tau_\varepsilon}\, f_\varepsilon^{(2)} - (\mathbf{v}-\mathbf{u})\cdot\left[f^e\,\frac{\partial\,\mathbf{u}}{\partial t^{(2)}} + f^{(1)}\,\frac{D^{(1)}\mathbf{u}}{D\, t^{(1)}}\right]. \tag{5.102}$$

The integral of the previous equation over the velocity space leads to the correct expression for the internal energy equation (5.12), but the heat flux $\mathbf{q}_\lambda$ involves the thermal relaxation time constant, i.e. $\mathbf{q}_\lambda = -2\,\rho\, e\,\tau_\varepsilon\,\nabla e$, instead of the usual relaxation constant as previously discussed. Among other things, this allows us to properly tune the desired Prandtl number $Pr = \tau/(2\,\tau_\varepsilon)$.

The distribution function f and the energy distribution function f_ε mime the behavior of real particles with regard to fluid flow and transferred kinetic energy, respectively. The pseudo-kinetic description splits the information transferred by real particles in two different mesoscopic species interacting with each other, which define a virtual mixture. The coupling term among the species of the virtual mixture is the heat dissipation term. This example allows us to understand that the development of reliable mesoscopic tools for gaseous mixtures could be relevant for thermal models too. For this reason, even though in the present work we are mainly interested in the fluid flow of carbon dioxide within microscopic structures, some work has been carried out for improving present models for gaseous mixtures.

5.4.5 Boundary conditions

The coding of boundary conditions is an essential part of any numerical method, but it becomes quite critical for the LBM. In this case, some boundary conditions are

needed for the discrete distribution functions in order to recover the desired boundary conditions for the macroscopic moments. Essentially, it is not possible to directly include the desired values for the macroscopic moments in the code but they must be converted in terms of constraints for the discrete distribution functions first.

There are at least five different types of boundary conditions (BCs) in the LBM [102, 144].

1. *Periodic* BCs are often used, even though they are sometimes not realistic, because of easiness of coding: they are usually applied to all the lattice components of the distribution functions.

2. *Inflow* BCs which essentially set the inlet distribution function equal to the equilibrium distribution function with both desired velocity and density in order to reproduce a given mass flow rate or with the desired velocity and density extrapolated from the computed flow [145].

3. *Outflow* BCs can be very difficult to deal with and they usually involve the equilibrium distribution function together with a proper combination of desired and extrapolated macroscopic quantities [145].

4. *Wall* BCs which can include both *no-slip* and *slip* conditions according to the local Knudsen number, i.e. the actual dynamics of interaction between fluid and solid obstructions.

The last condition is particularly relevant for numerical simulations of fluid flow in porous media [152], because in this case the fluid flow regime can continuously change according to the local characteristic of the pore size.

In order to briefly explain the different fluid flow regimes and how they can be described by the LBM, let us consider an infinitely deep channel stretching in the

Table 5.2: Flow regimes for different Mach number (Ma) and Reynolds number (Re) combinations [146]. The Knudsen number (Kn) is reported too. Channel height to its length, i.e H/L, is considered to be small.

		Re	
Ma	$O(H/L)$	$O(1)$	$O(L/H)$
$O(H/L)$	$Kn = O(1)$ Creeping micro-flow	$Kn = O(H/L)$ Moderate micro-flow	$Kn = O(H^2/L^2)$ Low Mach Fanno Flow
$O(1)$	$Kn = O(L/H)$ Transonic free-molecular flow	$Kn = O(1)$ Transonic micro-flow	$Kn = O(H/L)$ Transonic Fanno Flow
$O(L/H)$	$Kn = O(L^2/H^2)$ Hypersonic free-molecular flow	$Kn = O(L/H)$ Hypersonic free-molecular flow	$Kn = O(1)$ Hypersonic Fanno Flow

x direction (y identifies the transverse direction). Let us suppose that the distance D separates two slabs along the transverse direction y and that the length L can be considered a good characteristic dimension of the fluid flow along the axial direction x. Many different fluid flow regimes can exist according to the actual values of three dimensionless parameters, i.e the Mach number (Ma), the Reynolds number (Re) and the Knudsen number which is proportional to the ratio of the previous ones ($Kn \propto Ma/Re$) [146]. The dimensionless parameters appear in the dimensionless fluid equations and control the flow regime. Within the context of the Chapman-Enskog perturbation expansion, they can independently have three values, i.e. small $O(H/L)$, moderate $O(1)$ and large $O(L/H)$, leading to nine independent flow regimes. Tab. 5.2 shows these combinations together with their corresponding Knudsen number regimes [146]. Note that the lower diagonal of this matrix is characterized by Knudsen numbers indicating that a continuum-flow theory using the Navier-Stokes equations

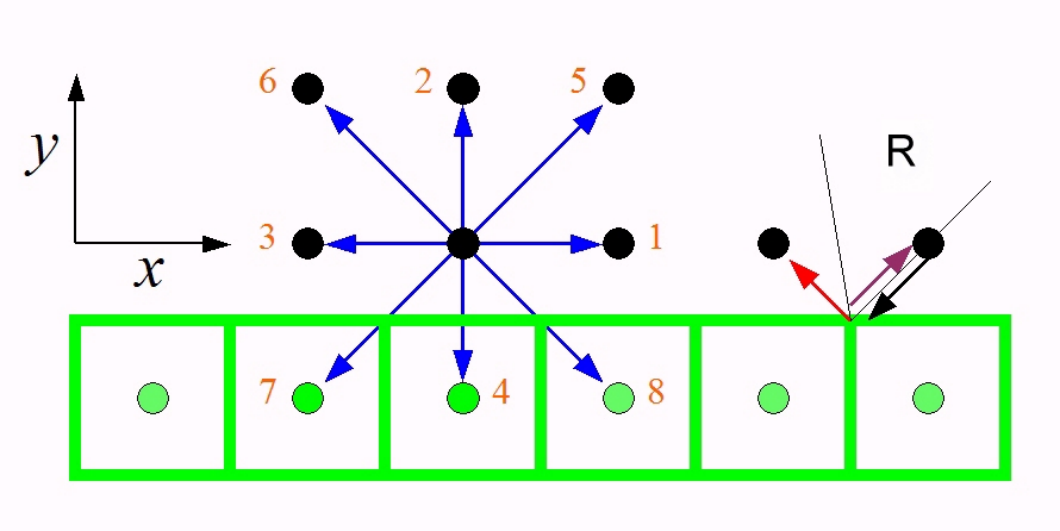

Figure 5.1: Integration between the D2Q9 lattice and the bottom solid wall of the infinitely deep channel. In the right side, an allowed microscopic velocity pointing at the wall and the possible paths due to wall interaction, i.e. complete reflection or complete flipping along former incoming direction, are reported too.

is not appropriate.

It is worth to point out that when the fluid flow regime does not satisfy the underlying hypothesis of the continuum-flow theory, the Navier-Stokes equations should not be used any more [147]. However for moderate rarefied regimes, it is possible to introduce a boundary condition, called *slip-flow* boundary condition, which represents the first-order correction to the NavierStokes equations to account for non-equilibrium effects [148]. The slip-flow condition essentially prescribes a velocity discontinuity at the wall, proportional to the local Knudsen number. This velocity jump is completely unphysical and it must be considered a numerical trick in order to avoid the resolution of the Knudsen layer by means of the Boltzmann equation [147].

In the LBM framework, the fluid flow velocity at the wall can be freely tuned and some works exist which simulate moderate rarefied fluid flows by means of slip-flow condition [149,150]. Unfortunately, sometimes it is not so easy to distinguish between

the numerical inaccuracies due to the implemented algorithm for treatment of the fluid-wall interaction and the desired correction to the usual macroscopic equations in the continuum limit. For this reason, the wall treatment will be discussed.

Let us consider again the infinitely deep channel introduced previously. In this two-dimensional domain, the fluid flow due to a fixed external force field along the axial direction x is characterized, in the low Reynolds number limit, by a parabolic velocity profile for steady state conditions. This test reference case is usually referred to as Poiseuille flow. The integration between the mesoscopic lattice and the bottom solid wall is reported in Fig. 5.1. The generic component of the allowed microscopic velocity pointing at the wall (right side of the previous figure) can be completely reflected or completely flipped along its former incoming direction. No other possibilities are allowed because of the regularity of the lattice. The flipping of the incoming particles is also called *bounce-back rule*. In the following, the linear combination of the previous alternatives is investigated. The analysis reported in the paper of He et al. [151] has been generalized in order to appreciate the effects of possible reflections too.

First of all, let us consider the term which takes into account the effects due to the external force field in Eq. (5.77). Its treatment can be simplified because here we are mainly interested in the first order moments, involved in the definition of the macroscopic velocity. The first order moment of the external force term reads

$$\begin{aligned} \rho\,\mathbf{g} &= \sum_{\lambda=0}^{8} \varsigma^{\lambda}\mathbf{v}^{\lambda}\left(\frac{d}{\sqrt{e}}\,\mathbf{k}^{\lambda\star}\cdot\mathbf{g}\right) \approx \sum_{\lambda=0}^{8} \varsigma^{\lambda}\mathbf{v}^{\lambda}\left(\frac{3\,\rho}{c^2}\,\mathbf{v}^{\lambda}\cdot\mathbf{g}\right) \\ &= \sum_{\lambda=0}^{8} \varsigma^{\lambda}\mathbf{v}^{\lambda}\left(\frac{\rho}{6\,c^2\,\varsigma^{\lambda}}\,\mathbf{v}^{\lambda}\cdot\mathbf{g}\right) = \sum_{\lambda=0}^{8} \varsigma^{\lambda}\mathbf{v}^{\lambda}\,\mu^{\lambda}/\delta t. \end{aligned} \tag{5.103}$$

where

$$\mu^{\lambda} = \frac{\rho\,\delta t}{6\,c^2\,\varsigma^{\lambda}}\,\mathbf{v}^{\lambda}\cdot\mathbf{g}. \tag{5.104}$$

This means that the simplified term μ^λ can be substituted to the original term with regard to the first order moments only. Introducing the simplified term in the discrete equation (5.77), leads to

$$\varphi^{\dagger\,\lambda} - \varphi^\lambda = -\omega\,\left(\varphi^\lambda - \varphi^{e\,\lambda}\right) + \mu^\lambda, \tag{5.105}$$

where $\varphi^{\dagger\,\lambda} = \varphi^\lambda(\mathbf{x} + \mathbf{v}\,\delta t, \mathbf{v}, t + \delta t)$, $\varphi^\lambda = \varphi^\lambda(\mathbf{x}, \mathbf{v}, t)$ and $\varphi^{e\,\lambda} = \varphi^{e\,\lambda\star}(\mathbf{x}, \mathbf{v}, t)$. Let us consider the steady state conditions only. In this case, the discrete lattice viscosities along the axial direction do not change during the streaming step because the velocity profile is independent of x coordinate in the Poiseuille flow. This means that:

$$\varphi^\lambda = \varphi^{e\,\lambda} + \mu^\lambda/\omega, \tag{5.106}$$

for $\lambda = 1, 3$ (see labeling in Fig. 5.1). For all the other cases, it is possible to express the generic discrete distribution function by means of the value at the previous time step, i.e. the value of the distribution function at the previous grid node along the incoming direction. This yields

$$\varphi^\lambda = (1-\omega)\,\varphi^{\ddagger\,\lambda} + \omega\,\varphi^{\ddagger\,e\,\lambda} + \mu^\lambda, \tag{5.107}$$

for all $\lambda \neq 1, 3$ (see labeling in Fig. 5.1), where $\varphi^{\ddagger\,\lambda} = \varphi^\lambda(\mathbf{x} - \mathbf{v}\,\delta t, \mathbf{v}, t - \delta t)$. Applying Eqs. (5.106) and (5.107) to all the discrete lattice velocities the following results are recovered:

$$\varphi_1^1 = \rho\,\left[1 + 3\,\frac{u_{x,1}}{c} + 3\left(\frac{u_{x,1}}{c}\right)^2\right] + \mu_1^1/\omega, \tag{5.108}$$

$$\varphi_1^2 = \varphi_0^4 = (1-\omega)\,\varphi_1^4 + \omega\,\rho\,\left[1 - \frac{3}{2}\,\left(\frac{u_{x,1}}{c}\right)^2\right] + \mu_1^2, \tag{5.109}$$

$$\varphi_1^3 = \rho\,\left[1 - 3\,\frac{u_{x,1}}{c} + 3\left(\frac{u_{x,1}}{c}\right)^2\right] + \mu_1^3/\omega, \tag{5.110}$$

$$\varphi_1^4 = (1-\omega)\,\varphi_2^4 + \omega\,\rho\,\left[1 - \frac{3}{2}\,\left(\frac{u_{x,2}}{c}\right)^2\right] + \mu_1^4, \tag{5.111}$$

$$\begin{aligned}\varphi_1^5 &= (1-R)\,\varphi_0^7 + R\,\varphi_0^8 = \\ &+(1-R)\left\{(1-\omega)\,\varphi_1^7 + \omega\,\rho\,\left[1 - 3\,\frac{u_{x,1}}{c} + 3\left(\frac{u_{x,1}}{c}\right)^2\right] + \mu_1^7\right\} \\ &+R\left\{(1-\omega)\,\varphi_1^8 + \omega\,\rho\,\left[1 + 3\,\frac{u_{x,1}}{c} + 3\left(\frac{u_{x,1}}{c}\right)^2\right] + \mu_1^8\right\},\end{aligned} \tag{5.112}$$

$$\begin{aligned}\varphi_1^6 &= (1-R)\,\varphi_0^8 + R\,\varphi_0^7 = \\ &+(1-R)\left\{(1-\omega)\,\varphi_1^8 + \omega\,\rho\,\left[1 + 3\,\frac{u_{x,1}}{c} + 3\left(\frac{u_{x,1}}{c}\right)^2\right] + \mu_1^8\right\} \\ &+R\left\{(1-\omega)\,\varphi_1^7 + \omega\,\rho\,\left[1 - 3\,\frac{u_{x,1}}{c} + 3\left(\frac{u_{x,1}}{c}\right)^2\right] + \mu_1^7\right\},\end{aligned} \tag{5.113}$$

$$\varphi_1^7 = (1-\omega)\,\varphi_2^7 + \omega\,\rho\,\left[1 - 3\,\frac{u_{x,2}}{c} + 3\left(\frac{u_{x,2}}{c}\right)^2\right] + \mu_1^7, \tag{5.114}$$

$$\varphi_1^8 = (1-\omega)\,\varphi_2^8 + \omega\,\rho\,\left[1 + 3\,\frac{u_{x,2}}{c} + 3\left(\frac{u_{x,2}}{c}\right)^2\right] + \mu_1^8, \tag{5.115}$$

where $u_{x,1}$ and $u_{x,2}$ are the values of the macroscopic velocity at the grid node closer to the bottom wall and at the next grid node along the traverse direction, respectively. The tunable parameter R has been introduced in order to include in the wall interaction rule both the ideal reflection case $R = 1$ and the ideal slip back along the incoming direction $R = 0$. The macroscopic velocity at the grid node closer to the bottom wall can be expressed by definition as

$$\rho\,u_{x,1} = c\sum_{\lambda=0}^{8}\varsigma^\lambda\,v_x^\lambda\,\varphi_1^\lambda = \rho\,u_{x,1}\,\Lambda_1 + \rho\,u_{x,2}\,\Lambda_2 + \rho\,g_x\,\delta t\,\Lambda_g, \tag{5.116}$$

where Λ_1, Λ_2 and Λ_g are proper functions of ω. The Poiseuille flow has been assumed because an analytical solution exists for the low Reynolds number limit, namely

$$u_x(y) = \frac{H^2\,g_x}{2\,\nu}\,\frac{y}{H}\,\left(1 - \frac{y}{H}\right) + u_w, \tag{5.117}$$

where u_w is the velocity at the wall eventually caused by the slip-flow condition. The previous analytical solution allows us to express both $u_{x,1}$ and $u_{x,2}$ as functions of the velocity at the wall. The final purpose of this calculation is to show what velocity

at the wall comes from a given wall interaction rule identified by the parameter R. If δy is the distance of the first centroid from the bottom wall, which is equal to half the discretization step ($\delta y = \delta x/2$), let us suppose that $\delta y \ll H$, i.e. that the discretization is fine enough. Hence the velocity at the wall can be expressed as

$$\frac{u_w}{c} = \left[\frac{(\Lambda_1/4 + 3\,\Lambda_2/4 - 1/4)\ Re_L + \Lambda_g}{1 - \Lambda_1 - \Lambda_2}\right] \frac{g_x\,\delta t}{c}, \tag{5.118}$$

where $Re_L = c\,H/\nu$ is the lattice Reynolds number. Introducing the definitions of Λ_1, Λ_2 and Λ_g in the previous equation, the final expression is recovered

$$\frac{u_w}{c} = \left\{\frac{R}{1-R}\left[\frac{Re_L}{4}\,\frac{2-\omega}{\omega} - 2\,\frac{1 - 5\,\omega + 3\,\omega^2}{\omega\,(2-\omega)}\right] + \frac{1}{1-R}\,\frac{2 - 4\,\omega + 3\,\omega^2}{\omega\,(2-\omega)}\right\}\,\frac{g_x\,\delta t}{c}. \tag{5.119}$$

The velocity at the wall is made of two parts: the first, leading, part is proportional to the lattice Reynolds number while the second term does not depend on it. The popular bounce-back rule ($R = 0$) allows us to recover the no-slip boundary condition, i.e. $u_w = 0$, with first order accuracy in time. In particular, the bounce-back rule always induces a positive error which increases for values of the dimensionless frequency close to the limits of the allowed range ($0 \leq \omega \leq 2$). On the other hand, when ideal reflection is also allowed ($R \neq 0$), the previous formula can be simplified as

$$\frac{u_w}{c} \approx \frac{R}{1-R}\left(\frac{Re_L}{4}\right)\left(\frac{2-\omega}{\omega}\right)\,\frac{g_x\,\delta t}{c}. \tag{5.120}$$

The previous relation expresses that the velocity at the wall is a monotonic increasing function of the parameter R used to mix together the bounce-back rule and the ideal reflection rule. In particular if the ideal reflection rule is considered ($R \to 1$), then the velocity at the wall tends to infinity because the wall does not apply a viscous stress for compensating the external force field and the fluid tends to accelerate indefinitely. The previous relation can be used to implement the slip-flow condition for moderately rarefied gases by tuning the parameter R.

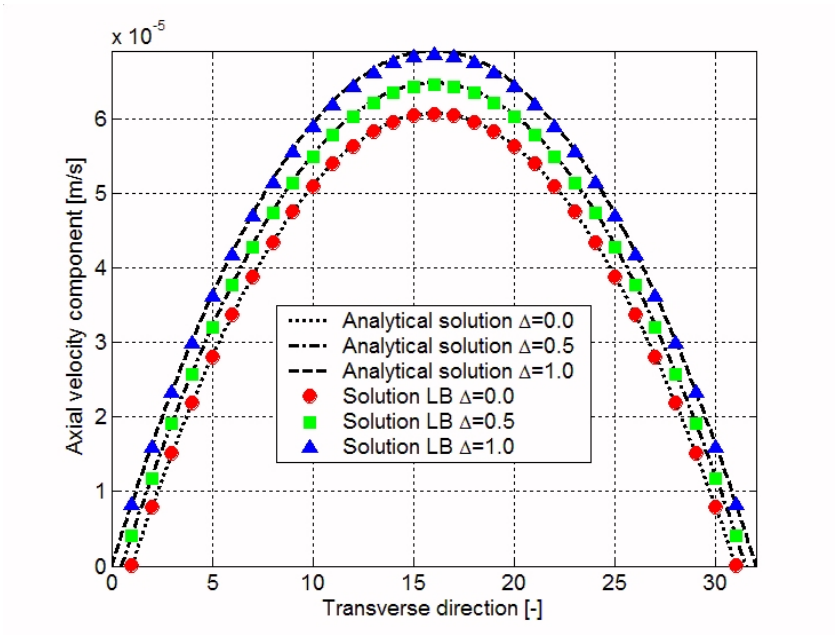

Figure 5.2: Numerical results for the Poiseuille flow obtained by means of the improved bounce-back rule [152], which allows us to freely locate the wall with respect to the spatial discretization nodes.

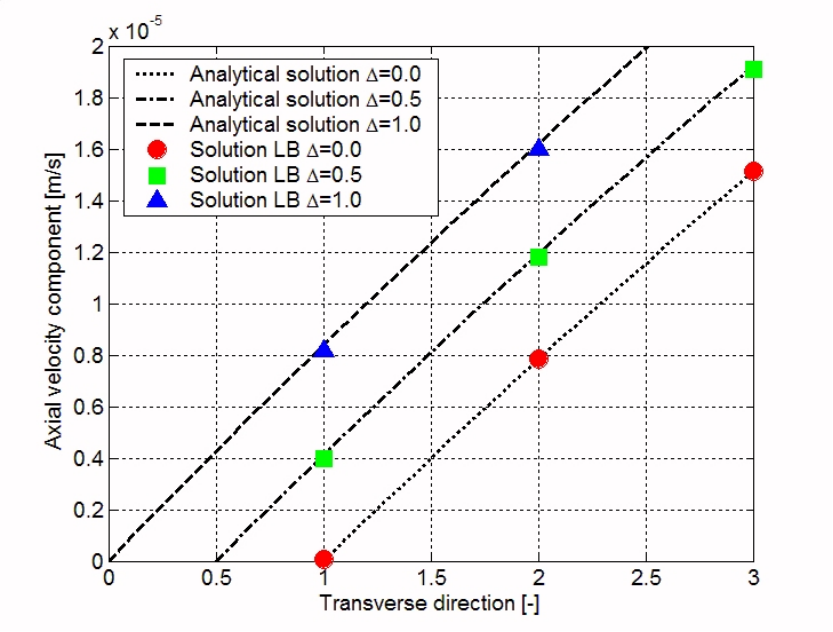

Figure 5.3: Numerical results for the Poiseuille flow obtained by means of the improved bounce-back rule [152], which allows us to freely locate the wall with respect to the spatial discretization nodes. The portion of the computational domain closer to the wall is reported.

Some more accurate boundary conditions for the LBM exist, which fit the second order accuracy no-slip boundary conditions on a surface of arbitrary form lying between the nodes of a regular lattice [152–154]. The possibility to freely locate the solid wall between two consecutive grid nodes widens the application field of LBM. In Fig. 5.2, and, more clearly, in Fig. 5.3 some results obtained by applying the improved bounce-back rule, proposed by Filippova and Hänel [152], are reported for the Poiseuille flow. Even though the grid nodes where the calculation is performed are always the same, the numerical results show a good agreement with the analytical solutions obtained by considering different locations for both walls. In particular, Δ is the ratio of the distance between the wall and the closer grid node with regard to the discretization step. The usual bounce-back rule is recovered for $\Delta = 1/2$.

The challenges of the new boundary conditions are strictly tied to the current trend of including features coming originally from other numerical techniques in LBM. While the original LBM was severely grid-bound and awkward in front of realistically complex geometries, many variants have been developed today that cure the initial flaw. The success of these improvements for the future will critically depend on which extent they will be able to handle complex geometries without compromising the original LBM assets of simplicity for parallel computing [104].

5.5 Lattice Boltzmann models for gaseous mixtures

Even though in the present work we are mainly interested in the fluid flow of carbon dioxide within microscopic structures, in this section present models based on LBM for gaseous mixtures are analyzed. As previously outlined, a relevant interest about gaseous mixtures exists and this includes virtual mixtures too, i.e. mixtures

made by virtual species which carry some fractions of information in order to realize a pseudo-kinetic description of the phenomenon.

For this reason, a lot of work has been performed in recent years in order to produce reliable lattice Boltzmann models for multi-component fluids and, in particular, for mixtures composed by miscible species [155–161]. The problem is to find a proper way, within the framework of a simplified kinetic model, for describing the interactions among different particles. Once this milestone is defined, the extension of the model to reactive flows is straightforward [162, 163] and it will essentially involve additional source terms in the species equations according to the reaction rate. Unfortunately, most existing lattice Boltzmann models for mixtures [155–163] are based on heuristic assumptions or prescribe too much constraints for setting the microscopic parameters, which finally imply an idealized macroscopic description. The older models [155–158, 162, 163] were based on the single-fluid approach, which allows us to produce a set of hydrodynamic equations for the whole mixture. Essentially, considering the mixture properties in the Maxwellian distribution functions that are involved in the simplified collisional operators, each species will be forced to evolve towards the mixture equilibrium conditions. This approach is acceptable when the species share similar characteristics, but it cannot be defined a truly multi-component description. On the other hand, some models [159–161] based on the two-fluid approach have been proposed. In this approach, each species relaxes towards its equilibrium configuration according to its specific relaxation time and some coupling must be considered in order to describe the collisions among different species. Some models [159, 160] adopt a *force coupling* in the momentum equations, which derives from a linearized kinetic term. This technique allows us to describe the effects of collisions among particles of different species by means of an approximated forcing term. Recently, another model

has been proposed, which tries to overcome this approximation [161]. In this case any approximation is avoided in the formal formulation of the model, but there is no discussion about the effects of this improvement in the hydrodynamic equations. The original paper [161] reports a Chapman-Enskog asymptotic analysis of a linearized version of the proposed model based on a simple *force coupling* in the momentum equations, which produces results similar to those of previous models.

The best way to understand the limits of *force coupling* and the possible ways to overcome them is to consider, once again the kinetic theory. It is well known that the lattice Boltzmann models can be directly derived from the kinetic models using some standard discretization procedures and proper approximations [164]. There is a significant amount of literature on gas mixtures within the kinetic theory framework [147,165]. In his doctoral thesis, Kolodner [166], following Grad's moment method, investigated what variables, in addition to the classical fundamental variables, must be considered in order to properly describe the phenomena occurring in binary mixtures. The classical work of Chapman and Cowling [165] was concerned with the determination of the transport coefficients for binary mixtures by means of the full Boltzmann equations. Among the simplified kinetic models, the first single-fluid model for binary mixtures is that due to Gross and Krook [167, 168], which is based on a BGK-like collisional operator. Sirovich [169] proposed to linearize the equations of the previous model and proposed his very popular model, although it should be noted that the equations obtained by Sirovich are non linear, since the linearization was done around a local Maxwellian [170]. This model historically started the two-fluid approach. Trying to generalize Sirovich's results, Hamel [171, 172] proposed a simplified kinetic model which was able to include both single-fluid and two-fluid approaches, by considering multiple equilibrium distribution functions in-

volving the respective species velocities and the mixture velocity. Unfortunately, in the original paper [172], no Chapman-Enskog asymptotic analysis of the model was reported and the transport properties were discussed by using the coefficients appearing in Sirovich's equation. In order to reduce the computational efforts, the linearized kinetic models became very popular and they were mathematically formalized [173]. More recently it has been pointed out that none of the previous models reduce to a BGK-like equation when mechanical identical components are considered, despite the fact that all of them are based on a BGK-like equation for each species [174]. This means that none of the previous models satisfies the indifferentiability principle, i.e. the fact that when all the species are identical one recovers the equation for a single component gas, which is correctly satisfied by a single-fluid model, recently proposed [175].

On the track of Hamel's work, a two-fluid simplified kinetic model is proposed here[1] and only small changes are introduced in order to satisfy the indifferentiability principle when cross collisions prevail. The model is formulated in such a way as to recover the conventional BGK equations for the limiting case of non-interacting particles and the consistent single-fluid approach for ideally coupled particles. The hydrodynamic equations are fully derived by means of the Chapman-Enskog asymptotic analysis, which allows us to point out that the model is characterized by an additional coupling among the species, called *viscous coupling* to distinguish it from the *force coupling* previously considered. A strategy for setting the mesoscopic parameters of the model in order to recover the desired transport coefficients is proposed. Finally, a Lattice Boltzmann (discretized) version of the previous model and a strategy for

[1]Part of the contents discussed in this chapter was submitted for publication:

- P. Asinari, "Viscous coupling based lattice Boltzmann model for binary mixtures", submitted to *Physics of Fluids* (2004).

setting the lattice mesoscopic parameters are discussed too. In the present work, only isothermal conditions and nearly incompressible flows are considered, because they are enough to analyze the effects of *viscous coupling*. In the model derivation, the properties of the Maxwell molecule are assumed. Only the problem of binary gas mixtures is considered. The full generalization of the method to gas mixtures is quite straightforward, as only few changes are required.

5.5.1 Kinetic theory of binary mixtures

Let us consider a mixture simply composed of two types of particles, labeled a and b. The simultaneous Boltzmann equations for the binary system are [147, 165]:

$$\frac{\partial f_a}{\partial t} + \mathbf{v} \cdot \nabla f_a + \mathbf{g}_a \cdot \nabla_{\mathbf{v}} f_a = Q_{a\,a} + Q_{a\,b}, \tag{5.121}$$

$$\frac{\partial f_b}{\partial t} + \mathbf{v} \cdot \nabla f_b + \mathbf{g}_b \cdot \nabla_{\mathbf{v}} f_b = Q_{b\,b} + Q_{b\,a}, \tag{5.122}$$

where $Q_{a\,a}$ and $Q_{b\,b}$ are the collisional terms which describe the collisions among particles of the same type (self collisions), while $Q_{a\,b}$ and $Q_{b\,a}$ are the collisional terms due to the interactions among different species (cross collisions). Each collisional term has a well-known structure similar to the collisional operator involved in the Boltzmann equation for the single fluid. The time evolution of the distribution function for each species is affected both by collisions with particles of the same type and with particles of different type. These two phenomena are the kinetic driving forces of the equilibration process for the whole mixture. A simplified kinetic model which allows us to separately describe both driving forces, as it happens for the original Boltzmann equations, would be desirable. Essentially, the key idea is to substitute the previous collisional terms with simplified ones $Q(f, f) \rightarrow J(f)$, which are selected with a BGK-like structure. In the following only the equation for a generic species

$\sigma = a, b$ will be considered. The simplified kinetic equation has the general form:

$$\frac{\partial f_\sigma}{\partial t} + \mathbf{v} \cdot \nabla f_\sigma + \mathbf{g}_\sigma \cdot \nabla_{\mathbf{v}} f_\sigma = -\frac{1}{\tau_\sigma} \left[f_\sigma - f_\sigma^e \right] - \frac{1}{\tau_{m\,\sigma}} \left[f_\sigma - f_{\sigma(m)}^e \right], \tag{5.123}$$

where τ_σ is the relaxation time constant for self collisions, $\tau_{m\,\sigma}$ is the relaxation time constant for the cross collisions, f_σ^e is a Maxwellian distribution function of the specific velocity, while $f_{\sigma(m)}^e$ is a Maxwellian distribution function of a characteristic mixture velocity. The explicit expressions of the previous Maxwellians are:

$$f_\sigma^e = \frac{\rho_\sigma}{m_\sigma \left(2\pi e_\sigma\right)^{D/2}} \exp\left[-\frac{\left(\mathbf{v} - \mathbf{u}_\sigma\right)^2}{2\, e_\sigma} \right], \tag{5.124}$$

$$f_{\sigma(m)}^e = \frac{\rho_\sigma}{m_\sigma \left(2\pi e_\sigma\right)^{D/2}} \exp\left[-\frac{\left(\mathbf{v} - \mathbf{u}_x\right)^2}{2\, e_\sigma} \right], \tag{5.125}$$

where ρ_σ is the density, m_σ is the particle mass and $\mathbf{u}_\sigma$ is the macroscopic velocity, while e_σ and $\mathbf{u}_x$ are tunable parameters of the model. The parameters $\tau_{m\,\sigma}$ and $\mathbf{u}_x$ are not independently tunable parameters. In order to satisfy the local momentum conservation for the whole mixture, the following condition must hold:

$$\sum_\sigma \int m_\sigma\, \mathbf{v} \left[f_\sigma - f_{\sigma(m)}^e \right] / \tau_{m\,\sigma}\, d\mathbf{v} = \sum_\sigma \rho_\sigma \left(\mathbf{u}_\sigma - \mathbf{u}_x \right) / \tau_{m\,\sigma} = 0. \tag{5.126}$$

The tunable parameters of the previous model may be easily obtained by demanding that the moments of the model equations yield, in addition to the conservation equations, the correct ratio for the times characterizing the relaxation of the velocity and temperature differences [170]. In this way the results of Hamel [171] are recovered without any approximation and the characteristic mixture velocity can be identified with the mass averaged velocity $\mathbf{u}_x = \mathbf{u}_m$, where

$$\mathbf{u}_m = \frac{\sum_\sigma m_\sigma \mathbf{u}_\sigma}{\sum_\sigma m_\sigma}. \tag{5.127}$$

The local momentum conservation given by Eq. (5.126) implies that the quantity $\rho_\sigma / (m_\sigma \tau_{m\,\sigma})$ must be a constant and so the cross-collision relaxation time constants

differ one another. It is easy to check that Hamel's model does not satisfy the indifferentiability principle. In the following, a strategy for setting the tunable parameters will be proposed, which essentially allows realizing a smooth transition from the two-fluid approach to the single-fluid approach. For this reason the characteristic velocity will be set in such a way as to guarantee the indifferentiability principle at least for the fully-coupled configuration, when the mixture evolves as a single fluid. The characteristic velocity of the mixture can be identified with the barycentric velocity

$$\mathbf{u}_x = \mathbf{u} = \sum_\sigma x_\sigma \mathbf{u}_\sigma \tag{5.128}$$

where $x_\sigma = \rho_\sigma / \sum_\sigma \rho_\sigma$ is the mass concentration of the generic species. In this case, the local momentum conservation given by Eq. (5.126) implies $\tau_{m\,a} = \tau_{m\,b} = \tau_m$. It easy to check that if cross collisions prevail, the summation of the BKG-like kinetic equations for each species allows us to recover a BGK-like kinetic equation for the mixture.

The Chapman-Enskog asymptotic analysis of the previous kinetic model yields (see Appendix A):

$$\frac{\partial \rho_\sigma}{\partial t} + \nabla \cdot (\rho_\sigma \mathbf{u}_\sigma) = 0, \tag{5.129}$$

$$\begin{aligned} \frac{\partial (\rho_\sigma \mathbf{u}_\sigma)}{\partial t} &+ \nabla \cdot \left[(1-\alpha_\sigma)\, \rho_\sigma \mathbf{u}_\sigma \otimes \mathbf{u}_\sigma + \alpha_\sigma\, \rho_\sigma \mathbf{u} \otimes \mathbf{u} \right. \\ &+ \left. \alpha_\sigma \rho_\sigma \mathbf{u}_{\alpha(\sigma)} \otimes \mathbf{w}_\sigma + \alpha_\sigma \rho_\sigma \mathbf{w}_\sigma \otimes \mathbf{u}_{\alpha(\sigma)} \right] = \\ &- \nabla (\rho_\sigma e_\sigma) + \rho_\sigma \mathbf{g}_\sigma - \frac{1}{\tau_m} \rho_\sigma \mathbf{w}_\sigma \\ &+ \nabla \cdot \left\{ \alpha_\sigma \rho_\sigma e_\sigma \tau_m \left[\nabla \mathbf{u}_{\alpha(\sigma)} + \nabla \mathbf{u}_{\alpha(\sigma)}^T \right] \right\}, \end{aligned} \tag{5.130}$$

where $\alpha_\sigma = \tau_\sigma / (\tau_\sigma + \tau_m)$ is a bounded function of the relaxation time constants such as $0 \leq \alpha_\sigma \leq 1$, $\mathbf{w}_\sigma = \mathbf{u}_\sigma - \mathbf{u}$ is the diffusion velocity with regard to the barycentric velocity and $\mathbf{u}_{\alpha(\sigma)} = (1-\alpha_\sigma)\, \mathbf{u}_\sigma + \alpha_\sigma \mathbf{u}$ is a linear combination between the specific

velocity and the barycentric velocity. Unlike what happens at macroscopic level when the usual BGK equation is considered, in the previous Eq. (5.130) the relaxation time constants affect the advection term, the viscous term and an internal forcing term, which directly allows us to exchange momentum among the species. In a mesoscopic framework, a strategy for setting the relaxation time constants of the model is needed.

The system of macroscopic equations derived by the usual BGK equation for non-interacting species can be easily recovered by considering $\alpha_\sigma \to 0$. Two cases are possible: $1/\tau_\sigma \to \infty$ and $1/\tau_m \to 0$, but only the second one is allowed because it produces a non-zero viscosity $\alpha_\sigma \tau_m \to \tau_\sigma$. In a similar way, the system of macroscopic equations derived by the single-fluid BGK-like equation for ideally miscible components can be easily recovered by considering $\alpha_\sigma \to 1$. Two cases are possible: $1/\tau_m \to \infty$ and $1/\tau_\sigma \to 0$, but only the second one is allowed because it produces a non-zero viscosity $\alpha_\sigma \tau_m \to \tau_m$. The previous discussion allows us to prove that all the relaxation frequencies of the model must be bounded from above. Let us define $1/\tau_\sigma^0$ and $1/\tau_m^0$ the maximum value for the specific relaxation frequency and for the single-fluid relaxation frequency, respectively. Let us introduce two additional tunable parameters which are defined in the following way:

$$\chi = \frac{1/\tau_\sigma}{1/\tau_\sigma^0}, \tag{5.131}$$

$$\epsilon = \frac{1/\tau_m}{1/\tau_m^0}. \tag{5.132}$$

For simplicity, unique value of the parameter χ for all the species will be considered. In this way, the whole set of relaxation frequencies is uniquely identified by a point $P(\epsilon, \chi)$ on the plane $[0,1] \times [0,1] \subset \mathbb{R}^2$, which will be called Hamel's plane. For example, the point $P(0,1)$ on Hamel's plane identifies mixtures of non-interacting

species and implies the following macroscopic momentum equation:

$$\frac{\partial\left(\rho_\sigma \mathbf{u}_\sigma\right)}{\partial t}+\nabla\cdot\left[\rho_\sigma \mathbf{u}_\sigma\otimes\mathbf{u}_\sigma\right]=-\nabla\left(\rho_\sigma e_\sigma\right)+\rho_\sigma \mathbf{g}_\sigma+\nabla\cdot\left[\rho_\sigma e_\sigma \tau_\sigma^0\left(\nabla\mathbf{u}_\sigma+\nabla\mathbf{u}_\sigma^T\right)\right]. \quad (5.133)$$

By assuming $\rho_\sigma e_\sigma = p_\sigma$ and $e_\sigma \tau_\sigma^0 = \nu_\sigma$, where p_σ is the partial pressure and ν_σ is the kinematic viscosity for the generic species, the Navier-Stokes equation is recovered. This allows us to identify the value of the internal energy $e_\sigma = p_\sigma/\rho_\sigma$ and the minimum value of the relaxation time $\tau_\sigma^0 = \nu_\sigma/e_\sigma$.

The point $P(1,0)$ on Hamel's plane identifies the mixtures which can be described by the single-fluid approach. In this case, the momentum equation reads

$$\begin{aligned}&\frac{\partial\left(\rho_\sigma \mathbf{u}_\sigma\right)}{\partial t}+\nabla\cdot\left[\rho_\sigma \mathbf{u}\otimes\mathbf{u}+\rho_\sigma \mathbf{u}\otimes\mathbf{w}_\sigma+\rho_\sigma \mathbf{w}_\sigma\otimes\mathbf{u}\right]=\\&-\nabla\left(\rho_\sigma e_\sigma\right)+\rho_\sigma \mathbf{g}_\sigma-\frac{1}{\tau_m^0}\rho_\sigma \mathbf{w}_\sigma+\nabla\cdot\left[\rho_\sigma e_\sigma \tau_m^0\left(\nabla\mathbf{u}+\nabla\mathbf{u}^T\right)\right]. \quad (5.134)\end{aligned}$$

The identification process is not obvious, because the relaxation time constant τ_m^0 is involved in two different terms: the internal forcing term and the viscous term. In the models derived by the single-fluid approach [157], the usual practice identifies the internal forcing term as the leading effect of the diffusion process and this allows us to relate the relaxation time constant τ_m^0 with the diffusion coefficient. In particular, for high diffusive processes $1/\tau_m^0 \to \infty$ and the internal forcing term yields the ideal coupling among the species, i.e. $\mathbf{u}_\sigma \approx \mathbf{u}$. Unfortunately this means also $\tau_m^0 \to 0$, and so the obtained results are valid only when the viscous effects can be neglected [147]. Even though the two-fluid approach [159] interprets in the same way the internal forcing term, it allows us to tune it independently of the mixture viscosity, which will be a linear combination of the component viscosities. Unfortunately, the mixture viscosity can be a very complex function of the component viscosities [179] and the linear approximation may be valid only in the simplest cases. A complete discussion of the usual two-fluid approach is reported in the next section.

In the following, a different strategy is proposed. By summing the momentum equations for the species (5.134) and recalling the definition of barycentric velocity, the momentum equation for the mixture is recovered:

$$\frac{\partial(\rho\,\mathbf{u})}{\partial t} + \nabla\cdot(\rho\,\mathbf{u}\otimes\mathbf{u}) = -\nabla(\rho\,e) + \rho\,\mathbf{g} + \nabla\cdot\left[\rho\,e\,\tau_m^0\left(\nabla\mathbf{u} + \nabla\mathbf{u}^T\right)\right], \qquad (5.135)$$

where $\rho = \sum_\sigma \rho_\sigma$ is the mixture density, $e = \sum_\sigma x_\sigma\, e_\sigma = p/\rho$ is the mixture internal energy, $p = \sum_\sigma p_\sigma$ is the mixture pressure and $\mathbf{g} = \sum_\sigma x_\sigma\,\mathbf{g}_\sigma$ is the mass averaged effect of the external field. In order to recover the Navier-Stokes momentum equation for the mixture, the minimum value of the cross-collision relaxation time constants must be $\tau_m^0 = \nu_m/e$, where ν_m is the mixture kinematic viscosity. According to the mesoscopic framework, this strategy allows us to recover any experimental mixture viscosity instead of conjecturing a simplified value based on the component viscosities. Unfortunately, there is no proof that this strategy of setting the relaxation time constants ensures the ideal coupling among the species, i.e. $\mathbf{u}_\sigma \approx \mathbf{u}$, as it should be expected by the single-fluid approach. Moreover, the behavior of the model for mixtures which cannot be considered either fully-decoupled or ideally diffusive, which means for $0 < \alpha_\sigma < 1$, is not clear.

Let us consider a given number of different mixtures in the same isothermal condition: each mixture is made by components which share the same characteristics in terms of mass concentrations, molecular weights, kinematic viscosities and only differ in terms of diffusivity, that is, coupling strength. Equivalently, let us analyze a given mixture in isothermal conditions but for different temperature values and suppose that temperature affects diffusivity more than what happens for other thermo-physical properties. In both cases, it is possible to exclusively vary the coupling strength among the species. On Hamel's plane, we can smoothly move from the fully-decoupled configuration $P(0,1)$ to the ideally diffusive configuration $P(1,0)$ and

the set of the intermediate points $P_H(\chi_H, \epsilon)$ defines a curve. If we arbitrarily adopt the parameter ϵ as an index of the coupling strength, this means that some function $\chi_H(\epsilon)$, which smoothly describes the intermediate configurations such that $\chi_H(0) = 1$ and $\chi_H(1) = 0$, will exist. The function $\chi_H(\epsilon)$ will be called Hamel's function and determines the behavior of the kinetic model by means of the function α_σ involved in Eq. (5.130). This function can be reformulated by means of the new variables:

$$\alpha_\sigma(\epsilon) = \frac{\epsilon\,\gamma_\sigma}{\chi_H + \epsilon\,\gamma_\sigma}, \tag{5.136}$$

where $\gamma_\sigma = (x_\sigma\,\nu_\sigma)/(y_\sigma\,\nu_m)$ and $y_\sigma = p_\sigma/\sum_\sigma p_\sigma$ is the volume concentration for the generic species. The general analysis of Eq. (5.130) can be quite difficult.

5.5.2 Force coupling versus viscous coupling

For simplicity, let us consider an infinitely long channel in the x-direction (y identifies the transverse direction). When a single fluid realizes a laminar flow through it, the typical conditions of the Poiseuille flow are recovered. In the following, a binary mixture will be considered. In spite of its simplicity, this test problem allows us to find a general expression for Hamel's function: the effectiveness of this result will be verified by numerical simulations for two dimensional domains too. In the low Mach number limit, the inertial effects described by the left hand side of Eq. (5.130) can be neglected. In the same limit, the velocity field is essentially solenoidal (divergence free) and the effects due to the pressure gradient are negligible too, when ideal gases are considered. Under these hypotheses Eq. (5.130) becomes:

$$\mathbf{V}\,\frac{\partial^2\,\mathbf{u}^x}{\partial\,y^2} = \epsilon\,\mathbf{F}\,\mathbf{u}^x - \mathbf{a}^x, \tag{5.137}$$

where $\mathbf{V}$ is the viscosity matrix, $\mathbf{F}$ is the matrix which describes the internal force coupling, $\mathbf{u}^x = [\,u_a^x, u_b^x\,]^T$ is a vector collecting the x components of the specific veloc-

ities and $\mathbf{a}^x = [\,\rho_a\, g_a^x, \rho_b\, g_b^x\,]^T$ is a vector collecting the x components of the external field. The elements of the viscosity matrix are:

$$V_{11}(\epsilon) = \rho_a\,\nu_a\,\frac{\chi_H + \epsilon\, x_a\,\gamma_a}{\left[\,\chi_H + \epsilon\,\gamma_a\,\right]^2} \tag{5.138}$$

$$V_{12}(\epsilon) = \rho_a\,\nu_a\,\frac{\epsilon\, x_b\,\gamma_a}{\left[\,\chi_H + \epsilon\,\gamma_a\right]^2} \tag{5.139}$$

$$V_{21}(\epsilon) = \rho_b\,\nu_b\,\frac{\epsilon\, x_a\,\gamma_b}{\left[\,\chi_H + \epsilon\,\gamma_b\,\right]^2} \tag{5.140}$$

$$V_{22}(\epsilon) = \rho_b\,\nu_b\,\frac{\chi_H + \epsilon\, x_b\,\gamma_b}{\left[\,\chi_H + \epsilon\,\gamma_b\,\right]^2}. \tag{5.141}$$

The matrix which describes the internal force coupling is:

$$\mathbf{F} = x_a\, x_b\,\frac{\rho\, e}{\nu_m}\,\begin{bmatrix} +1 & -1 \\ -1 & +1 \end{bmatrix}. \tag{5.142}$$

The *force coupling* can be defined internal because $det\,(\mathbf{F}) = 0$. In order to analyze the solutions of the previous system, given by the Eqs. (5.137), let us discuss the determinant of the matrix $\mathbf{V}$:

$$det\,(\mathbf{V}) = \frac{\rho_a\,\nu_a\,\rho_b\,\nu_b}{\left[\,\chi_H + \epsilon\,\gamma_a\,\right]^2\,\left[\,\chi_H + \epsilon\,\gamma_b\,\right]^2}\,\left[\chi_H^2 + 2\,\chi_H\,\epsilon\,\left(\,x_a\,\gamma_a + x_b\,\gamma_b\,\right)\right] \geq 0. \tag{5.143}$$

In particular for any $\epsilon \in [0, 1)$, the determinant is positive and the inverse matrix $\mathbf{V}^{-1}$ exists. For this reason, Eq. 5.137 can be rewritten in the following way:

$$\frac{\partial^2\,\mathbf{u}^x}{\partial\, y^2} = \epsilon\,\mathbf{V}^{-1}\,\mathbf{F}\,\mathbf{u}^x - \mathbf{V}^{-1}\,\mathbf{a}^x, \tag{5.144}$$

This system of equations can be diagonalized. The result is:

$$\frac{\partial^2\,\hat{\mathbf{u}}^x}{\partial\, y^2} = \epsilon\,\mathbf{D}\,\hat{\mathbf{u}}^x - \mathbf{b}^x, \tag{5.145}$$

where $\mathbf{D} = \mathbf{E}^{-1}(\mathbf{V}^{-1}\,\mathbf{F})\,\mathbf{E}$ is the diagonal matrix formed by the eigenvalues of the matrix $(\mathbf{V}^{-1}\,\mathbf{F})$, $\mathbf{E}$ is the matrix formed by the columns of the right eigenvectors of the matrix $(\mathbf{V}^{-1}\,\mathbf{F})$ and $\mathbf{b}^x = \mathbf{E}^{-1}\mathbf{V}^{-1}\,\mathbf{a}^x$ is the modified forcing term. Independently

from the mixture properties, the system of equations is characterized by a null eigenvalue and a positive eigenvalue: let us suppose $D_{11} = 0$ and $D_{22} \geq 0$. The equation which corresponds to the null eigenvalue is:

$$\frac{\partial^2 \hat{u}_1^x}{\partial y^2} = -\frac{\rho_a \, g_a^x + \rho_b \, g_b^x}{\rho \, \nu_c} < 0, \tag{5.146}$$

where $\hat{u}_1^x$ and ν_c are defined as

$$\hat{u}_1^x(\epsilon) = \frac{V_{11}(\epsilon) + V_{21}(\epsilon)}{\rho \, \nu_c(\epsilon)} \, u_a^x + \frac{V_{12}(\epsilon) + V_{22}(\epsilon)}{\rho \, \nu_c(\epsilon)} \, u_b^x, \tag{5.147}$$

$$\nu_c(\epsilon) = \frac{x_a \, \nu_a}{\chi_H + \epsilon \, \gamma_a} + \frac{x_b \, \nu_b}{\chi_H + \epsilon \, \gamma_b}. \tag{5.148}$$

The equation which corresponds to the positive eigenvalue is:

$$\frac{\partial^2 \hat{u}_2^x}{\partial y^2} = + \epsilon \, x_a \, x_b \, \frac{\rho \, e}{\nu_m} \, \frac{\rho \, \nu_c}{det \, (\mathbf{V})} \, \hat{u}_2^x - b_2^x. \tag{5.149}$$

where $\hat{u}_2^x$ is defined as

$$\hat{u}_2^x(\epsilon) = \frac{V_{11}(\epsilon) + V_{21}(\epsilon)}{\rho \, \nu_c(\epsilon)} \, (\, u_b^x - u_a^x \,) \, . \tag{5.150}$$

Equation (5.146) admits parabolic solutions with negative curvature regardless of the mixtures properties. On the other hand, Eq. (5.149) admits parabolic solutions if and only if the components of the mixture do not interact with each other ($\epsilon = 0$). In this case, the physical situation is the same usually considered in Poiseuille flow: the viscous matrix $\mathbf{V}$ is diagonal and the solutions in terms of the original variables u_a^x and u_b^x will be parabolic too because they come from linear combinations of the diagonalized variables $\hat{u}_1^x(0)$ and $\hat{u}_2^x(0)$. In particular, the diagonalized velocity $\hat{u}_1^x(0) = z_a \, u_a^x + z_b \, u_b^x$ reduces to the viscous velocity for the mixture $\mathbf{u}_\nu$ which is:

$$\mathbf{u}_\nu = \sum_\sigma z_\sigma \, \mathbf{u}_\sigma, \tag{5.151}$$

where $z_\sigma = (x_\sigma \, \nu_\sigma) / \sum_\sigma (x_\sigma \, \nu_\sigma)$. In the general case $\epsilon \neq 0$, the coupling among species introduces exponential solutions because the coefficient multiplying $\hat{u}_2^x$ on the right

hand side of Eq. (5.149) is strictly positive. The internal *force coupling* changes the nature of the solutions.

The particular case of $\epsilon = 1$ must be discussed separately. In this case, the system of equations is singular and a solution may exist if and only if the forcing term satisfies a compatibility condition. Considering $\epsilon = 1$ in the system (5.137) and applying the difference between the first and the second equation, the compatibility condition is obtained:

$$x_a \, x_b \, \frac{e}{\nu_m} \, (\, u_a^x - u_b^x \,) = x_a \, y_b \, g_a^x - x_b \, y_a \, g_b^x. \tag{5.152}$$

If the forcing terms due to the external field are such that $x_a \, y_b \, g_a^x = x_b \, y_a \, g_b^x$, then the solution of the system of equations is unique, i.e. $u_a^x = u_b^x$. Let us suppose to model a mixture affected by a given forcing term $\rho \, g^x = \rho_a \, g_a^x + \rho_b \, g_b^x$. This forcing term acts as a source term in the mixture momentum equation (5.135). In the porous media simulations, it is quite usual to describe the effects of the pressure gradient as a forcing term. For the mixtures, where only the total value of the pressure gradient is known, the splitting of the forcing term among the momentum equations for the components can be made by means of the previous compatibility condition. If the source term for a generic species is called $\rho_\sigma \, g_\sigma^x$, then the compatibility condition prescribes that $\rho_\sigma \, g_\sigma^x = y_\sigma \rho \, g^x$, i.e. the splitting of the forcing term must be made on the basis of the volume concentrations.

An important feature of the proposed kinetic model is that the model allows us to tune the determinant of the viscous matrix $\mathbf{V}$ by means of the coupling strength ϵ. For this reason, the mixtures characterized by ideally miscible components can be very easily described by setting $\epsilon = 1$, i.e. a finite value. In the usual two-fluid models, the ideally miscible configuration is an asymptotic limiting case, which only in principle can be recovered by increasing the coupling force [159]. For the lattice

Boltzmann models, some stability constraints exist which do not allow us to consider forcing terms too strong and this makes the usual way to recover the ideally miscible configuration actually impracticable. Since the proposed model simulates the coupling among species by means of the viscous matrix $\mathbf{V}$ more than by means of the force matrix $\mathbf{F}$, it will be called a *viscous coupling* based model.

The previous discussion suggests a way to calculate Hamel's function. For intermediate coupling strengths, the diagonalized velocity $\hat{u}_1^x(\epsilon)$ can be expressed in the following way:

$$\hat{u}_1^x(\epsilon) = u_\nu^x + \left[\frac{V_{11}(\epsilon) + V_{21}(\epsilon)}{\rho\,\nu_c(\epsilon)} - z_a\right]\left(\,u_a^x - u_b^x\,\right). \tag{5.153}$$

When the difference among the species velocities is large, the components of the mixture are characterized by weak interactions and the diagonalized velocity is equivalent to the viscous mixture velocity $\hat{u}_1^x(\epsilon) \approx \hat{u}_1^x(0) = u_\nu^x$, as previously discussed for the Poiseuille flow. For strong interactions among species, the components velocities essentially become the same and all the possible velocity averages produce the same result. In both cases, the second term involved in the right hand side of Eq. (5.153) is negligible for different reasons. This suggests to consider the approximation $\hat{u}_1^x(\epsilon) \approx u_\nu^x$ acceptable for any coupling strength. In this way, according to Eq. (5.146), Hamel's function essentially affects the viscous velocity of the mixture by means of the critical viscosity given by Eq. (5.148). The proper value of the critical viscosity can be tuned in order to reproduce the experimental data for the viscous velocity of the mixture. It is reasonable to assume that, for an intermediate coupling strength, the critical viscosity belongs to the range defined by the mass averaged viscosity $\nu_c(0) = \sum_\sigma x_\sigma \nu_\sigma$ and by the mixture viscosity for the ideally miscible configuration $\nu_c(1) = \nu_m$. Since Hamel's function is bounded $0 \leq \chi_H \leq 1$, some constraints exist for the way to connect the previous values of critical viscosity. In

particular, the linear strategy, which means

$$\nu_c(\epsilon) = \sum_\sigma \frac{x_\sigma\,\nu_\sigma}{\chi_H + \epsilon\,\gamma_\sigma} = (1-\epsilon)\sum_\sigma x_\sigma \nu_\sigma + \epsilon\,\nu_m, \tag{5.154}$$

is allowed for any configuration such as $\nu_m \geq 1/2\,\sum_\sigma x_\sigma\,\nu_\sigma$. The previous constraint can be easily verified by the fact that the upper bound of the critical viscosity is $\nu_c^{max} = \nu_m/\epsilon$ and this imposes a maximum rate of change for the critical viscosity, when ideally miscible components are considered. Anyway, a connecting path always exists, but for $\nu_m \leq 1/2\,\sum_\sigma x_\sigma\,\nu_\sigma$ it is not linear. The condition (5.154) allows us to calculate Hamel's function, which is the last parameter needed to define the kinetic model.

5.5.3 Linearized kinetic models

The main difficulty of Hamel's model is due to the fact that the zero-order approximation of the velocity distribution function is a linear combination of Maxwellian functions, which, in general, is not a Maxwellian itself (see Appendix A). This is a direct consequence of the fact that, in the simplified collisional operator, two different Maxwellian distribution functions are involved. If the species velocity $\mathbf{u}_\sigma$ does not differ too much from the barycentric velocity $\mathbf{u}$, this mathematical complication is not needed and it can be avoided by means of an asymptotic approximation. It is interesting to point out that, in principle, a linearized model can be considered valid only for configurations close to the constitutive hypotheses used to derive it: in this case, that the cross collisions are so relevant to force the species velocity to be close to the barycentric velocity.

Equation (5.123) can be recast in the following form:

$$\frac{\partial f_\sigma}{\partial t} + \mathbf{v}\cdot\nabla f_\sigma + \mathbf{g}_\sigma\cdot\nabla_{\mathbf{v}} f_\sigma = -\frac{1}{\alpha_\sigma\,\tau_m}\left[f_\sigma - f_\sigma^e\right] - \frac{1}{\tau_m}\left[f_\sigma^e - f_{\sigma(m)}^e\right]. \tag{5.155}$$

In order to simplify the last term on the right hand side of the previous equation, it is possible to expand f^e_σ around $f^e_{\sigma(m)}$ or, equivalently, to expand $f^e_{\sigma(m)}$ around f^e_σ, in the limiting case that the specific velocity and the barycentric velocity are sufficiently similar. The asymptotic formulas are:

$$f^e_\sigma = f^e_{\sigma(m)} + \frac{f^e_{\sigma(m)}}{e_\sigma} (\mathbf{v} - \mathbf{u}) \cdot (\mathbf{u}_\sigma - \mathbf{u}) + O\left(|\mathbf{u}|^3\right), \tag{5.156}$$

and

$$f^e_{\sigma(m)} = f^e_\sigma + \frac{f^e_\sigma}{e_\sigma} (\mathbf{v} - \mathbf{u}_\sigma) \cdot (\mathbf{u} - \mathbf{u}_\sigma) + O\left(|\mathbf{u}|^3\right). \tag{5.157}$$

Neglecting the higher order terms and considering a linear combination of the previous formulas by means of a dimensionless parameter $0 \leq \beta \leq 1$, a set of approximations for the difference between the Maxwellian distribution functions can be obtained:

$$f^e_\sigma - f^e_{\sigma(m)} \approx \left[\beta \frac{f_{\sigma(m)}}{e_\sigma} (\mathbf{v} - \mathbf{u}) + (1 - \beta) \frac{f^e_\sigma}{e_\sigma} (\mathbf{v} - \mathbf{u}_\sigma)\right] \cdot (\mathbf{u}_\sigma - \mathbf{u}). \tag{5.158}$$

Substituting the previous approximation in Eq. (5.155) yields:

$$\begin{aligned} \frac{\partial f_\sigma}{\partial t} &+ \mathbf{v} \cdot \nabla f_\sigma + \mathbf{g}_\sigma \cdot \nabla_{\mathbf{v}} f_\sigma = -\frac{1}{\alpha_\sigma \tau_m} \left[f_\sigma - f^e_\sigma\right] \\ &- \frac{f^e_{\sigma(m)}}{e_\sigma} \frac{\beta}{\tau_m} (\mathbf{v} - \mathbf{u}) \cdot \mathbf{w}_\sigma - \frac{f^e_\sigma}{e_\sigma} \frac{1 - \beta}{\tau_m} (\mathbf{v} - \mathbf{u}_\sigma) \cdot \mathbf{w}_\sigma \end{aligned} \tag{5.159}$$

Considering $\beta = 0$, the kinetic model originally proposed by Sirovich can be recovered [169]. The additional terms in Eq. (5.159) do not affect the zero-order approximation of the distribution function involved in the asymptotic analysis. For this reason, even though some coupling among species exists, the zero order approximation of the distribution function is still Maxwellian. Essentially, the additional terms are similar to the terms which appear in the Chapman-Enskog asymptotic analysis when the external force field is considered: see Eq. (A.9) in Appendix A. It is well known that only the moments of the forcing term up to the second order are involved in the previous analysis. In particular, all the approximations (5.158) produce the same

results for both zero and first-order moments, while they differ for the second-order moments. Let us consider, for example, the following second-order moment:

$$\int m_\sigma \, \mathbf{v} \otimes \mathbf{v} \, \left[f^e_\sigma - f^e_{\sigma(m)} \right] \, d\mathbf{v} \approx \rho_\sigma \left[2 \left(1 - \beta \right) \mathbf{u}_\sigma \otimes \mathbf{u}_\sigma - 2\beta \, \mathbf{u} \otimes \mathbf{u} + \left(2\beta - 1 \right) \left(\mathbf{u}_\sigma \otimes \mathbf{u} + \mathbf{u} \otimes \mathbf{u}_\sigma \right) \right] . \quad (5.160)$$

It is possible to recover the result due to the original Maxwellian distribution functions, if and only if the approximation characterized by $\beta = 1/2$ is considered. In fact, it is well known that the central difference approximation ($\beta = 1/2$) produces better results than one-side approximations ($\beta = 1$ or $\beta = 0$, where the last is considered by Sirovich's model). It is possible to conclude that Sirovich's model considers only one possible approximation, which is not the most accurate.

The Chapman-Enskog asymptotic analysis of the linearized models can be easily performed by analogy with the analysis of Hamel's model (see Appendix A). The continuity equation for each species is the same of Hamel's model and it is described by Eq. (5.129). The momentum equation is:

$$\frac{\partial \left(\rho_\sigma \mathbf{u}_\sigma \right)}{\partial t} + \nabla \cdot \left(\rho_\sigma \mathbf{u}_\sigma \otimes \mathbf{u}_\sigma + 2\beta \, \alpha_\sigma \rho_\sigma \mathbf{w}_\sigma \otimes \mathbf{w}_\sigma \right) = -\nabla \left(e_\sigma \rho_\sigma \right) + \rho_\sigma \, \mathbf{g}_\sigma - \frac{1}{\tau_m} \rho_\sigma \mathbf{w}_\sigma + \nabla \cdot \left[\alpha_\sigma \, \rho_\sigma \, e_\sigma \, \tau_m \, \left(\nabla \mathbf{u}_\sigma + \nabla \mathbf{u}_\sigma^T \right) \right] . \quad (5.161)$$

All the linearized models produce a coupling force proportional to the diffusion velocity $\mathbf{w}_\sigma$. In some linearized models ($\beta \neq 0$), the diffusion velocity can affect the advection term but in none of them the diffusion velocity can affect the viscous term, which is usually the leading term in the low Mach number limit. If we consider once more the infinitely deep channel discussed in the previous section and in particular Eq. (5.137), all the linearized models are characterized by a diagonal viscous matrix $\mathbf{V}$. This means that the determinant of the viscous matrix is always strictly positive and *viscous coupling* is not possible.

Again, the problem is finding a method for correlating the microscopic relaxation time constants with the macroscopic transport coefficients. The most usual strategy will be discussed [159]. First of all, if the specific relaxation time constant τ_σ is set in such a way that:

$$\tau_\sigma = \frac{\nu_\sigma \, \tau_m}{e_\sigma \, \tau_m - \nu_\sigma}, \tag{5.162}$$

then the component viscosity is decoupled by the diffusion process because $\alpha_\sigma \, e_\sigma \, \tau_m = \nu_\sigma$ and Eq. (5.161) exactly recovers the Navier-Stokes momentum equation. Negative values of the relaxation time constants τ_σ are possible because in the linearized kinetic equation (5.155) only the quantity $\alpha_\sigma \, \tau_m$ is involved. The cross collision relaxation time constant τ_m can be tuned according to the mutual diffusion coefficient. The difference between the two Navier-Stokes equations for each species (a and b) leads to the following equation:

$$\frac{1}{\tau_m} \, (\mathbf{u}_a - \mathbf{u}_b) = -\frac{\rho^2 \, e}{\rho_a \, \rho_b} \, \mathbf{d} + \nabla^2 \left(\nu_a \, \mathbf{u}_a - \nu_b \, \mathbf{u}_b \right), \tag{5.163}$$

where the inertial effects have been neglected and the driving force is:

$$\mathbf{d} = \frac{\rho_a \, \rho_b}{\rho^2 \, e} \left[\frac{1}{\rho_a} \nabla \left(\rho_a \, e_a \right) - \frac{1}{\rho_b} \nabla \left(\rho_b \, e_b \right) - \mathbf{g}_a + \mathbf{g}_b \right] \approx \frac{\rho_a \, \rho_b}{\rho \, p} \left(\mathbf{g}_b - \mathbf{g}_a \right). \tag{5.164}$$

When isothermal flows in the low Mach number limit are considered, and no additional source terms in the continuity equations due to chemical reactions exist, the density gradients can be neglected and the driving force is mainly due to the external force field. The viscous effects in Eq. (5.163) are usually negligible too because it can be assumed that the derivatives are slowly varying with regard to the diffusion process [159]. If the cross collision relaxation time constant is set in such a way that

$$\tau_m = \frac{m_a \, m_b}{\left(m_a + m_b \right)^2} \, \frac{D}{e}, \tag{5.165}$$

where D is the mutual diffusion coefficient, then the expression for the velocity difference is recovered [178]:

$$\mathbf{u}_a - \mathbf{u}_b = -\frac{\rho^2}{\rho_a\,\rho_b}\,\frac{m_a\,m_b}{(m_a+m_b)^2}\,D\,\mathbf{d} \approx -\frac{m_a\,m_b}{(m_a+m_b)^2}\,\frac{D}{e}\,(\mathbf{g}_b - \mathbf{g}_a)\,. \tag{5.166}$$

For non-reactive isothermal flows in the low Mach number limit, the linearized two-fluid models realize the coupling among the species by means of a forcing term in the momentum equation, which essentially depends on the splitting of the external field acting on the mixture. For this reason, they may be called *force coupling* based models. Let us suppose to model a mixture affected by a given external field $\rho\,\mathbf{g}$, which could be, for example, a given pressure gradient, and let us suppose to adopt the splitting based on the volume concentrations, as discussed in the previous section. In this case, the coupling force is:

$$\mathbf{u}_a - \mathbf{u}_b \approx -\frac{m_a\,m_b}{(m_a+m_b)^2}\,\frac{D}{e}\,\frac{\rho}{\rho_a\,\rho_b}\,(x_a\,y_b - x_b\,y_a)\;\mathbf{g}. \tag{5.167}$$

It is evident that the coupling force is zero for mixtures characterized by $x_a\,y_b = x_b\,y_a$, independently of the mutual diffusion coefficient. Even though a different force splitting may be adopted in order to avoid this problem, it seems somehow artificial to use the external force field for simulating the internal coupling among species. In this case, the coupling based on the viscous effects of the diffusion velocity is a practical way to overcome the previous difficulties. The coupling strength can be easily set according to the experimental data concerning fluid flow of both mixture and components. Otherwise, for large diffusion coefficients, the coupling strength can be tuned in order to reproduce the desired momentum exchange among the species. In fact, since the *force coupling* is included in Hamel's model anyway, it is possible to tune the cross-collision relaxation time constants according to Eq. (5.165) and the coupling strength will be consequently defined as $\epsilon = \tau_m^0/\tau_m$. The final formula is:

$$\epsilon = \frac{\nu_m}{D} \frac{(m_a + m_b)^2}{m_a\, m_b}. \tag{5.168}$$

Recalling the results of the previous section, Hamel's model allows us to recover the ideally miscible configuration for $\epsilon = 1$. It is possible to consider the previous expression as the formal definition of the coupling strength for the linearized models, too. The linearized models allow us to recover the ideally miscible configuration only in the asymptotic limit $\epsilon \to \infty$ (in the linearized models ϵ is not bounded from above). This result proves that the *viscous coupling* is more effective than the *force coupling* because a lower (finite) value of the coupling strength is enough to reproduce the single-fluid approach.

The usual strategy for setting the relaxation time constants has an important consequence. When very high coupling strengths are considered, it is possible to assume $\mathbf{u}_\sigma \approx \mathbf{u}$. In this case, summing the species momentum equations (5.161), it is possible to obtain the momentum equation for the barycentric velocity and it is easy to verify that the value of the mixture viscosity for ideally miscible components coincides with the mass averaged viscosity $\sum_\sigma x_\sigma \nu_\sigma$. From the experimental point of view, this formula is valid as a first approximation: actually the mixture viscosity can be a very complicate function of the mixture properties [179]. Also in this case, the problem can be solved by modifying the strategy for setting the relaxation time constants, as previously done for Hamel's model. The mixture viscosity becomes a tunable parameter but this is not sufficient to describe the ideally miscible configuration because the viscous matrix, involved in Eq. (5.137), is always non-singular.

5.5.4 Lattice Boltzmann model for binary mixtures

In the following section, a lattice Boltzmann model for binary mixtures based on Hamel's model, defined by the Eqs. (5.123, 5.124, 5.125, 5.128), is constructed.

The two dimensional $D2Q9$ lattice will be used. Since only discrete velocities are allowed, the problem reduces to compute the generic discretized distribution function f_σ^λ, which is essentially the value of the velocity distribution function when the i-th discrete velocity is considered $f_\sigma^\lambda(t,\mathbf{x}) = f_\sigma(t,\mathbf{x},\mathbf{v}^\lambda)$. In this way, the original kinetic equation, which is an integro-differential equation, reduces to a system of differential equations:

$$\frac{\partial f_\sigma^\lambda}{\partial t} + \mathbf{v}^\lambda \cdot \nabla f_\sigma^\lambda + \mathbf{g}_\sigma \cdot \nabla_{\mathbf{v}} f_\sigma^\lambda = -\frac{\chi_H}{\tau_\sigma^0}\left[f_\sigma^\lambda - f_\sigma^{e\,\lambda}\right] - \frac{\epsilon}{\tau_m^0}\left[f_\sigma^\lambda - f_{\sigma(m)}^{e\,\lambda}\right], \tag{5.169}$$

for any $0 \leq \lambda \leq 8$. The kinetic term which takes into account the effects of the external force field can be simplified. This practice is based on the fact that the non-equilibrium distribution function does not differ too much from the equilibrium distribution with regard to the microscopic velocity, in the fluid regime limit [176]. In this way, the following approximation can be adopted:

$$-\nabla_{\mathbf{v}} f_\sigma^\lambda \approx -\nabla_{\mathbf{v}} f_\sigma^{e\,\lambda} = (1-\alpha_\sigma)\frac{f_\sigma^{e\,\lambda}}{e_\sigma}\left(\mathbf{v}^\lambda - \mathbf{u}_\sigma\right) + \alpha_\sigma \frac{f_{\sigma(m)}^{e\,\lambda}}{e_\sigma}\left(\mathbf{v}^\lambda - \mathbf{u}\right). \tag{5.170}$$

Substituting the previous approximation in the equation for the discretized distribution function yields:

$$\begin{aligned}\frac{\partial f_\sigma^\lambda}{\partial t} \quad &+ \quad \mathbf{v}^\lambda \cdot \nabla f_\sigma^\lambda = -\frac{\chi_H}{\tau_\sigma^0}\left[f_\sigma^\lambda - f_\sigma^{e\,\lambda}\right] - \frac{\epsilon}{\tau_m^0}\left[f_\sigma^\lambda - f_{\sigma(m)}^{e\,\lambda}\right] \\ &+ \quad (1-\alpha_\sigma)\frac{f_\sigma^{e\,\lambda}}{e_\sigma}\left(\mathbf{v}^\lambda - \mathbf{u}_\sigma\right)\cdot \mathbf{g}_\sigma + \alpha_\sigma \frac{f_{\sigma(m)}^{e\,\lambda}}{e_\sigma}\left(\mathbf{v}^\lambda - \mathbf{u}\right)\cdot \mathbf{g}_\sigma. \end{aligned} \tag{5.171}$$

Since only the discrete distribution functions for the lattice microscopic velocities are considered, an interpolation test function must be adopted to calculate the macroscopic moments. The key idea is to reduce the statistical moments of the continuous distribution function to weighted summations of the discretized distribution functions by means of proper quadrature formulas. The interpolation test function should be assumed in such a way as to include the equilibrium distribution function as a particular case, in order to allow us to recover the equilibrium conditions. The problem

is that the equilibrium distribution function is an exponential function, while the moments are polynomial forms of the macroscopic quantities. This mismatch can be easily overcome by continuous integration but not by a quadrature formula, which cannot change the nature of the interpolation test function. For this reason the equilibrium distribution function must be approximated with a polynomial form too. If the low Mach number limit is considered, then the equilibrium distribution function can be linearized around the state at rest. For the Maxwellian distribution function centered on the specific velocity, this approximation yields:

$$f_\sigma^{e\,\lambda} \approx \frac{\rho_\sigma}{m_\sigma \left(2\pi e_\sigma\right)^{D/2}} \exp\left[-\frac{(\mathbf{v}^\lambda)^2}{2\,e_\sigma}\right]\left[1+\frac{\mathbf{v}^\lambda\cdot\mathbf{u}_\sigma}{e_\sigma}+\frac{\left(\mathbf{v}^\lambda\cdot\mathbf{u}_\sigma\right)^2}{2\,e_\sigma^2}-\frac{\mathbf{u}_\sigma^2}{2\,e_\sigma}\right], \qquad (5.172)$$

and, similarly, for the Maxwellian distribution function centered on the barycentric velocity:

$$f_{\sigma(m)}^{e\,\lambda} \approx \frac{\rho_\sigma}{m_\sigma \left(2\pi e_\sigma\right)^{D/2}} \exp\left[-\frac{(\mathbf{v}^\lambda)^2}{2\,e_\sigma}\right]\left[1+\frac{\mathbf{v}^\lambda\cdot\mathbf{u}}{e_\sigma}+\frac{\left(\mathbf{v}^\lambda\cdot\mathbf{u}\right)^2}{2\,e_\sigma^2}-\frac{\mathbf{u}^2}{2\,e_\sigma}\right], \qquad (5.173)$$

where, in both cases, only the terms up to the second-order in the macroscopic velocities have been considered. Equation (5.171) can be formulated by introducing some auxiliary variables:

$$\begin{aligned}\frac{\partial\varphi_\sigma^\lambda}{\partial t} \;&+\; \mathbf{v}^\lambda\cdot\nabla\varphi_\sigma^\lambda = -\frac{\chi_H}{\tau_\sigma^0}\left[\varphi_\sigma^\lambda-\varphi_\sigma^{e\,\lambda}\right]-\frac{\epsilon}{\tau_m^0}\left[\varphi_\sigma^\lambda-\varphi_{\sigma(m)}^{e\,\lambda}\right]\\ &+\; (1-\alpha_\sigma)\,\frac{\varphi_\sigma^{e\,\lambda}}{e_\sigma}\left(\mathbf{v}^\lambda-\mathbf{u}_\sigma\right)\cdot\mathbf{g}_\sigma+\alpha_\sigma\frac{\varphi_{\sigma(m)}^{e\,\lambda}}{e_\sigma}\left(\mathbf{v}^\lambda-\mathbf{u}\right)\cdot\mathbf{g}_\sigma, \qquad (5.174)\end{aligned}$$

where $\varphi_\sigma^\lambda = f_\sigma^\lambda/Q_\sigma^\lambda$, $\varphi_\sigma^{e\,\lambda} = f_\sigma^{e\,\lambda}/Q_\sigma^\lambda$, $\varphi_{\sigma(m)}^{e\,\lambda} = f_{\sigma(m)}^{e\,\lambda}/Q_\sigma^\lambda$ and

$$Q_\sigma^\lambda = \frac{1}{m_\sigma\left(2\pi\,e_\sigma\right)^{D/2}}\exp\left[-\frac{(\mathbf{v}^\lambda)^2}{2\,e_\sigma}\right]. \qquad (5.175)$$

Since the deviation of the distribution function from the one at rest is also small in the fluid regime limit, it can be assumed that the function φ_σ^λ belongs to the same class of functions which includes the equilibrium functions $\varphi_\sigma^{e\,\lambda}$ and $\varphi_{\sigma(m)}^{e\,\lambda}$, i.e. the class of

the D-dimensional second-order polynomial forms. The unknown parameters involved into the interpolation test function can be determined by using the calculated values of the distribution function for the lattice microscopic velocities. Once the interpolation test function is well defined [127], the quadrature formulas for the calculation of the macroscopic moments can be obtained. In this case they are:

$$\rho_\sigma = \sum_{\lambda=0}^{8} \varsigma^\lambda \, \varphi_\sigma^\lambda \,, \tag{5.176}$$

$$\rho_\sigma \, \mathbf{u}_\sigma = \sum_{\lambda=0}^{8} \varsigma^\lambda \, \mathbf{v}^\lambda \, \varphi_\sigma^\lambda \,, \tag{5.177}$$

where ς^λ are the same weight factors given by Eq. (5.64). Since only the terms up to the second-order in the macroscopic quantities have been considered in the approximations (5.172, 5.173), the forcing terms in Eq. (5.174) can be simplified by neglecting higher order terms. It is well known that considering different-order approximations can lead to numerical inaccuracies. Since the acceleration due to the external force field can be considered of the first-order, the terms multiplying the acceleration must be of the first-order with regard to the macroscopic velocities [132]. For this reason, the equations for the discretized distribution functions become:

$$\frac{\partial \varphi_\sigma^\lambda}{\partial t} + \mathbf{v}^\lambda \cdot \nabla \varphi_\sigma^\lambda = -\frac{\chi_H}{\tau_\sigma^0} \left[\varphi_\sigma^\lambda - \varphi_\sigma^{e\,\lambda} \right] - \frac{\epsilon}{\tau_m^0} \left[\varphi_\sigma^\lambda - \varphi_{\sigma(m)}^{e\,\lambda} \right] + \frac{1}{\sqrt{e_\sigma}} \, \mathbf{k}_{\alpha(\sigma)}^\lambda \cdot \mathbf{g}_\sigma, \tag{5.178}$$

where

$$\mathbf{k}_{\alpha(\sigma)}^\lambda = \rho_\sigma \left[\frac{\mathbf{v}^\lambda - \mathbf{u}_{\alpha(\sigma)}}{\sqrt{e_\sigma}} + \frac{\mathbf{v}^\lambda \cdot \mathbf{u}_{\alpha(\sigma)}}{\sqrt{e_\sigma^3}} \, \mathbf{v}^\lambda \right]. \tag{5.179}$$

For recovering Eq. (5.178), the property that the vector $\mathbf{k}_{\alpha(\sigma)}^\lambda$ is linear with regard to the macroscopic velocities has been used.

The left hand side of Eq. (5.178) is essentially a substantial derivative and it involves a known microscopic velocity of the lattice, defined by Eq. (5.63). The ordinary derivatives can be numerically estimated by considering the rate of change for

a finite time step δt smaller than the characteristic time scales of the phenomena. The spurious terms, which derive from the previous approximation at the hydrodynamic level, are called discrete lattice effects. In order to cancel the discrete lattice effects, some corrections are need. Let us introduce the following corrected velocities [132, 133]:

$$\rho_\sigma \, \mathbf{u}^\star_\sigma = \sum_{\lambda=0}^{8} \varsigma^\lambda \, \mathbf{v}^\lambda \, \varphi^\lambda_\sigma - \rho_\sigma \, (\mathbf{w}^\star_\sigma/\tau_m - \mathbf{g}_\sigma) \, \delta t/2. \tag{5.180}$$

The corrected barycentric velocity $\mathbf{u}^\star = \sum_\sigma x_\sigma \mathbf{u}^\star_\sigma$ is consequently defined too. Similarly the corrected equilibrium distribution function $\varphi^{e\,\lambda\star}_\sigma$ centered on the specific velocity $\mathbf{u}^\star_\sigma$ and the corrected equilibrium distribution function $\varphi^{e\,\lambda\star}_{\sigma(m)}$ centered on the barycentric velocity $\mathbf{u}^\star$ can be obtained. Thanks to these quantities, the final lattice Boltzmann method can be formulated:

$$\begin{aligned} \varphi^\lambda_\sigma \left(t + \delta t, \mathbf{x} + \mathbf{v}^\lambda \delta t\right) - \varphi^\lambda_\sigma \;&=\; -\chi_H \, \frac{\delta t}{\tau^0_\sigma} \left[\varphi^\lambda_\sigma - \varphi^{e\,\lambda\star}_\sigma\right] - \epsilon \, \frac{\delta t}{\tau^0_m} \left[\varphi^\lambda_\sigma - \varphi^{e\,\lambda\star}_{\sigma(m)}\right] \\ &+\; \frac{\delta t}{\sqrt{e_\sigma}} \, \mathbf{k}^{\lambda\star}_{\alpha(\sigma)} \cdot \left[\, d_\sigma \, \mathbf{g}_\sigma + (1 - d_\sigma) \; \mathbf{w}^\star_\sigma/\tau_m \,\right], \end{aligned} \tag{5.181}$$

where d_σ is defined as

$$d_\sigma = 1 - \frac{1}{2} \, \frac{\delta t}{\alpha_\sigma \, \tau_m} = 1 - \frac{\delta t}{2} \left(\frac{\chi_H}{\tau^0_\sigma} + \frac{\epsilon}{\tau^0_m}\right), \tag{5.182}$$

and it takes into account the discrete lattice effects, while $\mathbf{k}^{\lambda\star}_{\alpha(\sigma)}$ is the quantity defined by Eq. (5.179) when the corrected velocities are considered. It is easy to check that, in the continuous limit $\delta t \to 0$, the corrected equations coincide with the previous Eqs. (5.178). The corrected specific velocity involves the corrected diffusion velocity and, for this reason, Eq. (5.180) realizes an implicit formulation. This feature can be made evident by considering the definition of diffusion velocity:

$$\rho_\sigma \sum_k \left[(1 + \omega_m/2) \, \delta_{k\,\sigma} - x_{\,k} \, \omega_m/2 \,\right] \mathbf{u}^\star_k = \sum_{\lambda=0}^{8} \varsigma^\lambda \, \mathbf{v}^\lambda \, \varphi^\lambda_\sigma + \rho_\sigma \, \mathbf{g}_\sigma \, \delta t/2, \tag{5.183}$$

where $\omega_m = \delta t/\tau_m$ is the dimensionless frequency for the cross collisions. It is possible to derive an explicit formulation for the corrected velocities from the previous equation:

$$\rho_\sigma \, \mathbf{u}^\star_\sigma = \sum_k \left[\left(\frac{2}{2+\omega_m} \, \delta_{k\,\sigma} + \frac{\omega_m}{2+\omega_m} \, x_{\,k} \right) \left(\sum_{\lambda=0}^{8} \varsigma^\lambda \, \mathbf{v}^\lambda \, \varphi^\lambda_k + \rho_\sigma \, \mathbf{g}_{\,k} \, \delta t/2 \right) \right]. \quad (5.184)$$

When the cross collisions are negligible $\omega_m = 0$, the previous correction reduces to the usual definition for the corrected velocity given by Eq. (5.76), which has been modified in order to take into account the effects of the external field [158]. The final lattice Boltzmann method exactly recovers the following equations (see Appendix B):

$$\frac{\partial \rho_\sigma}{\partial t} + \nabla \cdot (\rho_\sigma \mathbf{u}^\star_\sigma) = 0, \quad (5.185)$$

$$\begin{aligned} \frac{\partial \left(\rho_\sigma \mathbf{u}_\sigma \right)}{\partial t} \;&+\; \nabla \cdot \left[(1-\alpha_\sigma) \, \rho_\sigma \mathbf{u}^\star_\sigma \otimes \mathbf{u}^\star_\sigma + \alpha_\sigma \, \rho_\sigma \mathbf{u}^\star \otimes \mathbf{u}^\star \right. \\ &+\; \left. \alpha_\sigma \rho_\sigma \mathbf{u}^\star_{\alpha(\sigma)} \otimes \mathbf{w}^\star_\sigma + \alpha_\sigma \rho_\sigma \mathbf{w}^\star_\sigma \otimes \mathbf{u}^\star_{\alpha(\sigma)} \right] = \\ &-\; \nabla \left(\rho_\sigma e_\sigma \right) + \rho_\sigma \mathbf{g}_\sigma - \frac{1}{\tau_m} \, \rho_\sigma \mathbf{w}^\star_\sigma \\ &+\; \nabla \cdot \left\{ d_\sigma \, \alpha_\sigma \rho_\sigma e_\sigma \tau_m \left[\nabla \mathbf{u}^\star_{\alpha(\sigma)} + \nabla \mathbf{u}^{\star T}_{\alpha(\sigma)} \right] \right\}. \end{aligned} \quad (5.186)$$

The proposed lattice Boltzmann method involves additional lattice parameters and a proper strategy is needed in order to tune them. First of all, the constraints must be defined. The lattice grid size δx, the viscosity of the components ν_σ and the viscosity of the ideally coupled mixture ν_m are considered input data of the problem. The internal energies for the components e_σ can be freely tuned, since the energy equations are not solved. In particular, assuming $r_\sigma = e_\sigma/c^2$, the parameters r_σ can be set in such a way as to reproduce the exact pressure gradients in the momentum equations. On the other hand, the local stability analysis of the lattice Boltzmann model suggests that $r_\sigma = 1/3$ is the optimal value for improving the stability [134]. In the low Mach number limit, and when ideal gases are considered, both effects of

density gradients and of the pressure gradients are negligible. For this reason, stability will be preferred to accuracy and the parameters will be accordingly selected.

Let us consider first the ideally non-interacting configuration, i.e when $1/\tau_m \to 0$. Let us define $\omega_\sigma^0 = \delta t^0/\tau_\sigma^0$ the dimensionless frequency for the generic component and c_σ^0 the lattice velocity for the generic component. Since the dimensionless frequency must be set in such a way as to respect the stability criterion $0 \leq \omega_\sigma^0 \leq 2$, the problem is to define c_σ^0 and τ_σ^0 in order to recover the desired lattice grid size δx and the kinematic viscosity for the single component ν_σ. The following formulas yield:

$$\tau_\sigma^0 = \frac{(2-\omega_\sigma^0)}{6\,(\omega_\sigma{}^0)^2}\,\frac{\delta x^2}{\nu_\sigma}, \tag{5.187}$$

$$c_\sigma^0 = \frac{\delta x}{\tau_\sigma^0\,\omega_\sigma^0} = \frac{6\,\omega_\sigma^0}{(2-\omega_\sigma^0)}\,\frac{\nu_\sigma}{\delta x}. \tag{5.188}$$

Since all the mixture components are computed on the same lattice, the lattice velocities must be all identical, i.e. $c_\sigma^0 = c^0$. This introduces a new constraint for the dimensionless frequencies. Let us suppose to label with a the component of the mixture characterized by the smallest viscosity: in this way $\nu_\sigma^0 \geq \nu_a^0$. The condition $c_\sigma^0 = c^0$ implies:

$$\omega_\sigma^0 = \frac{2\,\nu_a\,\omega_a^0}{\nu_\sigma\,(2-\omega_a^0) + \nu_a\,\omega_a^0} \leq \omega_a^0. \tag{5.189}$$

Selecting ω_a^0 in such a way that $0 \leq \omega_a^0 \leq 2$, then all the other dimensionless frequencies will follow from the previous condition and they will be $0 \leq \omega_\sigma^0 \leq 2$ too. In particular, the previous condition implies that the discretization time steps for all the components will be identical $\delta t^0 = \tau_\sigma^0\,\omega_\sigma^0 = \tau_a^0\,\omega_a^0$.

We can proceed in a similar way for the ideally miscible configuration. Let us define $\omega_m^0 = \delta t^0/\tau_m^0$ as the dimensionless frequency for the ideally miscible configuration. The following formulas hold:

$$\tau_m^0 = \frac{(2-\omega_m^0)}{6\,(\omega_m^0)^2}\,\frac{\delta x^2}{\nu_m}, \tag{5.190}$$

$$c_\sigma^m = \frac{\delta x}{\tau_m^0\,\omega_m^0} = \frac{6\,\omega_m^0}{(2-\omega_m^0)}\,\frac{\nu_m}{\delta x}. \tag{5.191}$$

In this case, the lattice velocities are naturally identical $c_\sigma^m = c^m$ and the same happens for the discretization time steps $\delta t^m = \tau_m^0\,\omega_m^0$. For an intermediate degree of coupling, the generalized expression of the discretization time step can be assumed as:

$$\delta t = \chi_H\,\delta t^0 + \epsilon\,\delta t^m = \chi_H\,\tau_a^0\omega_a^0 + \epsilon\,\tau_m^0\,\omega_m^0. \tag{5.192}$$

This allows us to calculate the intermediate values of the dimensionless frequencies:

$$\omega_\sigma = \delta t\,\frac{\chi_H}{\tau_\sigma^0} = \omega_\sigma^0\,\chi_H\,\left[\,\chi_H + \epsilon\,\theta\,\right], \tag{5.193}$$

$$\omega_m = \delta t\,\frac{\epsilon}{\tau_m^0} = \omega_m^0\,\epsilon\,\left[\,\chi_H/\theta + \epsilon\,\right], \tag{5.194}$$

where θ is defined as

$$\theta = \frac{\nu_\sigma}{\nu_m}\,\frac{(2-\omega_m^0)}{(2-\omega_\sigma^0)}\,\frac{\omega_\sigma^0}{\omega_m^0}. \tag{5.195}$$

The discussed strategy for setting the microscopic parameters allows us to reproduce the correct viscosities for the components in the ideally non-interacting limit and for the mixture in the ideally miscible limit. The coupling strength ϵ can be tuned by means of experimental data or by considering the diffusion coefficient for weakly interacting components. The discrete lattice effects depend on the coupling strength too and the expression for the parameter d_σ is:

$$d_\sigma = 1 - \left(1-d_\sigma^0\right)\,\chi_H^2 - (1-d_\sigma^m)\,\epsilon^2 - \frac{\chi_H\,\epsilon}{2}\,\left(\,\omega_\sigma^0\,\theta + \omega_m^0/\theta\right), \tag{5.196}$$

where $d_\sigma^0 = 1-\omega_\sigma^0/2$ and $d_\sigma^m = 1-\omega_m^0/2$ are the limiting cases for ideally non-interacting components and for ideally miscible components, respectively. As previously done for the continuous model, Hamel's function χ_H can be set in order to obtain the desired critical viscosity. In this case, the previous correlations must be

taken into account for the computation of the critical viscosity given by Eq. (5.148) in the discrete model:

$$\nu_c(\epsilon) = \frac{d_a\, c_a^2\, x_a\, \nu_a}{\chi_H\, d_a^0\, (c_a^0)^{\,2} + \epsilon\, d_a^m\, (c_a^m)^{\,2}\, \nu_a/\nu_m} + \frac{d_b\, c_b^2\, x_b\, \nu_b}{\chi_H\, d_b^0\, (c_b^0)^{\,2} + \epsilon\, d_b^m\, (c_b^m)^{\,2}\, \nu_b/\nu_m}. \quad (5.197)$$

Finally the compatibility condition for the discrete model must be modified too. Considering $\epsilon = 1$ in the system of discrete equations, analogous to the previous system of equations (5.137), and applying the difference between the first and second equation, the compatibility condition is obtained:

$$\frac{e}{\nu_m}\,(\,u_a^x - u_b^x\,) = g_a^x - g_b^x. \quad (5.198)$$

If the forcing terms due to the external field are such as $g_a^x = g_b^x$, then the solution of the system of equations is unique, i.e. $u_a^x = u_b^x$. Let us suppose to model a mixture affected by a given forcing term $\rho\, g^x = \rho_a\, g_a^x + \rho_b\, g_b^x$. For the mixture, where only the total value of the pressure gradient is known, the splitting of the forcing term among the momentum equations for the components can be made by means of the previous compatibility condition. If the source term for a generic species is called $\rho_\sigma\, g_\sigma^x$, then the compatibility condition for the discrete model prescribes that $\rho_\sigma\, g_\sigma^x = x_\sigma\, \rho\, g^x$, i.e. the splitting of the forcing term must be made on the basis of the mass concentrations. The difference with the continuous model is due to the fact that for the lattice Boltzmann model $e_\sigma = e = c^2/3$, while for the continuous model $e_\sigma = e\, y_\sigma/x_\sigma$. This feature of the discrete lattice model is a consequence of the stability constraint which has been assumed but it can be easily overcome by considering different values for the internal energy of each species, i.e. $r_\sigma \neq 1/3$.

Let us consider a two dimensional randomly generated porous medium. For the actual calculations, periodic boundary conditions in both directions are assumed. A given pressure gradient induces the flow of some binary mixtures through the porous

Table 5.3: Superficial velocities $M(u_\sigma^x)$ (averaged values over the whole porous medium) for single components of binary mixtures characterized by different coupling strengths. The critical viscosity is constantly equal to the averaged viscosity based on mass concentrations (case A), or varies according to the coupling strength with the assumed linear law (case B).

(A) $\nu_c(\epsilon) = \sum_\sigma x_\sigma \nu_\sigma$

ϵ $[-]$	χ_H $[-]$	ν_c $[m^2/s]$	ω_a $[-]$	ω_b $[-]$	ω_m $[-]$	$M(u_a^x)$ $[mm/s]$	$M(u_b^x)$ $[mm/s]$
0.000	1.000	3.750×10^{-6}	1.200	1.462	0.000	3.690	8.305
0.001	0.999	3.750×10^{-6}	1.199	1.460	0.001	3.753	8.196
0.002	0.998	3.750×10^{-6}	1.198	1.459	0.002	3.811	8.115
0.004	0.996	3.750×10^{-6}	1.196	1.457	0.004	3.937	7.943
0.008	0.992	3.750×10^{-6}	1.192	1.452	0.008	4.121	7.702
0.016	0.984	3.750×10^{-6}	1.184	1.442	0.016	4.281	7.323
0.032	0.968	3.750×10^{-6}	1.168	1.422	0.032	4.626	6.617
0.064	0.936	3.750×10^{-6}	1.135	1.382	0.064	4.913	6.187
0.126	0.827	3.750×10^{-6}	1.069	1.302	0.129	5.148	5.848
0.250	0.746	3.750×10^{-6}	0.934	1.138	0.263	5.234	5.567
0.500	0.495	3.750×10^{-6}	0.647	0.788	0.549	5.315	5.475
0.749	0.246	3.750×10^{-6}	0.336	0.410	0.860	5.383	5.424
0.989	0.010	3.750×10^{-6}	0.015	0.018	1.185	5.418	5.418

(B) $\nu_c(\epsilon) = (1-\epsilon)\sum_\sigma x_\sigma \nu_\sigma + \epsilon\,\nu_m \leq \sum_\sigma x_\sigma \nu_\sigma$

ϵ $[-]$	χ_H $[-]$	ν_c $[m^2/s]$	ω_a $[-]$	ω_b $[-]$	ω_m $[-]$	$M(u_a^x)$ $[mm/s]$	$M(u_b^x)$ $[mm/s]$
0.000	1.000	3.750×10^{-6}	1.200	1.462	0.000	3.690	8.305
0.001	0.999	3.749×10^{-6}	1.199	1.461	0.001	3.736	8.253
0.002	0.998	3.748×10^{-6}	1.199	1.460	0.002	3.776	8.173
0.003	0.997	3.747×10^{-6}	1.198	1.459	0.003	3.851	8.081
0.006	0.993	3.745×10^{-6}	1.195	1.458	0.005	3.977	7.903
0.012	0.987	3.739×10^{-6}	1.190	1.450	0.009	4.178	7.650
0.024	0.973	3.729×10^{-6}	1.180	1.437	0.019	4.523	7.226
0.048	0.946	3.708×10^{-6}	1.160	1.413	0.038	4.850	6.566
0.096	0.893	3.666×10^{-6}	1.119	1.362	0.077	5.217	6.250
0.191	0.791	3.582×10^{-6}	1.032	1.257	0.160	5.544	6.101
0.382	0.590	3.414×10^{-6}	0.839	1.021	0.349	6.043	6.261
0.573	0.398	3.246×10^{-6}	0.616	0.750	0.570	6.468	6.617
0.764	0.214	3.078×10^{-6}	0.361	0.440	0.827	7.099	7.174
0.994	0.006	2.875×10^{-6}	0.011	0.013	1.189	7.662	7.662

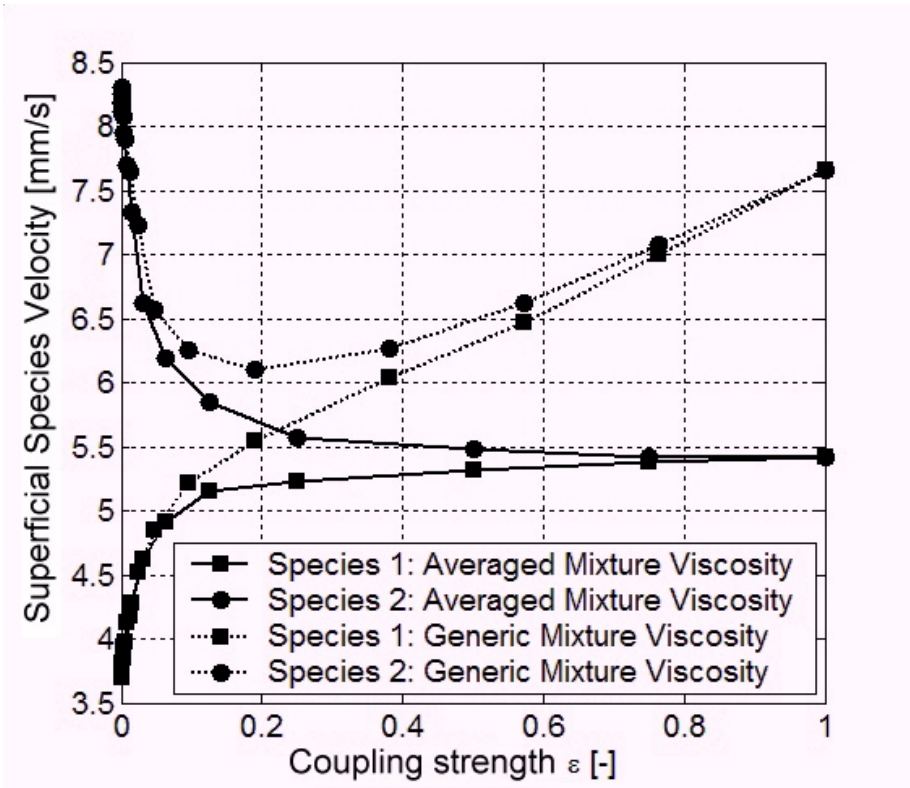

Figure 5.4: Superficial velocity for the components of the binary mixtures flowing in a randomly generated porous medium. Two cases are considered: in the first case, the fully-coupled mixture viscosity is set equal to the mass averaged viscosity and, in the second case, it is set equal to the generic experimental viscosity.

medium. Each mixture is characterized by a different coupling strength. From the physical point of view, we can imagine that each mixture is made of components characterized by different diffusivity but the same kinematic viscosity if considered alone or the same components for different values of temperature, which, again, mainly affects the diffusivity. This ideal experiment allows us to evaluate the effects of the cross collisions for the proposed model, its performance at macroscopic level and to verify the effectiveness of the tuning strategy for the relaxation time constants.

When the coupling strength is very small, the two species independently evolve according to their kinematic viscosities. When the coupling strength increases, i.e. when the cross collisions become important, the slower species try to slacken the other

species and vice versa. At the end, the result is that the two species are characterized by velocities much more similar in comparison with the results for the non-interacting configurations. For this reason, the barycentric velocity is enough to characterize the mixture for very high coupling strengths. This is the proper domain of the *single fluid* approach. The barycentric velocity of the mixture is affected by the mixture kinematic viscosity. A very popular experimental formula for the mixture kinematic viscosity is [179]:

$$\nu_m^r = \frac{x_a\,\nu_a}{1 + F_{a\,b}\,y_b/y_a} + \frac{x_b\,\nu_b}{1 + F_{b\,a}\,y_a/y_b}, \tag{5.199}$$

where $F_{a\,b}$ and $F_{b\,a}$ are positive corrective factors. In particular the experimental data show that the effective kinematic viscosity for the mixture is smaller than the averaged viscosity based on the mass concentrations of the components $\nu_m^r \leq \sum_\sigma x_\sigma \nu_\sigma$. In Tab. 5.3 and in Fig. 5.4 some numerical results are reported which have been calculated by the proposed discrete lattice model. In the first case, A, the fully-coupled mixture viscosity is set equal to the mass averaged kinematic viscosity $\nu_m = \sum_\sigma x_\sigma \nu_\sigma$ while, in the second case, B, it is set equal to a lower value $\nu_m = \nu_m^r \leq \sum_\sigma x_\sigma \nu_\sigma$. The proposed tuning strategy allows us to freely tune the fully-coupled mixture viscosity and it overcomes the constraints of the usual strategy for setting the relaxation time constants, which implies a fully-coupled viscosity constantly equal to the mass averaged viscosity [159]. Hamel's function has been set in such a way that the discrete critical viscosity given by Eq. (5.197) satisfies the linear equation (5.154). Even though the mathematical suitability of the proposed strategy has been previously discussed for the one dimensional case only, the numerical results confirm that it has a general effectiveness and it allows us to recover the desired behavior of the barycentric velocity with regard to the coupling strength for more complex computational domains too.

To summarize, we can point out the following conclusions about the discussed mesoscopic model for binary mixtures.

- The concept of binary mixtures in the framework of the LBM must be evaluated not only in literal meaning, because the interaction among different lattices is a general paradigm which can be fruitfully used to solve different coupled equations (see the discussion about virtual mixtures for multi-lattice models in the previous section).

- In order to reduce the computational needs, even though more discrete distribution functions are considered, they should share the same discretization of the space. In fact if the same spatial discretization and the same time step are considered, then all the distribution functions must share the same lattice velocity $c_\sigma = c$. This congruence condition is simply a numerical trick but it is necessary in order to make the computational demand reasonable.

- The mesoscopic tuning strategy must overcome the drawbacks of the congruence condition in order to include different relaxation dynamics on the same discretization of the phase space. A detailed tuning strategy has been discussed, aiming to achieve this goal. However since this strategy forces to consider values of the mesoscopic parameters which differ from the optimal ones required by stability, the universality of this strategy could be uncertain.

5.6 Developed numerical code

LBM is particularly successful for modeling flow through porous media, but it is computationally very expensive in terms of both floating point operations and storage needed to simulate real systems. For this reason, practical issues of implementation

can be very important in order to produce an efficient numerical code. Moreover, large parallel computing is a prerequisite for most lattice Boltzmann simulations, and computational limitations will continue to be a significant constraint for the foreseeable future for a wide range of porous medium systems [180].

A parallel numerical code which implements the lattice Boltzmann scheme discussed in the previous section was developed. A brief description of the main characteristics of the code is reported in the following and an example is discussed in order to understand the parallelization strategy and the consequent communications among computational nodes.

5.6.1 Flow chart

Essentially, the numerical code developed can be divided into two main parts: the Pre-processing Task and the Calculation Task.

1. *Pre-processing Task*

   (a) *Initialization*

   During this step, the parallel code is automatically copied on all the active nodes of the cluster by the *master node*. The master node is arbitrarily selected among the cluster machines in order to manage the I/O of the parallel code with all other *slave nodes*. Essentially the numerical code is always the same but different portions of it are activated according to the nature of the considered node. During this step, the user-defined input data are loaded by the master node, the lattice parameters are consequently calculated, stored in data structures and then sent to the slave nodes. Each node accordingly initializes some memory structures but the

memory allocation is still minimum because the actual dimensions of the problem have not been defined yet.

(b) *Grid refinement*

Randomly generated porous media can be uniquely defined by means of the *physical topology* which defines the locations of the solid obstructions with respect to the allowed fluid streams. Some additional details concerning how to produce a randomly generated porous medium will be discussed later on. It is worth to point out here that the spatial discretization step, used to simulate fluid flow in porous media, cannot be of the same order of the pore sizes, but rather it should be smaller, for producing reliable mesh-independent results. For this reason, during this step the physical topology of the porous medium is discretized by a given refinement ratio in order to produce a *computational topology* which is fine enough to be accurate.

(c) *Mesoscopic tuning strategy*

During this step, the microscopic lattice parameters are calculated according to the mesoscopic tuning strategy in order to match the user input data for the macroscopic transport coefficients. Essentially, the relaxation time constants τ_σ^0, τ_m^0 are calculated by means of Eqs. (5.187) and (5.190) and the lattice velocity, c, by means of Eq. (5.188) or Eq. (5.191). The grid refinement strongly affects the actual values of the lattice parameters. In particular it reduces the relaxation constants (τ_σ^0, $\tau_m^0 \propto \delta x^2$) and increases the lattice velocity ($c \propto \delta x^{-1}$). Since the dimensionless time frequencies must satisfy the stability constraint, the first effect is particularly critical because it forces to consider smaller time steps too.

(d) *Domain decomposition*

During this step, the computational domain is divided into smaller portions according to the decomposition strategy and each one of them is sent to a slave node of the cluster. In the following, a very easy strategy has been adopted which essentially leads to decompose the domain in equivalent-sized portions of the lattice distributed among each processor, without taking into account the pore distributions of the specific porous medium. This strategy has been selected because, for a homogeneous porous medium, some researchers suggest that the load imbalance among different processors is negligible [181, 182]. However, some limits exist for this easy decomposition [180] and they will be discussed in the next section. At this point, all the nodes of the cluster will perform the same operation on their sub-domain under the co-ordination of the master node.

(e) *Topology labeling*

Many previous implementations of LBM to simulate flow in porous media are based on a full lattice representation in which both fluid and solid lattice sites are stored and computed in a regular computational grid. The limits of this approach have been recently discussed in detail [180]. This approach leads to straightforward parallel processing implementations but is wasteful in floating point operations and storage. This is so because lattice points that fall within a solid phase are not needed to solve the flow field: one needs only to know their existence and geometric distribution [180]. For this reason, in the developed numerical code only the fluid cells are stored and computed. The available cells where the fluid flow can exist are identified by a *local labeling* without taking care of the

mutual arrangement. Having lost the natural ordering, neighboring nodes are no longer immediately known, so the neighboring information has to be added locally [180]. This can be easily obtained by means of the following auxiliary data structure

$$\langle L|_n = \left[n,\, i,\, j,\, n_E^1,\, n_N^2,\, n_W^3,\, n_S^4,\, n_{NE}^5,\, n_{NW}^6,\, n_{SW}^7,\, n_{SE}^8\right]. \tag{5.200}$$

For each fluid cell n, the physical coordinates (i and j in the two dimensional example) and the labels of the neighboring cells (n^λ) are stored (see Fig. 5.1 for labeling). This allows us to perform calculations in a serial form without taking care of the actual computational topology any more. Obviously filling the previous data structure can be quite demanding in terms of computational resources but, since this step is performed independently by each slave node, it is naturally parallel.

After the preliminary steps, the actual calculations can start.

2. *Calculation Task*

   (a) *Collision*

   As previously discussed, the collisional operator involved in Eq. (5.181) is assumed constant during each time step. This assumption introduces a second-order truncation error, which has been canceled out by means of the corrected velocities. The main advantage of this is the possibility to decouple the resolution of the BGK-like equation (5.181) into three easier steps, i.e. *moment calculation step*, *collision step* and *streaming step*. Once both the discrete Maxwellian equilibrium distribution functions, i.e. $\varphi_\sigma^{e\,\lambda\star}$ and $\varphi_{\sigma(m)}^{e\,\lambda\star}$, are evaluated by using the macroscopic quantities for the generic

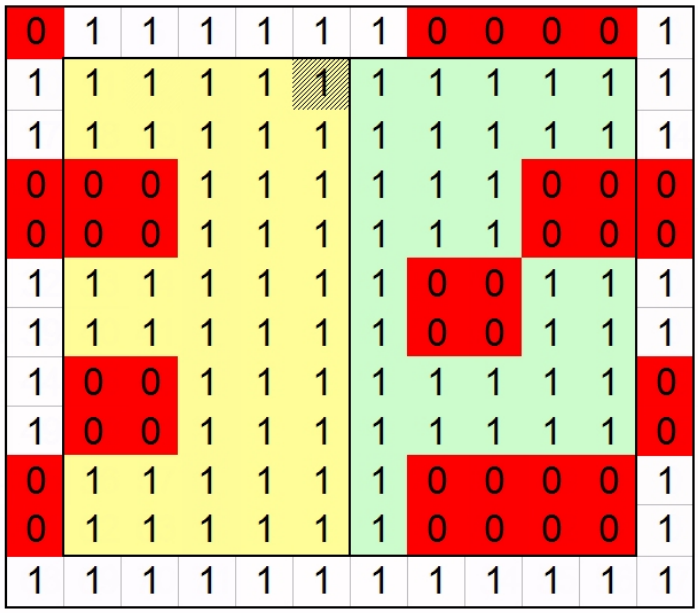

Figure 5.5: Simple example of randomly generated porous medium, where the solid obstructions are identified by the label "0". It must be imagined that the reported computational domain is repeated in both directions an infinite number of times because of the periodic boundary conditions.

species and for the mixture respectively, the following values

$$\begin{aligned} \varphi_\sigma^{\lambda\oplus} &= \varphi_\sigma^\lambda - \chi_H \frac{\delta t}{\tau_\sigma^0}\left[\varphi_\sigma^\lambda - \varphi_\sigma^{e\,\lambda\star}\right] - \epsilon\,\frac{\delta t}{\tau_m^0}\left[\varphi_\sigma^\lambda - \varphi_{\sigma(m)}^{e\,\lambda\star}\right] \\ &+ \frac{\delta t}{\sqrt{e_\sigma}}\,\mathbf{k}_{\alpha(\sigma)}^{\lambda\star}\cdot\left[\,d_\sigma\,\mathbf{g}_\sigma + (1-d_\sigma)\,\mathbf{w}_\sigma^\star/\tau_m\,\right], \end{aligned} \tag{5.201}$$

can be calculated and stored for each grid node. The splitting of the evolution equation (5.181) in two steps doubles the memory need because in this way two quantities, i.e. $\varphi_\sigma^{\lambda\oplus}$ and φ_σ^λ, must be stored for the same grid node.

(b) *Communications*

During this step, each node sends the boundary values of the discrete distribution functions to the corresponding nodes which are adjacent to the one considered in the global computational domain. In order to simplify the communications among slave nodes, some *ghost layers* of lattice points

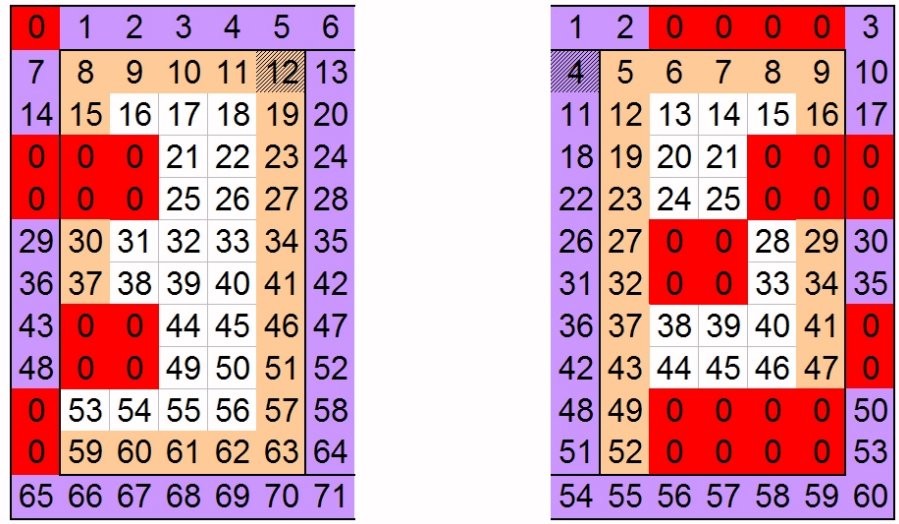

Figure 5.6: The computational domain reported in Fig. 5.5 has been split in two parts and a ghost one-cell-thick boundary of lattice cells has been added to each sub-domain. The sub-domain on the left is solved by the cluster node "0", while the sub-domain on the right is solved by the cluster node "1".

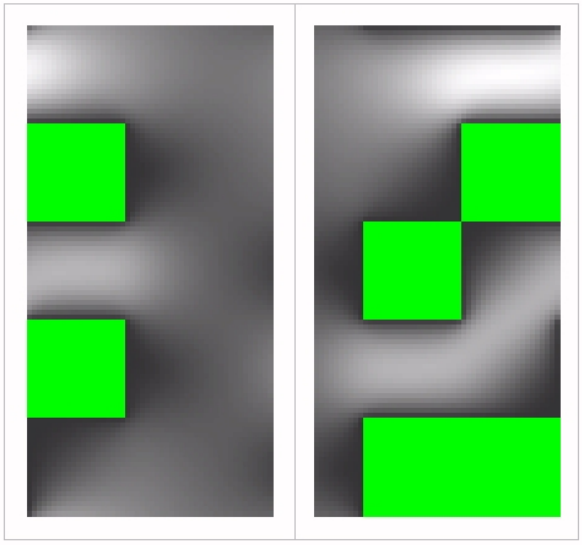

Figure 5.7: Velocity field contours of the fluid flow trough a randomly generated porous medium due to a given pressure gradient. Periodic boundary conditions in both directions are applied. The gray scale for the fluid cells has been tuned according to the local modulus of the velocity vector (lighter regions are characterized by higher velocities). The reported solution has been calculated by a simple two-node cluster and a refinement factor equal to 10.

Table 5.4: Communication tags among slave nodes for packaged data in a simple two-node cluster.

Sending Step													Receiving Step											
$0 \rightarrow 0$			$0 \rightarrow 1$			$1 \rightarrow 0$			$1 \rightarrow 1$				$0 \leftarrow 0$			$0 \leftarrow 1$			$1 \leftarrow 0$			$1 \leftarrow 1$		
λ	n_z	n	λ	n_z	n	λ	n_z	n	λ	n_z	n		λ	n_z	n	λ	n_z	n	λ	n_z	n	λ	n_z	n
2	1	8	**1**	**1**	**12**	1	1	9	2	1	5		2	1	1	1	1	13	1	1	10	2	1	2
2	2	9	1	2	19	1	2	16	2	2	6		2	2	2	1	2	20	1	2	17	4	1	55
2	3	10	1	3	23	1	3	29	2	3	7		2	3	3	1	3	24	1	3	30	4	2	56
2	4	11	1	4	27	1	4	34	2	4	8		2	4	4	1	4	28	1	4	35	4	3	57
2	5	12	1	5	34	1	5	41	2	5	9		2	5	5	1	5	35	1	5	50	4	4	58
4	1	59	1	6	41	1	6	47	4	1	52		4	1	66	1	6	42	1	6	53	4	5	59
4	2	60	1	7	46	3	1	5					4	2	67	1	7	47	**3**	**1**	**4**			
4	3	61	1	8	51	3	2	12					4	3	68	1	8	52	3	2	11			
4	4	62	1	9	57	3	3	19					4	4	69	1	9	58	3	3	18			
4	5	63	1	10	63	3	4	23					4	5	70	1	10	64	3	4	22			
			3	1	8	3	5	27								3	1	7	3	5	26			
			3	2	15	3	6	32								3	2	14	3	6	31			
			3	3	30	3	7	37								3	3	29	3	7	36			
			3	4	37	3	8	43								3	4	36	3	8	42			
			3	5	53	3	9	49								3	5	43	3	9	48			
			3	6	59	3	10	52								3	6	48	3	10	51			
			5	1	12	5	1	9								5	1	6	5	1	3			
			6	1	8	6	1	5								7	1	65	6	1	1			
			7	1	59	7	1	52								8	1	71	7	1	54			
			8	1	63														8	1	60			

have been added to each of the sub-domains. Let us consider for example the randomly generated porous medium reported in Fig. 5.5 and let us suppose to calculate the fluid flow trough it by means of a simple two-node cluster. The previous computational domain is split in two parts and a ghost one-cell-thick boundary of lattice cells is added. Then the local labeling is independently performed by each sub-domain. The final result is reported in Fig. 5.6. It is worth to point out that the additional boundaries are selected in such a way that the ghost cells for one sub-domain are computational cells for the other sub-domain. In the reported example, the cell locally labeled "12" in the sub-domain on the left (solved by the "node 0" of the cluster) corresponds to the cell locally labeled "4" in the sub-domain on the right (solved by the "node 1" of the cluster). Before proceeding with the streaming step, the values of the out-coming distribution functions must be sent to overwrite the incoming distribution functions in the corresponding ghost layers of the neighboring processors. In the reported example, the outcoming distribution functions at cell "12" for the sub-domain "0", i.e. $\varphi_\sigma^{5\oplus}$, $\varphi_\sigma^{1\oplus}$ and $\varphi_\sigma^{8\oplus}$ (see Fig. 5.1 for labeling), must overwrite the incoming distribution functions at cell "4" for the sub-domain "1". Because of the lattice simple structure, neighbor relationships between processors are readily known and there is no need to pass the local labeling of the fluid cell, which will be no more valid in the new sub-domain. In order to ensure the correct data exchange, both nodes independently produce two identification tags for the same data package. For the considered example, node "0" collects the discrete distribution functions of cell "12" in a data package and then it applies its identification

tag for sending it to node "1". This communication from node "0" to node "1", namely $0 \rightarrow 1$, will be

$$\langle D_S| = \left[0, 1, 1, 1, 12, \varphi_\sigma^{5\oplus}, \varphi_\sigma^{1\oplus}, \varphi_\sigma^{8\oplus}\right], \tag{5.202}$$

where the first elements of the vector are the sending node label (0), the receiving node label (1), the central direction (1) which identifies the sent triplet of discrete distribution functions (5,1,8), the sub-zone label (1) which allows us to distinguish triplets belonging to different cells but with the same central direction and, finally, the discretized distribution functions. The receiving node prepares a similar structure for the previous communication, namely $1 \leftarrow 0$, organized as follow

$$\langle D_R| = \left[1, 0, 3, 1, 4, \varphi_\sigma^{5\oplus}, \varphi_\sigma^{1\oplus}, \varphi_\sigma^{8\oplus}\right], \tag{5.203}$$

where the first elements of the vector are the receiving node label (1), the sending node label (0), the central direction flipped according to the bounce-back rule (3) which identifies the sent triplet of discrete distribution functions (5,1,8), the sub-zone label (1) and, finally, the discretized distribution functions. The previous data structures can properly match because, even though the local labeling is different ("12" for node "0" and "4" for node "1"), the central direction, and the sub-zone label are the same for both the nodes, if the same rule is used for labeling the cells. The receiving node simply overwrites the data fields and it has immediately the new label for the updated cell. All the communication tags for the simple two-node cluster are reported in Tab. 5.4, where the detailed example is reported in bold face. The same communication strategy can be applied for a larger number of cells due to grid refinement. In Fig. 5.7,

the numerical results for the discussed example are reported with a refinement factor equal to 10, which means that each cell shown in Fig. 5.5 has been simulated with 10×10 computational cells. All the nodes must be synchronized before proceeding to the streaming step for ensuring that the update of ghost layers has been completed, otherwise the interconnection among split sub-domains would not be correct.

(c) *Streaming*

The discrete distribution functions are updated by moving them according to the allowed directions of the considered lattice, namely

$$\varphi_\sigma^\lambda \left(t + \delta t, \mathbf{x} + \mathbf{v}^\lambda \delta t\right) = \varphi_\sigma^{\lambda\,\oplus}. \tag{5.204}$$

If the spatial grid has been constructed in such a way that it matches the lattice nature, i.e. $\delta x = c\,\delta t$, then the discrete distribution functions hop from the considered node to the neighboring ones.

(d) *Boundary conditions*

All the values of unknown discrete distribution functions for the inward-pointing links are evaluated. For links that refer to nodes out of the computational domain, Maxwellian distribution functions (inlet ports) or extrapolated data (outlet ports) are applied. For links out-coming from solid obstructions the wall interaction rule can be applied, which essentially is a linear combination of the bounce-back rule and the ideal reflection rule by means of parameter R. According to Eq. (5.120), the parameter R can be tuned in order to recover no-slip flow or slip flow depending to the local Knudsen number. The local Knudsen number requires an estimation of a local meaningful length for characterizing the fluid flow. This can be done

by means of the off-diagonal components of the stress tensor. In the LBM it is very easy to calculate every hydrodynamic moment for a single cell.

(e) *Moments*

During this step, the conserved hydrodynamic moments are calculated by means of the discrete distribution functions. At the same time, the previous quantities must be corrected according to Eq. (5.183) in order to cancel out the discrete lattice effects.

(f) *Convergence check*

All the steps of the calculation task must be repeated for every time step until the steady state conditions are obtained. Practically the calculation ends when a given convergence check is satisfied. The converge check can be a proper combination of the time rates of change for velocity and density/pressure fields.

5.6.2 Challenges of large parallel computing

The calculations by LBM for fluid flow in porous media can be quite demanding in terms of computational resources. Parallel computing is an useful tool for reducing the computational time and increasing the number of simulations to a reasonable value. Some details concerning parallel computing and the preliminary performance of the developed code are discussed in this section.

Before proceeding with the analysis of the parallel code, let us introduce some useful concepts:

- N, the number of nodes involved in the parallel calculation considered;
- WT_N, the wall clock time, which is the real physical time perceived by the final user;

Table 5.5: Scaling analysis for the test reference case reported in Fig. 5.8.

Number of Nodes [−]	Time due to Pre-processing Task [s]	Time due to Calculation Task [s]	Total Time [s]
1	407	1198	1605
4	22	403	425
8	7	195	202
16	2	114	116
32	1	81	82
48	<1	78	79

- $CT_N = WT_N \times N$, the CPU time which describes the calculation load for the cluster;
- CT_N^P, the pre-processing CPU time which describes the calculation load for the cluster due to the Pre-processing Task;
- CT_N^C, the calculation CPU time which describes the calculation load for the cluster due to the Calculation Task;
- $SpUp_N = WT_1/CT_N$, the speed-up efficiency which essentially compares the wall clock time due to single-node calculations (WT_1) and the actual CPU time due to the simultaneous utilization of N computational nodes ($CT_N = WT_N \times N$).
- $1/SpUp_N = (CT_N^P + CT_N^C)/WT_1$, the speed-up inefficiency which essentially compares the actual CPU time due to the simultaneous utilization of N computational nodes, subdivided between pre-processing and calculation time ($CT_N = CT_N^P + CT_N^C$), and the wall clock time due to single-node calculations (WT_1).

A reference test case shown in Fig. 5.8 has been reported for benchmarking. This makes use of a porous medium defined by a physical grid of 33×33 elementary cells,

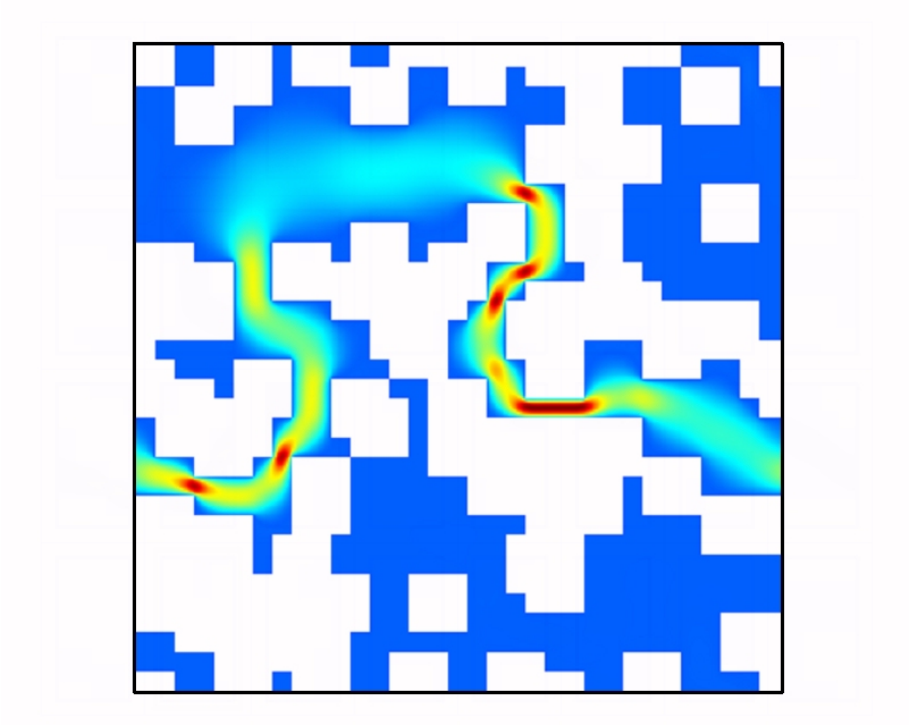

Figure 5.8: Velocity field contours of the fluid flow trough a randomly generated porous medium due to a given pressure gradient. Periodic boundary conditions in both directions are applied.

which can be available or not for fluid flow according to the porosity considered (50 %). The reported test is based on a single-class granulometry, which means that all the obstructions are characterized by the same size.

In order to produce mesh independent results, the computational grid size was chosen to be 8 times smaller than that of the physical one. For this reason, the number of computational cells increased (264×264) but only the cells available for fluid flow had to be considered (264×264×0.5 = 34,848). Since the discrete lattice considered is characterized by 9 microscopic velocities, the rough number of unknowns for this case is 313,632 (order 10^5), which is enough for benchmarking purposes. In the following calculations, an increasing number of nodes was considered (1, 4, 8, 16, 32, 48) in order to analyze the speed-up efficiency. The computational domain was automatically split

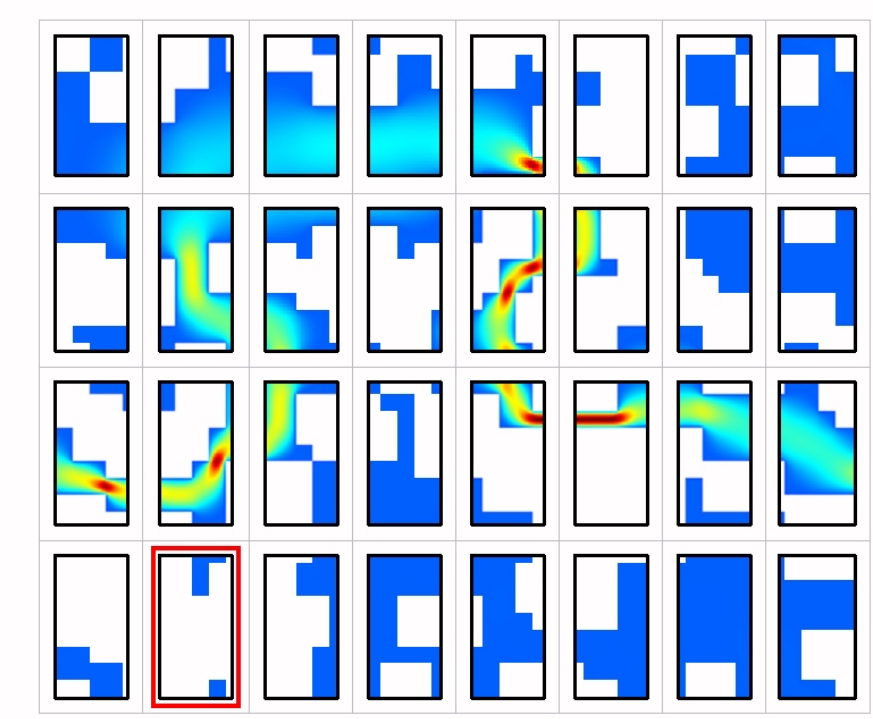

Figure 5.9: Velocity field contours of the fluid flow trough a randomly generated porous medium due to a given pressure gradient. Periodic boundary conditions in both directions are assumed. The reported solution has been calculated on a 32 node cluster.

by the code among the available nodes during the Pre-processing Task. The split parallel solution for the test reference case, when 32 computational nodes were used, is reported in Fig. 5.9. The numerical results for the scaling analysis are reported in Tab. 5.5. Finally, the calculated inefficiencies (reciprocal of the efficiency) are shown in Fig. 5.10.

The preliminary results are positive and a significant speed-up occurs, at least for a limited number of nodes ($N \leq 16$). For a higher number of nodes $N > 16$, the parallelization reduces its effectiveness. This is essentially due to unbalanced decomposition. Let us consider again Fig. 5.9, which shows the computational cells where the equations are solved. According to the considered porosity (50 %), the number of computational cells roughly equals the number of the solid cells where the

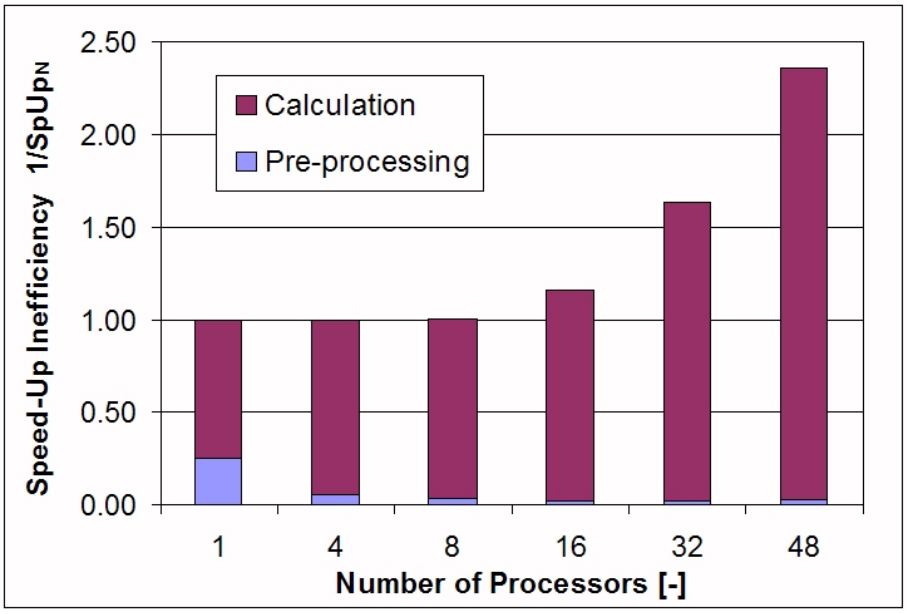

Figure 5.10: Speed-up inefficiency for the test reference case. For larger numbers of nodes the computational need due to Pre-processing Task becomes negligible.

equations are not solved. When the computational domain is decomposed among cluster nodes, this balance is no more satisfied for every node. For example, the bordered subdomain in Fig. 5.9 involves only few computational cells and, at a generic time step, the corresponding node will complete its work much faster than other overloaded nodes. Hence the code still needs some optimization. At any rate, the pre-processing receives a great benefit from parallelization and essentially does not affect the whole process time for a high number of nodes. The pre-processing is an additional step which simplifies the computational step on complex topologies and the parallel results confirm that it is a winning strategy for this problem.

The reported test reference case shows that even for simulations of a homogeneous porous geometry, substantial load imbalance can occur if a large number of processors is used [180]. The claim that for a homogeneous porous medium the load imbalance among different processors is negligible [181,182] cannot be considered a general result.

The reason is that homogeneity exists only at a sufficiently large scale for certain types of media and this assertion is not the case if a large number of processors are used [180].

The current parallel version of the code needs better strategies for domain decomposition in order to avoid the previous problem. The test reference case is enough to understand that this issue is particularly critical for a randomly generated porous medium. In particular, the elementary partitioning strategy shows its limits and in the end can reduce the effectiveness of parallelization. Some promising ideas are optimized rectilinear partitioning and most of all orthogonal recursive bisection [180,182]. In the first case, the grid is split into rectilinear-shaped sub-domains such that the workload is balanced. In the other case, orthogonal recursive bisection is a partitioning technique which subdivides the computational domain into equal parts of work by successively subdividing along orthogonal coordinate directions [182]. This second strategy is currently under investigation in order to implement it in the numerical code.

5.6.3 Practical issues of implementation

In this section, some practical issues of the parallel version of the developed lattice Boltzmann code are discussed. The current version of the code is composed of 54 functions (over 9,800 lines of code) and it has been developed from scratch in C++ in order to take advantage of flexible object-oriented programming and dynamic memory data structures.

The first issue means that C++ supports the data abstraction and the possibilities to express type hierarchies. This feature allows us to collect data together, which are logically related each other, as data fields of an unique structure and to work on

it by achieving solutions that would otherwise have required extra separate features. For example, all the discrete distribution functions are collected in the LatticeData structure and they are passed as unique data block to the different subroutines which define the main solver. Moreover, each data structure is characterized by some characteristic methods which allow us to perform specific tasks on the collected data. Considering again the example of the LatticeData structure, the hydrodynamic moments can be calculated by a call to a specific method belonging to the object class itself. The object-oriented programming can be integrated with pointers to data or pointers to data structures. In particular, for the streaming step there is no need to move the stored data in the physical memory but it is enough to modify the corresponding pointers, which are usually much smaller addresses pointing to previous quantities. Even though the same operations can be obtained by other languages, the previous operations are straightforward in C++.

In the framework of large parallel computing, data management based on dynamic memory allocation is even more important. In fact, the memory allocated by a particular node should be proportional to the actual size of the corresponding computational sub-domain assigned to it. In this way, the whole computational domain size can increase according to the number of nodes without requiring additional resources by each node. Otherwise the memory resources required by each node would be linked to the size of the whole problem, even though only a fraction of them would be actually used because of the domain decomposition.

The parallel numerical results were obtained on a cluster facility of the Virginia Tech (VT) Polytechnic Institute and State University (VA, U.S.A.). The VT cluster facility (ANANTHAM) is a 200 node Myrinet/switched Ethernet cluster. The essential hardware specifications of the individual nodes are:

- AMD Athlon 1.0 GHz CPU;
- 1 GB RAM,
- Myrinet PCI 64A (LANAI 7 CPU) 64 bit PCI SAN board,
- 100 Mbps Ethernet controller,
- 10.0 GB HDD (Maxtor 5400 RPM UDMA),

and the essential hardware specifications of the networking devices are:

- 7 Myrinet SAN switches (16 ports/switch each, for a total of 112 connections),
- 4 100 Mbps Ethernet switches (24 ports/switch each, for a total of 96 connections).

The essential software specifications are:

- Linux Operating System,
- MPICH 1.3 (includes C and C++ MPI bindings),
- OpenPBS 2.3 Portable Batch System (Batch Queueing System).

Essentially MPICH is a free communication library based on MPI technology [183]. This is an industry-standard library of routines for coordinating execution and communicating between processes in a parallel computing environment. Another VT cluster facility (SYSTEM-X) will be operational shortly and available for use with the developed code. This new facility is a 1100 Apple XServe G5 2.3 GHz dual processor cluster nodes (4 GB RAM, 80 GB HD), Mellanox switches / Cisco Gigabit Ethernet and it will be the fastest supercomputer at any academic institution in the world with its 12.25 Teraflops ("Top500 Data" for 2004).

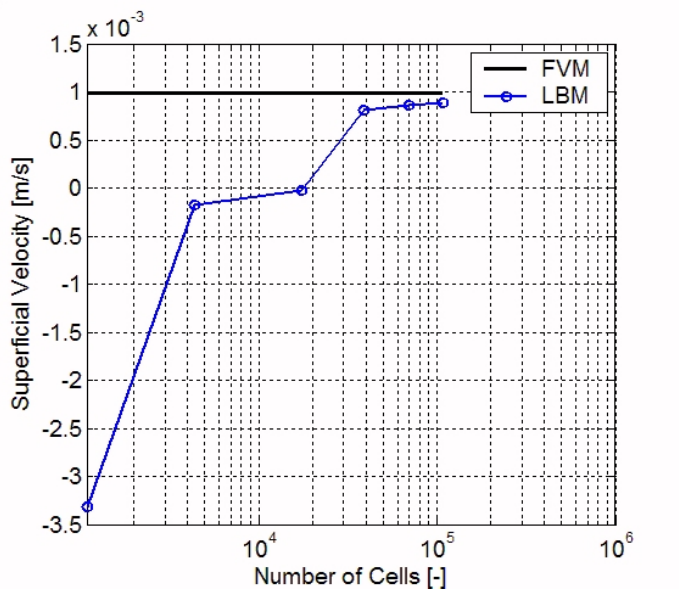

Figure 5.11: Comparison between the numerical results obtained by a commercial code based on FVM and the developed code based on LBM. The superficial velocity for the porous medium shown in Fig. 5.8 is reported. Some refinement factors are considered in order to verify the mesh-independence of the LBM results (FVM results are based on the maximum refinement).

5.6.4 Comparison with a conventional finite-volume solver

In order to validate the developed numerical code based on LBM, some benchmarking tests have been performed. In this section, a comparison with the commercial code FLUENT© based on a conventional finite volume method (FVM) is discussed.

The selected porous medium is the same previously considered and shown in Fig. 5.8. Essentially this porous medium is defined by a physical grid of 33×33 elementary cells, which can be available or not for the fluid flow according to the porosity considered (50 %). All the possible obstructions are characterized by the same size. The fluid flow in the porous medium is due to a given pressure gradient which has been implemented as a given forcing term in the momentum equation. This leads to a net fluid flow from the left to the right side of Fig. 5.8, where the contours of the velocity magnitude are reported by means of a properly filled scale.

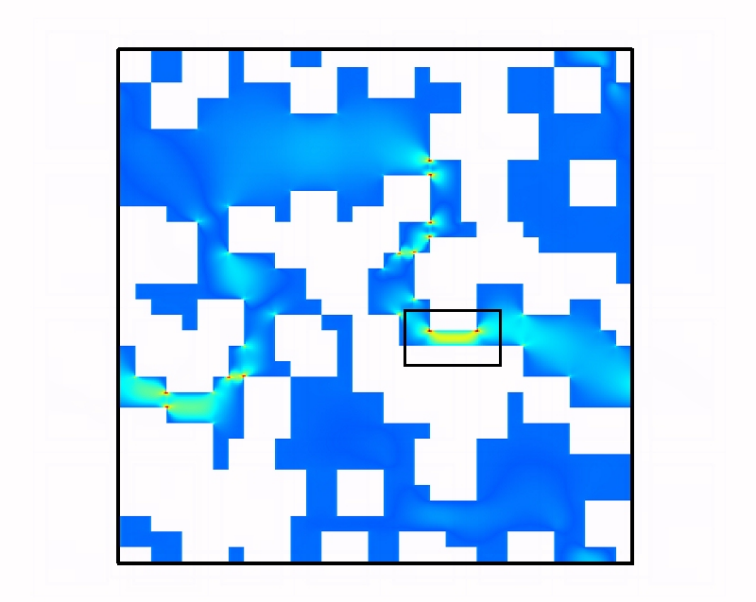

Figure 5.12: Contours of the discrepancy between velocity fields calculated by the FVM and the LBM with the the same maximum refinement factor (10). A proper filled scale normalized with the maximum local discrepancy which is roughly equal to 10% has been used.

The computational grid size was chosen once and for all to be 10 times smaller than that of the physical one in the calculations performed by FLUENT©, while a range of refinement factors (2, 4, 6, 8, 10) was chosen for the LBM calculations in order to verify that the results are effectively mesh-independent.

The numerical results of the superficial velocity for the considered porous medium due to both solvers are reported in Fig. 5.11. Even though the discrepancy between the two methods reduces by increasing the refinement factor, a residual non-negligible difference remains when the same maximum refinement factor (10) is considered. According to the multi-scale asymptotic analysis previously performed, the LBM is accurate up to second order in time and consequently in space within the fluid flow. Since the adopted discretization techniques considered by the FVM code have the same accuracy, the reason of the residual discrepancy could be ascribed to the

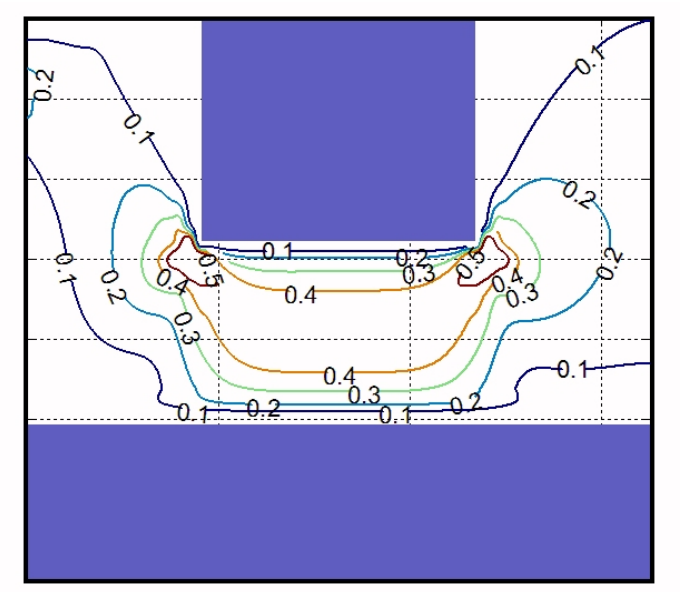

Figure 5.13: Contours of the discrepancy between velocity fields calculated by the FVM and the LBM with the the same maximum refinement factor (10) for the small portion shown in Fig. 5.12. The detailed labels of the contours are referred to the maximum local discrepancy which is roughly equal to 10%, i.e. label 0.5 identifies a discrepancy equal to 5%.

wall boundary treatment of LBM. This conjecture is confirmed by the contours of the discrepancy between the velocity fields reported in Figs. 5.12 and 5.13. The maximum local discrepancies are located close to the corners, where the bounce-back rule is no more able to ensure properly the no-slip boundary condition. In Fig. 5.13, the contours are reported for the small portion of the porous medium marked in Fig. 5.12 and they allow us to better understand that effectively the problem is located at the corners where the discrepancy is larger.

From the mathematical point of view, searching for a wall interaction rule at the generic corner which is able to satisfy the no-slip boundary condition seems an ill-posed problem, because the number of in-coming links of the discrete distribution function is not enough to ensure the zero velocity at both corner sides. Better wall interaction rules should be formulated.

5.7 Technological application

Discussing the relevant technological topics of the transcritical refrigerating cycles based on carbon dioxide, the important role of sealing has been outlined. The high working pressures of these transcritical cycles suggests that to seal carbon dioxide and minimize the leakage of the joints could be a critical issue for long-term operating devices. Since the current carbon dioxide circuits have several joints that need to be connected, sealing is a key design element [184].

Essentially there are two technologies which seem promising in order to realize reliable connections for carbon dioxide circuits:

- the *metal gaskets*, which offer the required low leakage rate but are usually more expensive;
- and the *rubber* or *polymeric gaskets*, which are characterized by higher permeation rate but are usually cheaper.

In addition to cost reasons, the previous technologies should be compared with regard to the possibility of realizing self-sealing. Depending on safety aspects when handling the system there might be requirements to avoid danger when opening a pressurized system. Actually, the trend in the regulation for carbon dioxide seems to avoid self-sealing systems, because they would create pressure drop, additional parts and costs. Hence low price and fixed installation are both reasons leading to prefer gaskets based on elastomers.

Despite the previous advantages, these gaskets could be characterized by unacceptable permeation losses. Unfortunately, especially carbon dioxide combines thermodynamic properties that lead to a high solubility as well as a moderate diffusion velocity in elastomers. Compared to other natural gases the permeation rate is there-

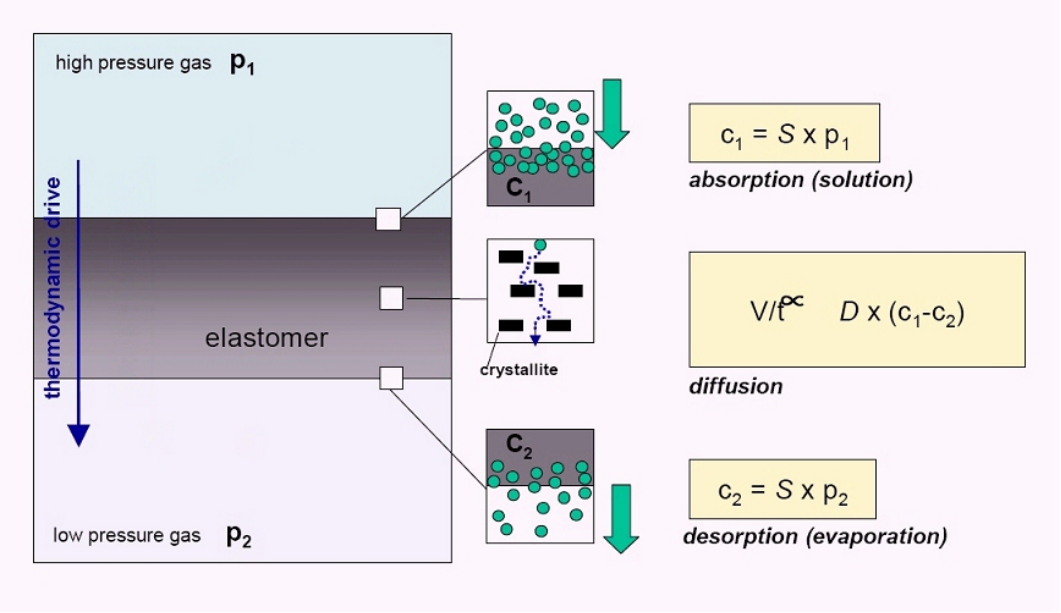

Figure 5.14: Entire permeation process of a gas through out a plane elastomer sample [184].

fore significantly higher.

The entire permeation process for a gas throughout a plane elastomer sample is reported in Fig. 5.14. As soon as a fluid is in contact with the surface of an elastomer for a sufficient time, gases can dissolve into the elastomer and move further by diffusion. The solution and transport process may cause modifications of the elastomer physical properties, which often lead to a decrease of the resistance to explosive decompression. The entire permeation process of a gas throughout a plane elastomer sample at moderately high pressures can be divided in three steps. Firstly the gas dissolves into the surface of the sample (absorption) according to Henry's law. The concentration of the gas dissolved is a linear function of the applied gas pressure with the slope proportional to Henry's coefficient. Hence gas diffusion from high pressure to low pressure side is governed by Fick's law, and finally evaporation into the low pressure gas region involves again Henry's law. The whole phenomenon

can be characterized by the permeation coefficient (permeability), which is defined as the product of diffusion coefficient and solubility coefficient [184, 185].

In the present application, the inlet and the outlet absorption phenomena will be neglected and for this reason the whole gas permeation is essentially governed by diffusion. The final goal is to calculate the diffusion velocity of carbon dioxide due to the applied pressure gradient throughout randomly generated porous media which mimic the microscopic topologies of actual elastomers.

5.7.1 Problem definition

First of all, the physical topology of the porous medium which mimics the microscopic structure of the elastomer must be defined. As discussed previously, the physical topology defines the locations of the solid obstructions with regard to the allowed fluid streams. At extreme pressures, the microscopic permeability of an elastomer is no longer a constant, but is reduced by the modification of the microscopic structure. This fluid-structure interaction will be neglected in the following calculations and the microscopic structure will be considered fixed. Otherwise it would be possible to take into account the effects due to compression and fluid-structure interaction by considering a reduced effective porosity.

The microscopic structure of the porous media can be measured directly by means of computer tomography, estimated by simulating the manufacturing process or randomly generated on the basis of an experimental granulometry law. The current version of the developed numerical code considers two-dimensional computational domains only and this limits strongly the possibility to compare the results of the numerical simulations with actual experimental measurements. For this reason, even though it represents the most promising opportunity of the proposed method, the

Table 5.6: Two randomly generated porous media with the same porosity (50%) but different granulometry laws: in topology (a) all the obstructions have the same size (3×3), while in topology (b) four different classes exist (1×1, 2×2, 3×3, 4×4).

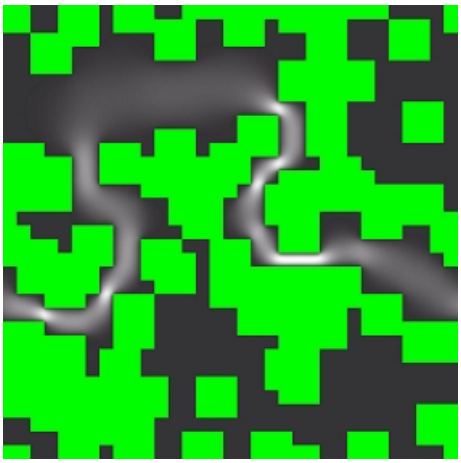

(a) Single-class granulometry.

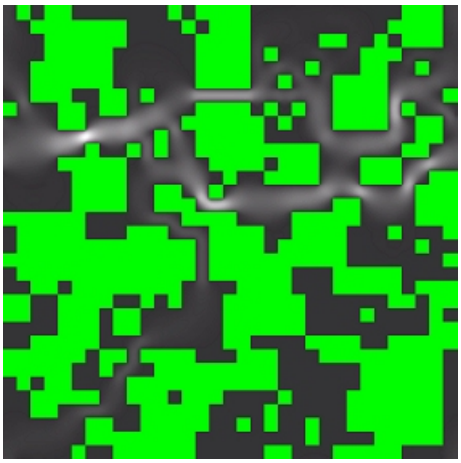

(b) Multi-class granulometry.

direct measurement by means of computer tomography has been discarded in this preliminary phase. For similar reasons, the considered porosities are unrealistically higher than actual ones of practical gaskets, which are characterized by modest permeation velocities.

In the following calculations, the porous media will be randomly generated by means of a *granulometry law*. Essentially a porous medium is made by many solid obstructions which can have different sizes and the the granulometry law gives the probability of finding obstructions characterized by a given size. Let us define N_i^s the number of obstructions with a given size A_i^s and C^s the number of granulometry classes, i.e. the number of sets collecting obstructions with the same size. If the physical topology has N available cells which can be randomly occupied by the obstructions, then the porosity Π of the porous medium is

$$\Pi = 1 - \frac{1}{N} \sum_{i=1}^{C^s} N_i^s \, A_i^s. \tag{5.205}$$

The labeling of obstruction classes can be done in such a way as to consider the smaller

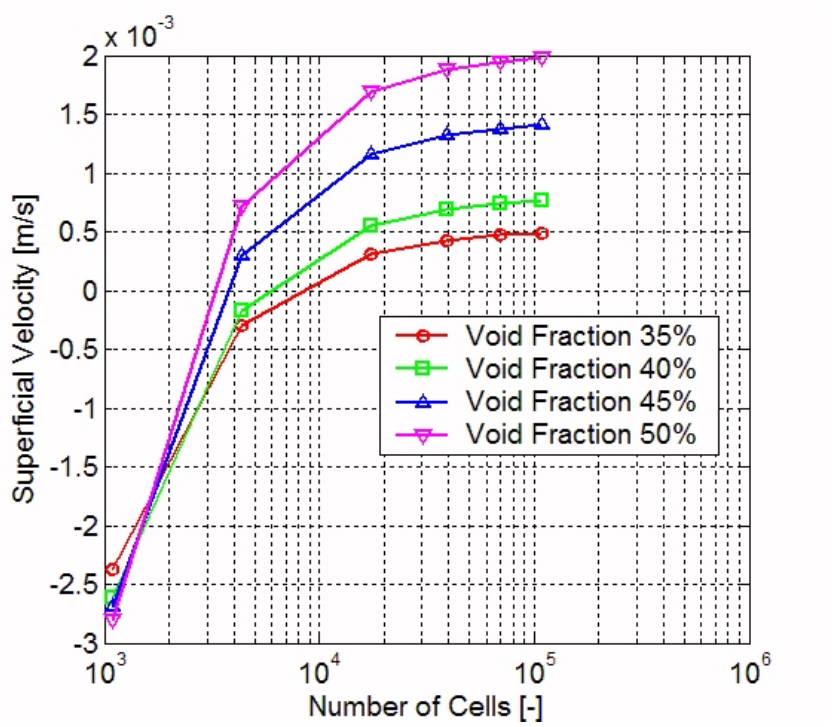

Figure 5.15: Superficial velocities for porous media characterized by different porosities. Some increasing refinement factors are considered.

obstructions first, namely $A_i^s = (i)^2$. The granulometry law gives the numerosity N_i^s of the generic class as a function of the previous labeling, i.e. as a function of the size, namely

$$N_i^s = \frac{K^s}{(i)^p} = \frac{1}{(i)^p} \frac{(1-\Pi)\, N}{\sum_{i=1}^{C^s} (i)^{2-p}}, \tag{5.206}$$

where K^s is a constant which can be expressed by Eq. (5.205) in order to make evident the relationship with porosity and $p \geq 0$ is a free tunable parameter. If $p = 0$, then all the classes have the same numerosity $N_i^s = K^s$, while if $p = 2$, then each class gives the same contribution to the whole porosity because $N_i^s\, A_i^s = (1-\Pi)\, N/C^s$. In Tab. 5.6 two randomly generated porous media with the same porosity (50%) but different granulometry laws are reported. The porous medium (a) is made of obstructions with the same size (3×3), while the porous medium (b) has been generated by assuming $C^s = 4$ and $p = 2$.

Once the physical topology is defined, the computational topology can be defined by applying a refinement which is sufficient to ensure mesh independent results. In order to achieve this goal, some test cases with different porosities and different refinement ratios (2, 4, 6, 8, 10) have been considered. The numerical results for the superficial diffusion velocity are reported in Fig. 5.15. Reliable results are obtained with a refinement equal to 10, which means that a computational grid 10×10 is used to simulate the fluid flow in each physical cell. In this case, the numerical solutions very weakly depend on further increments of mesh size: the selected mesh has 330×330 elementary computational cells.

5.7.2 Numerical results

In this section, some numerical results are reported for characterizing the fluid flow of carbon dioxide in porous media with regard to the actual porosity and the applied pressure gradient. Since the developed numerical code is still two-dimensional, the physical likelihood of the microscopic topology has not been driven too far.

The computational domain considers a very small portion of a plane elastomer sample. Since the characteristic size of the computational domain is much smaller than the macroscopic thickness of the elastomer sample, periodic boundary conditions can be used if a portion of the bulk material far from both surfaces is considered. The usual macroscopic approach essentially combines Fick's and Henry's law in order to derive the general gas permeation equation, which can be expressed as

$$\rho \, \mathbf{u}_M = -k_P \, \nabla p. \tag{5.207}$$

In the previous equation, $\mathbf{u}_M$ is the averaged superficial diffusion velocity which can be estimated at macroscopic scale by integrating on the whole microscopic domain

the actual velocity field $\mathbf{u}$, namely

$$\mathbf{u}_M(x_c/2, y_c/2) = \frac{1}{x_c\, y_c} \int_0^{x_c} \int_0^{y_c} \mathbf{u}(x, y)\, dx\, dy, \tag{5.208}$$

where $x_c \times y_c$ are the sizes of the computational domain. The previous equation means that gas permeation from high to low pressure surface is governed by the pressure gradient according to the permeation coefficient k_P (permeability), which is defined as the product of diffusion coefficient and the solubility coefficient and has been shown to be pressure independent [184]. The previous equation can be expressed in dimensionless form, namely

$$Re_c^x = -Pe_c^x\, Gr_c^x, \tag{5.209}$$

where Re_c^x is the dimensionless Reynolds number, Pe_c^x is the dimensionless permeation coefficient, Gr_c^x is the dimensionless pressure gradient expressed as

$$Re_c^x = \frac{u_M^x\, \delta x_0}{\nu}, \tag{5.210}$$

$$Pe_c^x = \frac{k_P\, \nu}{\delta x_0^2}, \tag{5.211}$$

$$Gr_c^x = \frac{\delta x_0^3}{\rho\, \nu^2} \frac{\partial p}{\partial x}, \tag{5.212}$$

where δx_0 is the characteristic size of the smallest physical cell or equivalently of the smallest 1×1 obstruction.

The developed numerical code allows us to directly simulate the microscopic actual velocity field $\mathbf{u}$ and then, by means of Eq. (5.208), to calculate the averaged macroscopic velocity $\mathbf{u}_M$ and consequently the permeation coefficient too. For this reason, the developed numerical code allows us to calculate the permeation coefficient on the basis of the actual microscopic topology, instead of deriving it from experimental data. Even though common numerical codes for Navier-Stokes equations could

be used to solve the flow in each micro channel of the porous media, computational overhead and heavy post-processing render them unsuitable for solving the flow in porous material and obtaining the permeation constant. For the reported tests, the numerical tool could be any other conventional one and LBM has been considered for practical reasons of implementation. However, the methodological approach is mesoscopic because the averaged transport coefficient usually coming from experiments is directly calculated on the basis of a more fundamental phenomenon description.

Some numerical simulations have been performed in order to analyze the influence of different porous structures on the material permeation constant and to evaluate whether different structures with the same volume porosity behave differently with respect to fluid flow through them.

Unfortunately, the current version of the numerical code deals with computational domains which are much smaller than those required by accurate simulations of practical gaskets. For this reason, realistic porosities cannot be currently considered, because they are so small that the existence of, at least, one fluid stream in a computational domain, made of few grid nodes, cannot be ensured. The possibility of considering larger computational domains, i.e. of increasing the number of grid nodes, will allow us to describe much finer details of the microscopic topology, like, for example, the actual fluid streams concerning permeation, which are characterized by extremely reduced characteristic dimensions. For this reason in this work, the considered porosities were unrealistically larger than those of practical gaskets and, in particular, four porosities were selected (0.35%, 0.40%, 0.45%, 0.50%). Five increasing pressure gradients were considered, too.

For each combination in terms of porosity and applied pressure gradient, twenty randomly generated porous structures were analyzed, thus obtaining a distribution

Table 5.7: Randomly generated porous media.

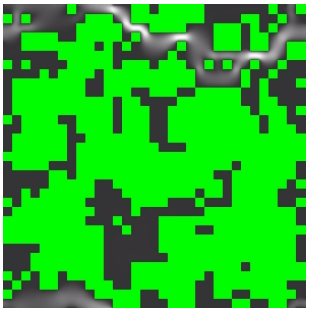

(a.1) Porosity 35%.

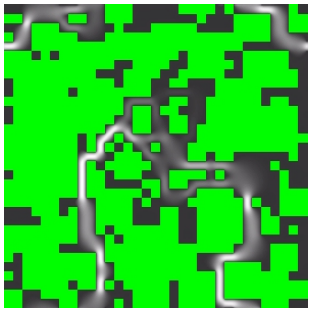

(a.2) Porosity 35%.

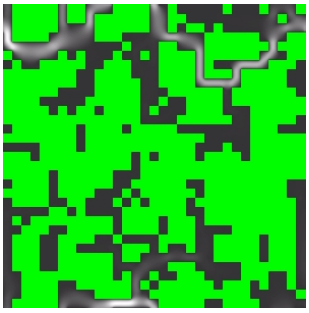

(a.3) Porosity 35%.

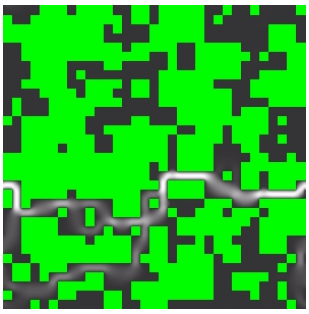

(b.1) Porosity 40%.

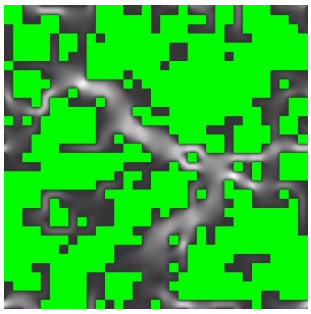

(b.2) Porosity 40%.

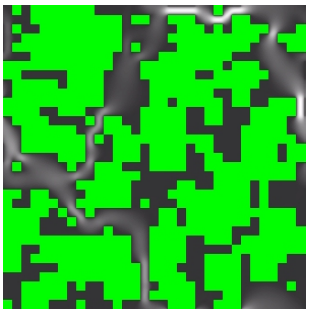

(b.3) Porosity 40%.

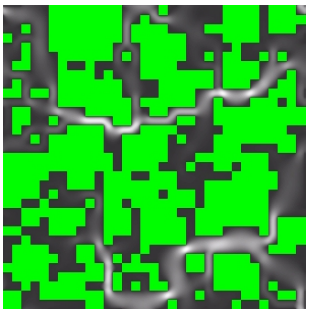

(c.1) Porosity 45%.

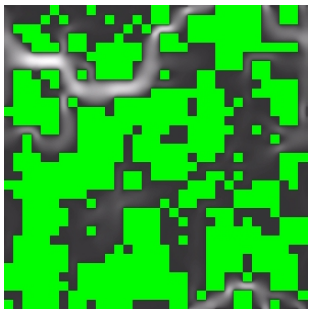

(c.2) Porosity 45%.

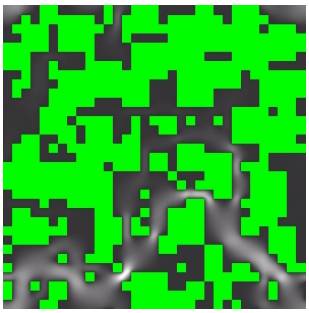

(c.3) Porosity 45%.

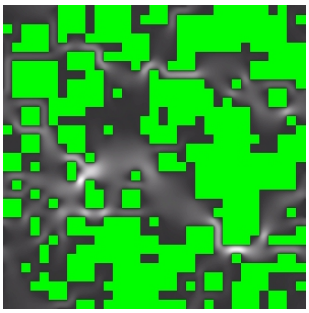

(d.1) Porosity 50%.

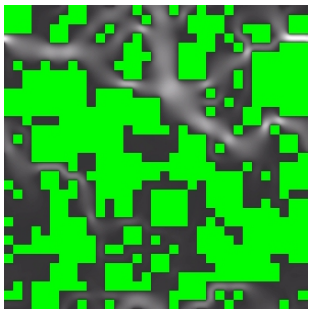

(d.2) Porosity 50%.

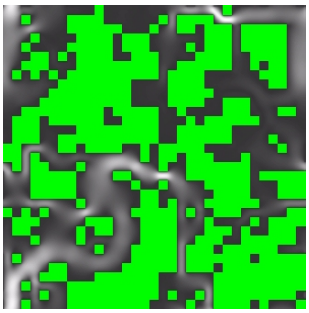

(d.3) Porosity 50%.

of values for the permeation constant. This last feature is usually neglected by the conventional approach, which considers macroscopic parameters sufficient to characterize uniquely the fluid flow and consequently the permeation constant. However, it is always possible to design, at least in principle, two different microscopic topologies characterized by the same macroscopic parameters, because they derive from some averaging procedures. For this reason, it is easy to prove that the macroscopic parameters are not sufficient to characterize the microscopic topology by considering figures reported in Tab. 5.7.

Each row of this table shows three porous media which share the same porosity and are subject to the same pressure gradient, but they lead to different velocity fields and consequently different averaged diffusion velocities. From the macroscopic point of view, it is clear that the three porous media have not the same permeation coefficient and that the porosity is not sufficient to uniquely characterize the microscopic fluid flow. For this reason, many equations have been proposed in order to calculate the permeation coefficient as a function of porosity and additional macroscopic parameters, like, for example, tortuosity. However, if more complex phenomena are considered (for example, reactive flows), the number of macroscopic parameters required to match the experimental data will increase accordingly and, at the end, it will be clear that a finite set of macroscopic parameters cannot exactly reproduce the actual microscopic phenomena.

The experimental plan was made of a $4 \times 5 \times 20$ factorial design, which required 400 numerical simulations. The numerical results are reported in Tab. 5.8. Taking advantage from the multiple simulations performed for each combination of porosity and applied pressure gradient, mean value and variance for the dimensionless Reynolds number of the fluid flow and the dimensionless permeability constant are

Table 5.8: Numerical results for fluid flow simulations in randomly generated porous media for varying porosity Π and increasing dimensionless pressure gradient $Gr_c^x = \delta x_0^3/(\rho\,\nu^2)\,(\partial p/\partial x)$. The mean value $M(x)$ and the corresponding variance $V(x)$ for the dimensionless momentum $Re_c^x = \delta x_0/\nu$ and the dimensionless permeation constant $Pe_c^x = k_D\,\nu/\delta x_0^2$.

		Gr_c^x				
Π		1.4E-05	7.0E-05	14.0E-05	70.1E-05	212.5E-05
0.35	$M(Re_c^x)$	2.70E-08	15.36E-08	30.64E-08	140.20E-08	422.64E-08
	$V(Re_c^x)$	1.28E-08	6.00E-08	15.42E-08	54.27E-08	143.61E-08
	$M(Pe_c^x)$	19.30E-04	21.91E-04	21.84E-04	20.00E-04	19.89E-04
	$V(Pe_c^x)$	9.15E-04	8.56E-04	11.00E-04	7.74E-04	6.76E-04
	V/M	0.4741	0.3906	0.5033	0.3871	0.3398
0.40	$M(Re_c^x)$	4.50E-08	23.82E-08	45.70E-08	187.62E-08	566.78E-08
	$V(Re_c^x)$	1.57E-08	9.76E-08	20.60E-08	122.02E-08	210.16E-08
	$M(Pe_c^x)$	32.12E-04	33.96E-04	32.58E-04	26.75E-04	26.67E-04
	$V(Pe_c^x)$	11.16E-04	13.92E-04	14.68E-04	17.40E-04	9.89E-04
	V/M	0.3489	0.4097	0.4508	0.6504	0.3708
0.45	$M(Re_c^x)$	6.19E-08	32.60E-08	75.42E-08	307.09E-08	804.26E-08
	$V(Re_c^x)$	2.17E-08	12.80E-08	23.97E-08	123.70E-08	303.00E-08
	$M(Pe_c^x)$	44.12E-04	46.49E-04	53.77E-04	43.79E-04	37.84E-04
	$V(Pe_c^x)$	15.50E-04	18.24E-04	17.09E-04	17.64E-04	14.26E-04
	V/M	0.3506	0.3926	0.3178	0.4028	0.3767
0.50	$M(Re_c^x)$	11.01E-08	56.33E-08	142.31E-08	641.20E-08	1666.96E-08
	$V(Re_c^x)$	5.37E-08	29.97E-08	64.15E-08	274.86E-08	1023.61E-08
	$M(Pe_c^x)$	78.46E-04	80.32E-04	101.46E-04	91.42E-04	78.43E-04
	$V(Pe_c^x)$	38.30E-04	42.74E-04	45.73E-04	39.19E-04	48.16E-04
	V/M	0.4877	0.5320	0.4508	0.4287	0.6141

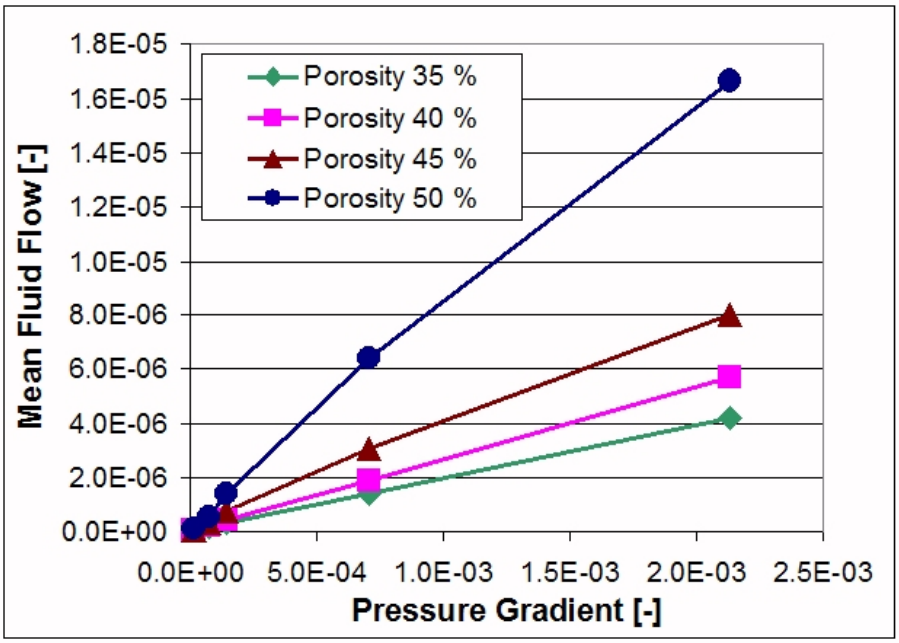

Figure 5.16: Mean values of the superficial velocity (Re_c^x) for porous media characterized by different porosities and subject to increasing pressure gradients (Gr_c^x).

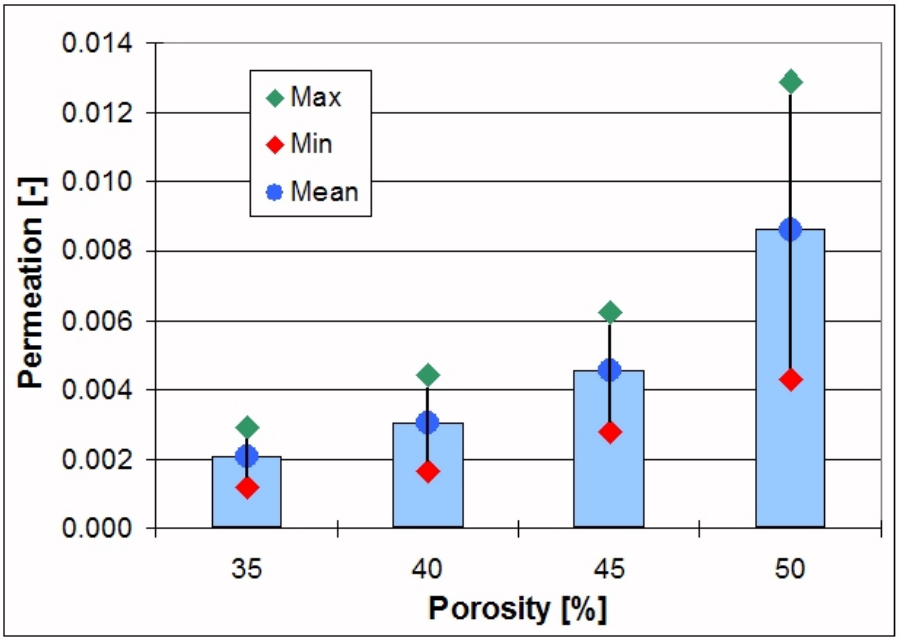

Figure 5.17: Mean values and corresponding variances of the calculated permeabilities (Pe_c^x) for different porosities.

reported. The analysis confirms the suitability of the linear law given by Eq. (5.209) for modeling fluid flow, because the dependence of velocity on the pressure gradient was found to be linear. This feature is evident in Fig. 5.16 where only the mean values are reported. Moreover numerical results confirm that the permeation coefficient dose not substantially depend on pressure [184, 185].

However, the permeability constant is found to vary considerably for different porous materials having the same volume porosity but different distributions of the solid particles in their structure. This confirms that porosity alone is not sufficient to properly characterize the material with regard to fluid flow. As Fig. 5.17 shows, the dependence of the permeation constant on material geometry greatly affects the accuracy of the estimation of the mass flow rate flowing through the porous media for a given pressure gradient. It is worth to point out that the variance of the permeation coefficients, i.e. the *absolute scattering* of the numerical results due to microscopic topology, obviously increases for higher porosities. On the other hand, the ratio between variance and average value of the permeation coefficient, i.e. the *relative scattering*, is substantially uncorrelated with porosity and applied pressure gradient. In fact, the results reported in Tab. 5.8 do not show a monotonic relationship between the relative scattering of the permeation coefficient, on the one hand, and both porosity and applied pressure gradient, on the other. This is probably due to the fact that twenty multiple simulations performed for each combination of porosity and applied pressure gradient are not sufficient for obtaining statistically consistent results concerning the relative scattering, which is much more difficult to be numerically investigated. It is obvious that a monotonic relationship of the relative scattering of the permeation coefficient with respect to porosity cannot exist, because, if null porosity (completely obstructed computational domain) or maximum

porosity (completely available computational domain) are considered, the fluid flow would be uniquely defined and the relative scattering would be consequently null. For this reason, if the relative scattering of the permeation coefficient has to be investigated, the number of simulations should be further increased in order to avoid the previous drawbacks.

The previous numerical results are preliminary because the two dimensional geometry and the maximum size of the computational domain strongly limits the actual practical importance of the simulations. However, the extension to three dimensional configurations does not change the substantial result, that is, the possibility for the microscopic topology to affect directly the macroscopic phenomena. For this application, thick elastomer slabs are usually considered and this naturally damps the scattering of the local fluid flow. This could not be the case for more complex flows, like those involving reactive flows.

5.8 Conclusions

In this chapter, a particular pseudo-kinetic technique for mesoscopic modeling, called Lattice Boltzmann Method (LBM), has been discussed and applied for simulating the microscopic flows of single species and/or mixtures in randomly generated porous media. This method offers some advantages reported in the following.

1. No linear system of algebraic equations must be solved and consequently there is no need for iterative procedures. The main solving loop is naturally a transient loop and this means that at each step the numerical solution satisfies the corresponding macroscopic equations with second order accuracy in both time and space.

2. There is no need for staggered grids because unphysical (chessboard-like [53]) solutions are automatically avoided. This means that both density/pressure and velocity are computed at the same locations. This feature is due to the fact that the advection term is discretized at kinetic level by approximating the substantial derivative which describes the time rate of change for the distribution function.

3. Additional local information is available in comparison with the conventional Finite Volume and Finite Element Method. As pointed out discussing the multi-relaxation-time formulation, the LBM can be considered a reformulation of the original Navier-Stokes equations by using the lower-order hydrodynamic modes as direct solving variables of the calculation. In this way, there is no need for interpolation in order to evaluate spatial gradients up to the second order because they are naturally included in the lower-order modes. For example, the Laplacian of the velocity field can be estimated in each cell without the need for involving neighboring cells.

4. Complex topologies can be efficiently included. Streaming step and bounce-back rule for implementing (both slip and no-slip) boundary conditions do not depend on the orientation of the solid obstructions. For this reason, the algorithm can be formulated without taking care of topological details (direction normal to the surface, available neighboring cells, ...).

5. The algorithm is naturally fitted for parallelization because the domain decomposition is eased by the existence of a lattice, the domain overlap needs to be only one cell wide and sub-domain boundary values are required only during the streaming step.

However some drawbacks still remain.

1. The solutions procedure is usually explicit in time for elementary formulations. This means that, if the lattice properties are set equal to physical ones, then the stability threshold ($\delta t/\tau < 2$) forces to consider very small time steps of the same order of the relaxation times, which for usual gases and ambient operating conditions are roughly equal to $10^{-11}/10^{-10}$ seconds. In this case, possible applications cannot extend further than micro-hydrodynamics. The problem is even more severe if some source terms in the continuity equations are considered in order to simulate, for example, chemical reactions. In this case, if direct simulation with lattice properties equal to physical ones is performed, then the whole simulation time would depend on the ratio between the source terms and the fixed time step and, in some cases, it could be quite long. The easy (but partial) way of solving the problem is to tune the lattice parameters in order to reproduce the same dimensionless groups which affect the fluid flow (Reynolds number, Prandtl number, Knudsen number, ...). This strategy works only when the considered phenomenon depend on few dimensionless groups. It is enough to consider a binary mixture with some chemical reactions for understanding that it is impossible to reproduce all the meaningful dimensionless groups at the same time without considering exactly the same physical properties.

2. The flexibility and the accuracy of models based on LBM depend on the whole number of tunable relaxation time constants because, in the best case, each one of them controls a macroscopic transport coefficient. If the relaxation time constants are few, then the consequent macroscopic picture of the phenomenon would be affected by an undesired (and unphysical in many cases) linking among the transport coefficients. For this reason, increasing the microscopic relaxation

time constants by multi-relaxation-time formulation or multi-lattice approach is very welcomed. However, sometimes this correlation among macroscopic transport coefficients due to relaxation time constants can open some useful insights into the investigated phenomenon. For example, discussing Hamel's model for binary mixtures allowed us to understand that cross collisions are responsible for both mutual diffusivity and viscous coupling among the species. For this reason, viscous coupling, i.e. modification of the stress tensor due to the presence of other gases, and mutual diffusivity can be explained by the same microscopic dynamics.

Chapter 6

Summary

For most engineering applications, microscopic dynamics merely determines material properties like fluid transport coefficients or porous medium permeability, which cannot be derived within the macroscopic framework. Since these material properties are simply measured experimentally, then the microscopic dynamics is largely irrelevant. From the practical point of view, in many cases simple heuristic formula can excellently work in order to calculate the averaged terms in simplified macroscopic equations used for taking into account the lower-scale phenomena.

In the previous chapters, a particular technological application, i.e. the transcritical refrigeration cycles with carbon dioxide, has been selected and four technological issues dealing with this application at different length scales (experimental test rig for airborne application, numerical simulation of compact heat exchangers, modeling of heat transfer phenomena close to the critical point and mesoscopic modeling of permeation by pseudo-kinetic methods), have been analyzed. Concerning the previous technological issues, it has been pointed out that some opportunities exist to usefully adopt a more fundamental modeling of lower-scale phenomena in order to solve practical problems. This is the case, for example, of undesired spurious conduction

in compact heat exchangers (which is not so relevant to justify the reduced diffusion of compact gascoolers), density fluctuations affecting the convective heat transfer (which are not the main responsible of discrepancies among heat transfer measurements) or unacceptable permeation rates of some gaskets (which is due essentially to the microscopic structure of the considered materials).

In this summary, a further (probably more important) remark is discussed. Even though in some specific cases a more fundamental explanation of the involved phenomena requires to overcome the usual averaged and/or homogenized models in order to recall the underlying phenomena, the microscopic dynamics is relegated to a subordinate role with respect to the high-level goals of engineering design. In conventional engineering, systems are built to achieve their goals by following rigid rules, which specify the detailed behavior of each of their component parts [105]. Their overall behavior must always be simple enough that complete prediction and often also analysis is possible. For this reason, microscopic dynamics must be suppressed because it is an intrinsically non-deterministic feature which could prevent from achieving the high-level goals. On the other hand, these dull machines resulting from conventional engineering design are not very suitable for dealing with complex unforeseeable situations. For example, it is evident that they realize lower performances than those of self-organizing biological systems.

This is the key point. Dull machines have no particular skill to manage complex situations because they are too simple themselves. They came from a design process which has systematically erased many effects coming from underlying microscopic dynamics and, in this way, any possibility of self-organization has been erased too. It is easy to see the counter-evidence of the previous remark. Let us consider again the Lattice Boltzmann Method. A generic model based on this method shows a coherent

self-organizing macroscopic behavior, called hydrodynamics, which can be described by means of the Navier-Stokes equations. For example in the simulation of fluid flow in porous media, these equations produce a velocity field coherent with the arrangement of the solid obstructions in the computational domain. From some points of view, the obtained velocity field can be considered as the "response" of the self-organizing system to a particular arrangement of the solid obstructions. The most surprising thing is that this self-organizing skill is not explicitly included in the LBM algorithm. The implemented coding rules are much simpler and they are based on collision and streaming only. The "response" in terms of complexity developed as a reaction to environmental stresses is not coded by rigid rules but naturally emerges from the underlying microscopic dynamics. The two essential ingredients of self-organizing complexity are the large number of components and the non-linear interaction among them. The clusters of artificial particles involved in LBM have both these features. After almost thirty years from the first lattice gas cellular automaton and almost fifteen years from the first lattice Boltzmann model, the most fascinating feature of these tools is still the self-organization attitude to deal with complexity.

How a large number of components can act together to perform complex tasks is not yet completely known. However if these principles could be found and applied, they would make a new form of engineering possible, which could be properly called *Complexity Engineering* [105].

Appendix A

Analysis of the Hamel model

An asymptotic analysis will be performed in order to recover the macroscopic equations for the lower-order moments, which derive from the simplified kinetic models defined by the previous Eqs. (5.123, 5.124, 5.125, 5.128). The Chapman-Enskog expansion technique [165] is very popular and it essentially consists of expanding the velocity distribution function in terms of a small parameter (Knudsen number) but not the macroscopic moments. It is well known that the Chapman-Enskog expansion can bring in solutions which are simply nonexistent [121,122], when the equations beyond the Navier-Stokes system are considered. Since in this case we limit our interest to the transport coefficients involved in the Navier-Stokes system, the Chapman-Enskog expansion will be considered.

Let us suppose to expand the velocity distribution function in terms of a small parameter K, which is proportional to the Knudsen number Kn:

$$f_\sigma = f_\sigma^{(0)} + K\, f_\sigma^{(1)} + K^2\, f_\sigma^{(2)} + \dots\,, \tag{A.1}$$

and to proceed in the same way for the partial derivatives:

$$\frac{\partial}{\partial\, t} = K\, \frac{\partial}{\partial\, t^{(1)}} + K^2\, \frac{\partial}{\partial\, t^{(2)}} + ..., \tag{A.2}$$

$$\frac{\partial}{\partial x_i} = K \frac{\partial}{\partial x_i^{(1)}} + ..., \tag{A.3}$$

$$\frac{\partial}{\partial v_i} = K \frac{\partial}{\partial v_i^{(1)}} + ... \tag{A.4}$$

The expansion of the gradient which involves the microscopic velocity (A.4) is quite unusual, but it is equivalent to the common practice of considering the effects of the external force field of the first order in the Knudsen number [164,177]. Both these approaches simplify the asymptotic analysis but nonetheless allow us to recover the correct source term in the momentum equation due to the external force field. Substituting the previous expansions in the kinetic model, given by Eqs. (5.123, 5.124, 5.125), a coupled hierarchy system of equations in the powers of K is obtained and the first elements of this system are:

$$f_\sigma^{(0)} = (1 - \alpha_\sigma) f_\sigma^e + \alpha_\sigma f_{\sigma(m)}^e, \tag{A.5}$$

$$\frac{\partial f_\sigma^{(0)}}{\partial t^{(1)}} + \mathbf{v} \cdot \nabla^{(1)} f_\sigma^{(0)} + \mathbf{g}_\sigma \cdot \nabla_{\mathbf{v}}^{(1)} f_\sigma^{(0)} = -\frac{1}{\alpha_\sigma \tau_m} f_\sigma^{(1)}, \tag{A.6}$$

$$\frac{\partial f_\sigma^{(0)}}{\partial t^{(2)}} + \frac{\partial f_\sigma^{(1)}}{\partial t^{(1)}} + \mathbf{v} \cdot \nabla^{(1)} f_\sigma^{(1)} + \mathbf{g}_\sigma \cdot \nabla_{\mathbf{v}}^{(1)} f_\sigma^{(1)} = -\frac{1}{\alpha_\sigma \tau_m} f_\sigma^{(2)}, \tag{A.7}$$

where $0 \leq \alpha_\sigma = \tau_\sigma / (\tau_\sigma + \tau_m) \leq 1$. The effects of the external force field in Eq. (A.7), which involves the terms $O(K^2)$, can be neglected. This practice is based on the fact that the non-equilibrium distribution function does not differ too much from the equilibrium distribution with regard to the microscopic velocity, in the fluid regime limit [176]. Equation (A.6) can be simplified by means of the first order of the expansion (A.5):

$$-\nabla_{\mathbf{v}}^{(1)} f_\sigma^{(0)} = (1 - \alpha_\sigma) \frac{f_\sigma^e}{e_\sigma} (\mathbf{v} - \mathbf{u}_\sigma) + \alpha_\sigma \frac{f_{\sigma(m)}^e}{e_\sigma} (\mathbf{v} - \mathbf{u}), \tag{A.8}$$

where the scale index of the velocity has been omitted $\mathbf{v}^{(1)} \rightarrow \mathbf{v}$ because it is the

dummy variable in the next integrals. Finally the system of equations becomes:

$$\begin{aligned}\frac{\partial f_\sigma^{(0)}}{\partial t^{(1)}} &+ \mathbf{v}\cdot\nabla^{(1)} f_\sigma^{(0)} = -\frac{1}{\alpha_\sigma\,\tau_m} f_\sigma^{(1)} \\ &+ (1-\alpha_\sigma)\,\frac{f_\sigma^e}{e_\sigma}\,\mathbf{g}_\sigma\cdot(\mathbf{v}-\mathbf{u}_\sigma) + \alpha_\sigma \frac{f_{\sigma(m)}^e}{e_\sigma}\,\mathbf{g}_\sigma\cdot(\mathbf{v}-\mathbf{u})\,, \qquad \text{(A.9)}\end{aligned}$$

$$\frac{\partial f_\sigma^{(0)}}{\partial t^{(2)}} + \frac{\partial f_\sigma^{(1)}}{\partial t^{(1)}} + \mathbf{v}\cdot\nabla^{(1)} f_\sigma^{(1)} = -\frac{1}{\alpha_\sigma\,\tau_m} f_\sigma^{(2)}. \qquad \text{(A.10)}$$

In order to recover the macroscopic equations for the moments of the velocity distribution function, the previous equations must be multiplied by the collisional invariants and then the integration over the microscopic velocity must be performed. Since the previous equations are coupled, this procedure will be useful only if the integral equations will be decoupled. In the single-fluid BGK model, it is easy to demonstrate that the higher-order terms due to the expansion of the distribution function, i.e. $f^{(\xi)}$ for $\forall\,\xi \geq 1$, do not affect the moments of the collisional invariants. In this case, since the first order of the expansion $f_\sigma^{(0)}$ is a linear combination of Maxwellian functions, which in general does not yield a Maxwellian function, this property does not hold anymore. The following similar conditions can be derived:

$$\int m_\sigma \sum_{\xi=1}^{\infty} K^\xi\, f_\sigma^{(\xi)}\, d\mathbf{v} = \int m_\sigma \left[f_\sigma - f_\sigma^{(0)}\right]\, d\mathbf{v} = 0, \qquad \text{(A.11)}$$

$$\begin{aligned}\sum_\sigma \frac{1}{\alpha_\sigma\,\tau_m} \int m_\sigma \mathbf{v} \sum_{\xi=1}^{\infty} K^\xi\, f_\sigma^{(\xi)}\, d\mathbf{v} &= \sum_\sigma \frac{1}{\alpha_\sigma\,\tau_m} \int m_\sigma \mathbf{v} \left[f_\sigma - f_\sigma^{(0)}\right]\, d\mathbf{v} \\ &= \frac{1}{\tau_m} \sum_\sigma \rho_\sigma\,(\mathbf{u}_\sigma - \mathbf{u}) = 0, \qquad \text{(A.12)}\end{aligned}$$

$$\begin{aligned}\sum_\sigma \frac{1}{\alpha_\sigma\,\tau_m} \int \frac{1}{2}\, m_\sigma\, \mathbf{v}^2 \sum_{\xi=1}^{\infty} K^\xi\, f_\sigma^{(\xi)}\, d\mathbf{v} &= \sum_\sigma \frac{1}{\alpha_\sigma\,\tau_m} \int \frac{1}{2}\, m_\sigma\, \mathbf{v}^2 \left[f_\sigma - f_\sigma^{(0)}\right]\, d\mathbf{v} \\ &= \frac{1}{2\,\tau_m} \sum_\sigma \rho_\sigma \left(\mathbf{u}_\sigma^2 - \mathbf{u}^2\right) \geq 0. \qquad \text{(A.13)}\end{aligned}$$

In particular, the condition (A.13) can be easily proved by remembering that the sum of the kinetic energies of the components must be greater than or equal to the

barycentric kinetic energy because of the deformation energy. This consideration allows us to suppose that each term of the series is positive and it can be upper bounded by the right hand side of the property (A.13). Since the previous relations must be satisfied for any small value of the parameter K, finally we obtain:

$$\int m_\sigma f_\sigma^{(\xi)}\, d\mathbf{v} = 0, \tag{A.14}$$

$$\sum_\sigma \mathbf{q}_\sigma^{(\xi)} = 0, \tag{A.15}$$

$$\sum_\sigma \varphi_\sigma^{(\xi)} \ll \frac{1}{2\,\tau_m} \sum_\sigma \rho_\sigma \left(\mathbf{u}_\sigma^2 - \mathbf{u}^2\right), \tag{A.16}$$

for any ξ-th perturbation ($\xi \geq 1$) of the velocity distribution function, where $\mathbf{q}_\sigma^{(\xi)}$ and $\varphi_\sigma^{(\xi)}$ are moments of the considered perturbation:

$$\mathbf{q}_\sigma^{(\xi)} = \frac{1}{\alpha_\sigma\,\tau_m} \int m_\sigma \mathbf{v} f_\sigma^{(\xi)}\, d\mathbf{v}, \tag{A.17}$$

$$\varphi_\sigma^{(\xi)} = \frac{1}{2\,\alpha_\sigma\,\tau_m} \int m_\sigma \mathbf{v}^2 f_\sigma^{(\xi)}\, d\mathbf{v}. \tag{A.18}$$

This means that the higher-order terms of the expansion for the distribution function can affect the moments of the collisional invariants for each species in such a way that the previous relations must hold.

Multiplying Eq. (A.9) by the collisional invariants and integrating over the microscopic velocity, the following equations are recovered:

$$\frac{\partial \rho_\sigma}{\partial t^{(1)}} + \nabla^{(1)} \cdot (\rho_\sigma \mathbf{u}_\sigma) = \alpha_\sigma\, \nabla^{(1)} \cdot (\rho_\sigma \mathbf{w}_\sigma), \tag{A.19}$$

$$\begin{aligned} \frac{\partial}{\partial t^{(1)}} \left[\rho_\sigma \left(\mathbf{u}_\sigma - \alpha_\sigma \mathbf{w}_\sigma\right)\right] \;&+\; \nabla^{(1)} \cdot \left[(1-\alpha_\sigma)\,\rho_\sigma \mathbf{u}_\sigma \otimes \mathbf{u}_\sigma + \alpha_\sigma\,\rho_\sigma \mathbf{u} \otimes \mathbf{u}\right] = \\ &- \; \nabla^{(1)} \left(\rho_\sigma e_\sigma\right) + \rho_\sigma \mathbf{g}_\sigma - \mathbf{q}_\sigma^{(1)}, \end{aligned} \tag{A.20}$$

$$\begin{aligned}\frac{\partial\left(\rho_\sigma e_\sigma^t\right)}{\partial t^{(1)}} &- \frac{\alpha_\sigma}{2}\frac{\partial}{\partial t^{(1)}}\left[\rho_\sigma\left(\mathbf{u}_\sigma^2-\mathbf{u}^2\right)\right]+\nabla^{(1)}\cdot\left[\rho_\sigma\left(e_\sigma^t\mathbf{u}_\sigma-\alpha_\sigma e_\sigma\mathbf{w}_\sigma\right)\right]= \\ &- \nabla^{(1)}\left[\rho_\sigma e_\sigma\left(\mathbf{u}_\sigma-\alpha_\sigma\mathbf{w}_\sigma\right)\right]+\frac{\alpha_\sigma}{2}\nabla^{(1)}\left[\rho_\sigma\left(\mathbf{u}_\sigma^2\mathbf{u}_\sigma-\mathbf{u}^2\mathbf{u}\right)\right] \\ &+ \rho_\sigma\left(\mathbf{u}_\sigma-\alpha_\sigma\mathbf{w}_\sigma\right)\cdot\mathbf{g}_\sigma-\varphi_\sigma^{(1)},\end{aligned} \tag{A.21}$$

where $\mathbf{w}_\sigma=\mathbf{u}_\sigma-\mathbf{u}$ is the diffusion velocity for the generic species and $e_\sigma^t=e_\sigma+\rho_\sigma\mathbf{u}_\sigma^2/2$ is the specific total energy.

Let us consider the effects of the first-order perturbation on the continuity equation. Multiplying Eq. (A.10) by the particle mass for the generic species, the following equation is recovered:

$$\frac{\partial\rho_\sigma}{\partial t^{(2)}}=-\alpha_\sigma\,\tau_m\,\nabla^{(1)}\cdot\mathbf{q}_\sigma^{(1)}. \tag{A.22}$$

In the derivation of the previous equation, Eqs. (A.19, A.20) have been applied. If Eq. (A.19) and Eq. (A.22) are summed, then the final result for the continuity equation is obtained:

$$\frac{\partial\rho_\sigma}{\partial t}+\nabla\cdot\left(\rho_\sigma\mathbf{u}_\sigma\right)=\alpha_\sigma\,\nabla\cdot\left[\rho_\sigma\mathbf{w}_\sigma-\tau_m\,\mathbf{q}_\sigma^{(1)}\right]. \tag{A.23}$$

According to the previously discussed definition given by Eq. (A.17), the general property given by Eq. (A.12) prescribes that the resultant of the vectors $\mathbf{q}_\sigma^{(1)}$, when all the mixture components are considered, must be zero, i.e. $\sum_\sigma\mathbf{q}_\sigma^{(1)}=0$. Since each parameter α_σ can be independently varied by setting the relaxation time constants for the corresponding species, the previous property implies that the vector $\mathbf{q}_\sigma^{(1)}$ cannot depend on α_σ. For this reason, the divergence involved in the right hand side of the previous equation does not explicitly depend on α_σ. In particular, if the relaxation time constants are properly set in such a way that $\alpha_\sigma=1$, then the considered model reduces to the single-fluid model with regard to the barycentric velocity. It has been shown by means of both Grad's moment method and the Chapman-Enskog expansion that this model satisfies the continuity equation [157,175]. For this reason,

it is possible to conclude that the $\mathbf{q}_\sigma^{(1)} = \rho_\sigma \mathbf{w}_\sigma / \tau_m$ and this result must be consider independent by the value of α_σ. For this reason, Eq. (A.23) reduces to Eq. (5.129).

Let us proceed in the same way for the momentum equation. Multiplying the previously discussed Eq. (A.10) by the particle momentum for the generic species and integrating over the microscopic velocity, the following equation is recovered:

$$\begin{aligned} \frac{\partial}{\partial t^{(2)}} \left[\rho_\sigma \left(\mathbf{u}_\sigma - \alpha_\sigma \mathbf{w}_\sigma \right) \right] &+ \alpha_\sigma \frac{\partial}{\partial t^{(1)}} \left(\rho_\sigma \mathbf{w}_\sigma \right) = \\ &- \nabla^{(1)} \cdot \left(\int m_\sigma \mathbf{v} \otimes \mathbf{v} \, f_\sigma^{(1)} \, d\mathbf{v} \right) - \mathbf{q}_\sigma^{(2)}. \end{aligned} \tag{A.24}$$

The previous Eqs. (A.19, A.20, A.21) will be used to simplify the analysis of the effects of the first-order perturbation to the momentum equation and in particular to calculate the integrals in the right hand side of the previous equation. Since the moments are linear integral forms of the distribution function, Eqs. (A.19, A.20, A.21) are essentially linear combinations of the Euler's equations for the generic species and for the single-fluid barycentric description. Unfortunately, these equations are non-linear with regard to the moments and for this reason it is convenient to reformulate them in the following way:

$$\frac{\partial \rho_\sigma}{\partial t^{(1)}} + \nabla^{(1)} \cdot \left[\rho_\sigma \mathbf{u}_{\alpha(\sigma)} \right] = 0, \tag{A.25}$$

$$\begin{aligned} \frac{\partial}{\partial t^{(1)}} \left[\rho_\sigma \mathbf{u}_{\alpha(\sigma)} \right] &+ \nabla^{(1)} \cdot \left[\rho_\sigma \mathbf{u}_{\alpha(\sigma)} \otimes \mathbf{u}_{\alpha(\sigma)} + \alpha_\sigma \left(1 - \alpha_\sigma \right) \rho_\sigma \mathbf{w}_\sigma \otimes \mathbf{w}_\sigma \right] = \\ &- \nabla^{(1)} \left(\rho_\sigma e_\sigma \right) + \rho_\sigma \mathbf{g}_\sigma - \mathbf{q}_\sigma^{(1)}, \end{aligned} \tag{A.26}$$

$$\begin{aligned} &\frac{\partial}{\partial t^{(1)}} \left(\rho_\sigma e_\sigma \right) + \frac{1}{2} \frac{\partial}{\partial t^{(1)}} \left[\rho_\sigma \mathbf{u}_{\alpha(\sigma)}^2 + \alpha_\sigma \left(1 - \alpha_\sigma \right) \rho_\sigma \mathbf{w}_\sigma^2 \right] + \nabla^{(1)} \cdot \left[\rho_\sigma \, e_\sigma \mathbf{u}_{\alpha(\sigma)} \right. \\ &\left. + O\left(|\mathbf{u}_{\alpha(\sigma)}|^3 \right) \right] = -\nabla^{(1)} \left[\rho_\sigma \, e_\sigma \mathbf{u}_{\alpha(\sigma)} \right] + \rho_\sigma \mathbf{g}_\sigma \cdot \mathbf{u}_{\alpha(\sigma)} - \varphi_\sigma^{(1)}, \end{aligned} \tag{A.27}$$

where $\mathbf{u}_{\alpha(\sigma)} = \left(1 - \alpha_\sigma \right) \mathbf{u}_\sigma + \alpha_\sigma \mathbf{u}$ is the linearly interpolated velocity. Since we are interested in the low Mach number limit, the terms which involve higher powers

of the velocities can be neglected. Applying Eqs. (A.25, A.26, A.27), the following expression can be recovered:

$$
\begin{aligned}
-\int m_\sigma \mathbf{v}\otimes\mathbf{v}\, f_\sigma^{(1)}\, d\mathbf{v} = -\alpha_\sigma\,\tau_m\,\Big[&\rho_\sigma e_\sigma \nabla\cdot\mathbf{u}_{\alpha(\sigma)} - \mathbf{u}_{\alpha(\sigma)}\cdot\mathbf{q}_\sigma^{(1)} + \varphi_\sigma^{(1)} \\
&+ \frac{1}{2}\,\alpha_\sigma\,(1-\alpha_\sigma)\,\frac{\partial\,(\rho_\sigma \mathbf{w}_\sigma^2)}{\partial t^{(1)}}\Big]\,\mathbf{I} + \alpha_\sigma\,\tau_m\,\Big[\rho_\sigma e_\sigma \nabla\mathbf{u}_{\alpha(\sigma)} + \rho_\sigma e_\sigma \nabla\mathbf{u}_{\alpha(\sigma)}^T \\
&- \mathbf{u}_{\alpha(\sigma)}\otimes\mathbf{q}_\sigma^{(1)} - \mathbf{q}_\sigma^{(1)}\otimes\mathbf{u}_{\alpha(\sigma)} + \alpha_\sigma\,(1-\alpha_\sigma)\,\frac{\partial}{\partial t^{(1)}}\,(\rho_\sigma \mathbf{w}_\sigma\otimes\mathbf{w}_\sigma)\Big]. \qquad \text{(A.28)}
\end{aligned}
$$

It is interesting to point out that the previous result does not depend on the external force field. If in both scalar and tensorial quadratic forms the effects due to the diffusion velocity are smaller than the effects due to the interpolated velocity, i.e. :

$$\mathbf{u}_{\alpha(\sigma)}^2 \;\gg\; \alpha_\sigma\,(1-\alpha_\sigma)\,\mathbf{w}_\sigma^2, \qquad \text{(A.29)}$$

$$\mathbf{u}_{\alpha(\sigma)}\otimes\mathbf{u}_{\alpha(\sigma)} \;\gg\; \alpha_\sigma\,(1-\alpha_\sigma)\,\mathbf{w}_\sigma\otimes\mathbf{w}_\sigma, \qquad \text{(A.30)}$$

then the time derivatives in the integral (A.28) can be neglected. Some hypotheses can be formulated about the effects due to the moments of the first-order perturbation too. According to the definition (A.17), the property (A.16) can be reformulated:

$$\sum_\sigma \varphi_\sigma^{(1)} \ll \frac{1}{2}\sum_\sigma \mathbf{q}_\sigma^{(1)}\cdot(\mathbf{u}_\sigma+\mathbf{u}) = \left[\sum_\sigma \mathbf{q}_\sigma^{(1)}\cdot\mathbf{u}_{\alpha(\sigma)}\right]_{\alpha_\sigma=1/2}. \qquad \text{(A.31)}$$

It is well known that both in fully-decoupled systems ($\alpha_\sigma = 0$) and in systems described by the single-fluid approach ($\alpha_\sigma = 1$), the moments of the perturbations do not affect the macroscopic equations. For the intermediate case ($\alpha_\sigma = 1/2$), the previous property demonstrates that the effects due to the lower-order moments of the perturbation prevail. As a first approximation, it is then reasonable to assume that the effects of $\varphi_\sigma^{(1)}$ can be neglected in Eq. (A.28). Substituting the simplified form of Eq. (A.28) into Eq. (A.24) and adding the result to Eq. (A.20), the momentum

equation for the generic species is obtained:

$$\begin{aligned}\frac{\partial\left(\rho_\sigma \mathbf{u}_\sigma\right)}{\partial t} &+ \nabla\cdot\left[\left(1-\alpha_\sigma\right)\rho_\sigma \mathbf{u}_\sigma\otimes\mathbf{u}_\sigma+\alpha_\sigma\,\rho_\sigma\mathbf{u}\otimes\mathbf{u}\right.\\ &+ \left.\alpha_\sigma\rho_\sigma\mathbf{u}_{\alpha(\sigma)}\otimes\mathbf{w}_\sigma+\alpha_\sigma\rho_\sigma\mathbf{w}_\sigma\otimes\mathbf{u}_{\alpha(\sigma)}\right]=\\ &- \nabla\left(\rho_\sigma e^c_\sigma\right)+\rho_\sigma\mathbf{g}_\sigma-\frac{1}{\tau_m}\,\rho_\sigma\mathbf{w}_\sigma\\ &+ \nabla\cdot\left\{\alpha_\sigma\rho_\sigma e_\sigma\tau_m\left[\nabla\mathbf{u}_{\alpha(\sigma)}+\nabla\mathbf{u}^T_{\alpha(\sigma)}\right]\right\},\end{aligned}\tag{A.32}$$

where e^c_σ is the corrected internal energy and its expression is:

$$e^c_\sigma = e_\sigma-\alpha_\sigma\,\mathbf{w}_\sigma\cdot\mathbf{u}_{\alpha(\sigma)}+\alpha_\sigma\,\tau_m\,e_\sigma\nabla\cdot\mathbf{u}_{\alpha(\sigma)}.\tag{A.33}$$

In the derivation of Eq. (A.33), it has been assumed that $|\mathbf{q}^{(1)}_\sigma| \gg |\mathbf{q}^{(2)}_\sigma|$ because the perturbations of the distribution function can be considered decreasing corrections of the previous terms in the expansion. In the small Mach number limit, the corrected internal energy can be confused with the internal energy, which is the leading term. For this reason, Eq. (A.32) reduces to Eq. (5.130).

Appendix B

Analysis of the discrete Hamel model

In this section, the Chapman-Enskog asymptotic analysis will be used in order to design a lattice Boltzmann model which recovers the performance of the continuous Hamel's model with second order accuracy in both time and space. In particular some corrections are needed for removing the unexpected discrete lattice effects. Let us start from the simple lattice Boltzmann model defined by Eqs. (5.178, 5.179). The macroscopic equations for the lower-order moments will be discussed. First of all, the left hand side of Eq. (5.178) is expanded by a Taylor series in δt up to the second order:

$$\frac{D_\lambda \varphi_\sigma^\lambda}{D t} + \frac{\delta t}{2} \frac{D_\lambda}{D t} \frac{D_\lambda \varphi_\sigma^\lambda}{D t} = -\frac{\chi_H}{\tau_\sigma^0} \left[\varphi_\sigma^\lambda - \varphi_\sigma^{e\,\lambda}\right] - \frac{\epsilon}{\tau_m^0} \left[\varphi_\sigma^\lambda - \varphi_{\sigma(m)}^{e\,\lambda}\right] + \frac{1}{\sqrt{e_\sigma}} \mathbf{k}_{\alpha(\sigma)}^\lambda \cdot \mathbf{g}_\sigma. \quad \text{(B.1)}$$

Then let us suppose to expand the normalized velocity distribution function φ_σ^λ in terms of a small parameter K, which is proportional to the Knudsen number Kn. The procedure is the same previously considered for the continuous model and it yields:

$$\varphi_\sigma^\lambda = \varphi_\sigma^{\lambda\,(0)} + K\,\varphi_\sigma^{\lambda\,(1)} + K^2\,\varphi_\sigma^{\lambda\,(2)} + \ldots\,. \quad \text{(B.2)}$$

We can analogously proceed for the partial derivatives given by Eqs. (A.2, A.3). In

this case, it is better to define a substantial derivative for the generic microscopic velocity of the lattice, by grouping together terms with the same order of magnitude:

$$\frac{D_\lambda^{(1)}}{D\,t^{(1)}} = \frac{\partial}{\partial\,t^{(1)}} + \mathbf{v}^\lambda \cdot \nabla^{(1)}. \tag{B.3}$$

Substituting the previous expansions in the simple model, a coupled hierarchy system of equations in the powers of K is obtained and the first elements of this system are:

$$\frac{D_\lambda^{(1)}\,\varphi_\sigma^{\lambda\,(0)}}{D\,t^{(1)}} = -\frac{1}{\alpha_\sigma\,\tau_m}\,\varphi_\sigma^{\lambda\,(1)} + \frac{1}{\sqrt{e_\sigma}}\,\mathbf{k}_{\alpha(\sigma)}^\lambda \cdot \mathbf{g}_\sigma, \tag{B.4}$$

$$\frac{\partial\varphi_\sigma^{\lambda\,(0)}}{\partial\,t^{(2)}} + \frac{D_\lambda^{(1)}\,\varphi_\sigma^{\lambda\,(1)}}{D\,t^{(1)}} + \frac{\delta t}{2}\,\frac{D_\lambda^{(1)}}{D\,t^{(1)}}\,\frac{D_\lambda^{(1)}\,\varphi_\sigma^{\lambda\,(0)}}{D\,t^{(1)}} = -\frac{1}{\alpha_\sigma\,\tau_m}\,\varphi_\sigma^{\lambda\,(2)}. \tag{B.5}$$

In particular the last term in the left hand side of Eq. (B.5) can be simplified by considering Eq. (B.4):

$$\frac{\partial\varphi_\sigma^{\lambda\,(0)}}{\partial\,t^{(2)}} + d_\sigma\,\frac{D_\lambda^{(1)}\,\varphi_\sigma^{\lambda\,(1)}}{D\,t^{(1)}} = -\frac{1}{\alpha_\sigma\,\tau_m}\,\varphi_\sigma^{\lambda\,(2)} - \frac{\delta t}{2\,\sqrt{e_\sigma}}\,\frac{D_\lambda^{(1)}}{D\,t^{(1)}}\,\left[\mathbf{k}_{\alpha(\sigma)}^\lambda \cdot \mathbf{g}_\sigma\right],$$

where

$$d_\sigma = 1 - \frac{1}{2}\,\frac{\delta t}{\alpha_\sigma\,\tau_m} = 1 - \frac{\delta t}{2}\left(\frac{\chi_H}{\tau_\sigma^0} + \frac{\epsilon}{\tau_m^0}\right). \tag{B.6}$$

The previous equations must be multiplied by the collisional invariants and then the integration on the microscopic velocity must be performed. Since Eq. (B.4) is analogous to Eq. (A.9) for the continuous model, the same results are obtained and the macroscopic equations (A.19, A.20) still hold for the simple model. The effects of the first-order perturbation on the continuity equation, involve the following sum:

$$\frac{1}{\alpha_\sigma\,\tau_m}\sum_{\lambda=0}^{8}\varsigma^\lambda\,\mathbf{v}^\lambda\,\varphi_\sigma^{\lambda\,(1)}, \tag{B.7}$$

which is equivalent to the vector $\mathbf{q}_\sigma^{(1)}$ for the continuous model. In order to calculate the previous quantity, Eq. (A.15) can be easily generalized for this case. In particular since this quantity can not depend on α_σ, it can not depend on the discrete lattice

effects too and this means that it must coincide with the vector $\mathbf{q}_\sigma^{(1)} = \rho_\sigma \mathbf{w}_\sigma / \tau_m$. An equivalent way to obtain the same result is to suppose that the diffusion velocity $\mathbf{w}_\sigma$ is a first-order term with regard to the parameter K:

$$\frac{1}{\alpha_\sigma \, \tau_m} \sum_{\lambda=0}^{8} \varsigma^\lambda \, \mathbf{v}^\lambda \sum_{\xi=1}^{\infty} K^{\,\xi} \, \varphi_\sigma^{\lambda\,(\xi)} = \frac{1}{\tau_m} \, \rho_\sigma \, \mathbf{w}_\sigma \, K. \tag{B.8}$$

Both approaches allow us to analyze the effects of the first-order perturbation on the continuity equation:

$$\frac{\partial \rho_\sigma}{\partial t^{(2)}} = -d_\alpha \, \alpha_\sigma \, \nabla^{(1)} \cdot (\rho_\sigma \, \mathbf{w}_\sigma) - \frac{\delta t}{2} \, \nabla^{(1)} \cdot (\rho_\sigma \, \mathbf{g}_\sigma) \, . \tag{B.9}$$

Summing the previous equation with Eq. (A.19), the continuity equation for the simple model is obtained:

$$\frac{\partial \rho_\sigma}{\partial t} + \nabla \cdot (\rho_\sigma \mathbf{u}_\sigma) = \frac{\delta t}{2} \, \nabla \cdot (\rho_\sigma \, \mathbf{l}_\sigma) \, , \tag{B.10}$$

where $\mathbf{l}_\sigma = \mathbf{w}_\sigma / \tau_m - \mathbf{g}_\sigma$ is the difference between the acceleration due to the internal coupling force and the external force field.

Let us proceed in the same way for the momentum equation. Multiplying Eq. (B.6) by the particle momentum for the generic species and integrating over the microscopic velocity, the following equation is recovered:

$$\begin{aligned} \frac{\partial}{\partial t^{(2)}} \left[\rho_\sigma \left(\mathbf{u}_\sigma - \alpha_\sigma \mathbf{w}_\sigma \right) \right] \; &+ \; \alpha_\sigma \, \frac{\partial}{\partial t^{(1)}} \left(\rho_\sigma \mathbf{w}_\sigma \right) = \frac{\delta t}{2} \, \frac{\partial}{\partial t^{(1)}} \left(\rho_\sigma \, \mathbf{l}_\sigma \right) \\ &- \; \frac{\delta t}{2} \, \nabla^{(1)} \cdot \left[\rho_\sigma \mathbf{u}_{\alpha(\sigma)} \otimes \mathbf{g}_\sigma + \rho_\sigma \mathbf{g}_\sigma \otimes \mathbf{u}_{\alpha(\sigma)} \right] \\ &- \; d_\sigma \, \nabla^{(1)} \cdot \left(\int m_\sigma \mathbf{v} \otimes \mathbf{v} \, f_\sigma^{(1)} \, d\mathbf{v} \right) , \end{aligned} \tag{B.11}$$

where the effects of the higher-order perturbations have been neglected. Applying Eqs. (A.25, A.26, A.27) and supposing that the effects due to both scalar and tensorial quadratic forms of the diffusion velocity are smaller than the effects due to the linearly

interpolated velocity, then:

$$
\begin{aligned}
-\int m_\sigma \mathbf{v}\otimes\mathbf{v}\, f_\sigma^{(1)}\, d\mathbf{v} &= \rho_\sigma\,(e_\sigma - e_\sigma^c)\,\mathbf{I} + \alpha_\sigma\,\tau_m\left[\rho_\sigma e_\sigma \nabla\mathbf{u}_{\alpha(\sigma)} + \rho_\sigma e_\sigma \nabla\mathbf{u}_{\alpha(\sigma)}^T\right. \\
&- \left.\rho_\sigma \mathbf{u}_{\alpha(\sigma)}\otimes\mathbf{w}_\sigma/\tau_m - \rho_\sigma\mathbf{w}_\sigma\otimes\mathbf{u}_{\alpha(\sigma)}/\tau_m\right]. \qquad \text{(B.12)}
\end{aligned}
$$

Considering the previous result, summing Eq. (B.11) with Eq. (A.20), the momentum equation for the simple model is obtained:

$$
\begin{aligned}
\frac{\partial(\rho_\sigma\mathbf{u}_\sigma)}{\partial t} &+ \nabla\cdot\left[(1-\alpha_\sigma)\,\rho_\sigma\mathbf{u}_\sigma\otimes\mathbf{u}_\sigma + \alpha_\sigma\,\rho_\sigma\mathbf{u}\otimes\mathbf{u} + \alpha_\sigma\rho_\sigma\mathbf{u}_{\alpha(\sigma)}\otimes\mathbf{w}_\sigma\right. \\
&+ \left.\alpha_\sigma\rho_\sigma\mathbf{w}_\sigma\otimes\mathbf{u}_{\alpha(\sigma)}\right] = -\nabla(\rho_\sigma e_\sigma) + \rho_\sigma\mathbf{g}_\sigma - \frac{1}{\tau_m}\rho_\sigma\mathbf{w}_\sigma \\
&+ \nabla\cdot\left\{d_\sigma\,\alpha_\sigma\rho_\sigma e_\sigma\tau_m\left[\nabla\mathbf{u}_{\alpha(\sigma)} + \nabla\mathbf{u}_{\alpha(\sigma)}^T\right]\right\} + \frac{\delta t}{2}\frac{\partial}{\partial t}(\rho_\sigma\,\mathbf{l}_\sigma) \\
&+ \frac{\delta t}{2}\nabla\cdot\left[\rho_\sigma\,\mathbf{u}_{\alpha(\sigma)}\otimes\mathbf{l}_\sigma + \rho_\sigma\,\mathbf{l}_\sigma\otimes\mathbf{u}_{\alpha(\sigma)}\right], \qquad \text{(B.13)}
\end{aligned}
$$

where $e_\sigma^c \approx e_\sigma$ has been assumed. Comparing Eqs. (B.10, B.13) with the macroscopic equations of the continuous Hamel's model given by Eqs. (5.129, 5.130), the discrete lattice effects are evident. Even though the macroscopic equations of the simple model recover the equations of the continuous model when $\delta t \to 0$, the simple model can not be considered acceptable and some corrections are needed. A recently suggested method for recovering the correct hydrodynamic equations will be generalized for the mixtures [132].

Let us introduce the following corrected velocities:

$$
\rho_\sigma\,\mathbf{u}_\sigma^\star = \sum_{\lambda=0}^{8}\varsigma^\lambda\,\mathbf{v}^\lambda\,\varphi_\sigma^\lambda + \rho_\sigma\,\mathbf{t}_\sigma^\star\,\delta t, \qquad \text{(B.14)}
$$

where $\mathbf{t}_\sigma^\star$ is an auxiliary vector. Consequently the corrected barycentric velocity $\mathbf{u}^\star = \sum_\sigma x_\sigma\mathbf{u}_\sigma^\star$ is defined too. Similarly the corrected equilibrium distribution function $\varphi_\sigma^{e\,\lambda\star}$ centered on the specific velocity $\mathbf{u}_\sigma^\star$ and the corrected equilibrium distribution function $\varphi_{\sigma(m)}^{e\,\lambda\star}$ centered on the barycentric velocity $\mathbf{u}^\star$ can be obtained. Let us introduce the

following guess lattice Boltzmann model:

$$\frac{D_\lambda\,\varphi_\sigma^\lambda}{D\,t}+\frac{\delta t}{2}\,\frac{D_\lambda}{D\,t}\,\frac{D_\lambda\,\varphi_\sigma^\lambda}{D\,t}=\;-\;\frac{\chi_H}{\tau_\sigma^0}\left[\varphi_\sigma^\lambda-\varphi_\sigma^{e\,\lambda\star}\right]-\frac{\epsilon}{\tau_m^0}\left[\varphi_\sigma^\lambda-\varphi_{\sigma(m)}^{e\,\lambda\star}\right]$$
$$+\;\frac{1}{\sqrt{e_\sigma}}\,\mathbf{k}_{\alpha(\sigma)}^{\lambda\star}\cdot\mathbf{g}_\sigma+\Theta_\sigma^{\lambda\star},\tag{B.15}$$

where $\mathbf{k}_{\alpha(\sigma)}^{\lambda\star}$ is the generalization of Eq. (5.179) when the corrected velocities are considered. The additional corrective factor $\Theta_\sigma^{\lambda\star}$ is defined as

$$\Theta_\sigma^{\lambda\star}=\rho_\sigma\,\left[-\frac{\delta t}{\alpha_\sigma\,\tau_m}\,\frac{\mathbf{t}_\sigma^\star\cdot\mathbf{v}^\lambda}{e_\sigma}+\frac{\mathbf{T}_\sigma^\star:\left(\mathbf{v}^\lambda\otimes\mathbf{v}^\lambda-e_\sigma\,\mathbf{I}\right)}{2\,e_\sigma^2}\right],\tag{B.16}$$

where $\mathbf{T}_\sigma^\star$ is an auxiliary tensor. The previous corrections to the simple model do not affect the first term of the expansion, i.e. $\varphi_\sigma^{\lambda\,(0)\star}=(1-\alpha_\sigma)\,\varphi_\sigma^{e\,\lambda\star}+\alpha_\sigma\,\varphi_{\sigma(m)}^{e\,\lambda\star}$. Using the previous result, the definition of the diffusion velocity, Eq. (B.14) and assuming that the additional term in the corrected velocities is of the first order in the Knudsen number because it is multiplied by the discretization time step, the property given by Eq. (B.8) can be generalized:

$$\frac{1}{\alpha_\sigma\,\tau_m}\sum_{\lambda=0}^{8}\varsigma^\lambda\,\mathbf{v}^\lambda\sum_{\xi=1}^{\infty}K^\xi\,\varphi_\sigma^{\lambda\,(\xi)\star}=\left(\frac{1}{\tau_m}\,\rho_\sigma\,\mathbf{w}_\sigma^\star-\frac{1}{\alpha_\sigma\,\tau_m}\,\rho_\sigma\,\mathbf{t}_\sigma^\star\,\delta t\right)\,K.\tag{B.17}$$

The previous corrections have been designed in such a way as to preserve the macroscopic Eqs. (A.19, A.20), if the velocities of the mixture components are redefined according to Eqs. (B.14). Proceeding in the usual way, the effects of the first-order perturbation on the continuity equation can be analyzed and summing this result to Eq. (A.19) the final form of the continuity equation is obtained:

$$\frac{\partial\rho_\sigma}{\partial t}+\nabla\cdot(\rho_\sigma\mathbf{u}_\sigma^\star)=\delta t\,\nabla\cdot\left[\rho_\sigma\,\left(\mathbf{l}_\sigma^\star/2+\mathbf{t}_\sigma^\star\right)\right].\tag{B.18}$$

The auxiliary vector can be set in such a way as to reproduce the performance of the continuous model with second order accuracy, i.e. $\mathbf{t}_\sigma^\star=-\mathbf{l}_\sigma^\star/2$.

Similarly the effects of the first-order perturbation on the momentum equation can be analyzed and summing this result to Eq. (A.20) the final form of the momentum

equation is obtained:

$$\begin{aligned}\frac{\partial\left(\rho_\sigma \mathbf{u}_\sigma\right)}{\partial t} &+ \nabla\cdot\big[(1-\alpha_\sigma)\,\rho_\sigma \mathbf{u}^\star_\sigma\otimes\mathbf{u}^\star_\sigma+\alpha_\sigma\,\rho_\sigma\mathbf{u}^\star\otimes\mathbf{u}^\star+\alpha_\sigma\rho_\sigma\mathbf{u}^\star_{\alpha(\sigma)}\otimes\mathbf{w}^\star_\sigma\\ &+ \alpha_\sigma\rho_\sigma\mathbf{w}^\star_\sigma\otimes\mathbf{u}^\star_{\alpha(\sigma)}\big]=-\nabla\left(\rho_\sigma e_\sigma\right)+\rho_\sigma\mathbf{g}_\sigma-\frac{1}{\tau_m}\,\rho_\sigma\mathbf{w}^\star_\sigma\\ &+ \nabla\cdot\left\{d_\sigma\,\alpha_\sigma\rho_\sigma e_\sigma\tau_m\left[\nabla\mathbf{u}^\star_{\alpha(\sigma)}+\nabla\mathbf{u}^{\star T}_{\alpha(\sigma)}\right]\right\}\\ &+ \frac{1}{2}\nabla\cdot\big[\delta t\,\rho_\sigma\,\mathbf{u}^\star_{\alpha(\sigma)}\otimes\mathbf{l}^\star_\sigma+\delta t\,\rho_\sigma\,\mathbf{l}^\star_\sigma\otimes\mathbf{u}^\star_{\alpha(\sigma)}\\ &- \alpha_\sigma\,\tau_m\,\rho_\sigma\,\left(\mathbf{T}^\star_\sigma+\mathbf{T}^{\star T}_\sigma\right)\big]. \end{aligned}\tag{B.19}$$

The auxiliary tensor can be set in such a way as to reproduce the performance of the continuous model with second order accuracy, i.e. $\mathbf{T}^\star_\sigma=\delta t\,\mathbf{u}^\star_{\alpha(\sigma)}\otimes\mathbf{l}^\star_\sigma/\left(\alpha_\sigma\,\tau_m\right)$. The previous results can be included in the definition of the corrective factor:

$$\Theta^{\lambda\star}_\sigma=\rho_\sigma\,\frac{\delta t}{2\,\alpha_\sigma\,\tau_m}\left[\frac{\mathbf{l}^\star_\sigma\cdot\mathbf{v}^\lambda}{e_\sigma}-\frac{\mathbf{u}^\star_{\alpha(\sigma)}\otimes\mathbf{l}^\star_\sigma:\left(\mathbf{v}^\lambda\otimes\mathbf{v}^\lambda-e_\sigma\,\mathbf{I}\right)}{e^2_\sigma}\right].\tag{B.20}$$

It is easy to verify that $\Theta^{\lambda\star}_\sigma=(1-d_\sigma)\,\mathbf{k}^{\lambda\star}_{\alpha(\sigma)}\cdot\mathbf{l}^\star_\sigma/\sqrt{e_\sigma}$. Substituting this result into the corrected Eq. (B.16), the final lattice Boltzmann model given by Eq. (5.181) is recovered. It is interesting to highlight that for non-interacting particles, i.e. when $1/\tau_m\to 0$, the discussed correction reduces to the well-known formula for the external force field only [132].

Bibliography

[1] M. J. Madou, Fundamentals of microfabrication: the science of miniaturization, CRC Press, Boca Raton (2002).

[2] Nanotechnology and MEMS 2003: The Race to Commercialize the Ultra-Small, Global Information, Inc. (GII) (2004).

[3] S. A. Campbell, The Science and Engineering of Microelectronics Fabrication, Oxford Series in Electrical Engineering, Oxford University Press (2000).

[4] R. R. Tummala, Microelectronics packaging handbook: technology drivers, Chapman and Hall (1997).

[5] A. Kersch, W. J. Morokoff, Transport simulation in microelectronics, Birkhäuser (1995).

[6] J. Figueras, A. M. Brosa, A. Ferré, Test Challenges in Nanometric CMOS Technologies, *Microelectronic Engineering*, Vol. 49, No. 1-2, pp. 119-133 (1999).

[7] J. Gautier, Beyond CMOS: quantum devices, *Microelectronic Engineering*, Vol. 39, No. 1-4, pp. 263-272 (1997).

[8] M. Gad-el-Hak (Editor), The MEMS handbook, CRC Press, Boca Raton, Florida (2001).

[9] J. W. Schultze, G. Staikov (Editors), Scaling down in Electrochemistry: Electrochemical Microsystem and Nanosystem Technology, *Proceedings of the 3rd International Symposium on Electrochemical Microsystem Technologies*, Garmisch/Partenkirchen, Germany, (2000), Reprinted from *Electrochimica Acta*, Vol. 47, No. 1-2 (2001).

[10] W. Ehrfeld, Electrochemistry and microsystems, *Electrochimica Acta*, Vol. 48, pp. 2857-2868 (2003).

[11] P. Gao, S. Le Person, M. Favre-Marinet, Scale effects on hydrodynamics and heat transfer in two-dimensional mini and microchannels, *International Journal of Thermal Sciences*, Vol. 41, pp. 1017-1027 (2002).

[12] J. Pettersen, A. Hafner, G. Skaugen, Development of compact heat exchangers for CO_2 air-conditioning systems, *International Journal of Refrigeration*, Vol. 21, No. 3, pp. 180-193 (1998).

[13] S. M. Flockhart, R. S. Dhariwal, Experimental and numerical investigation into the flow characteristics of channels etched in 100 Silicon, *Journal of Fluids Engineering*, Vol. 120, pp. 291295 (1998).

[14] B. Gromoll, Micro cooling systems for high density packaging, *Revue Generale de Thermique*, Vol. 37, pp. 781787 (1998).

[15] T. Chován, A. Guttman, Microfabricated devices in biotechnology and biochemical processing, *Trends in Biotechnology*, Vol. 20, No. 3 (2002).

[16] S. J. Haswell, V. Skelton, Chemical and biochemical microreactors, *Trends in Analytical Chemistry*, Vol. 19, pp. 389395 (2000).

[17] R. R. A. Syms, D.F. Moore, Optical MEMS for telecoms, *Materials Today*, Vol. 5, No. 7-8 (2002).

[18] A. Bejan, Shape and Structure, from Engineering to Nature, Cambridge University Press (2000).

[19] J. C. Ordoneza, A. Bejan, R. S. Cherry, Designed porous media: Optimally nonuniform flow structures connecting one point with more points, *International Journal of Thermal Sciences*, Vol. 42, No. 9, pp. 857-870 (2003).

[20] M.-H. Kim, J. Pettersen, C. W. Bullard, Fundamental process and system design issues in CO_2 vapor compression systems, *Progress in Energy and Combustion Science*, Vol. 30, pp. 119-174 (2004).

[21] Use of natural working fluids in air conditioning, *Natural fluid vapour cycle Task 6.3, Confidential report with Power Optimized Aircraft POA* (2002).

[22] S. B. Riffat, C. F. Afonso, A. C. Oliveira, D.A. Reay, Natural refrigerants for refrigeration and air-conditioning system, *Applied Thermal Engineering*, Vol. 17, No. 1, pp. 33-42 (1997).

[23] Y. Hwang, M. Ohadi, R. Radermacher, Natural refrigerants, *Mechanical Engineering*, Vol. 120, No. 10, pp. 96-99 (1998).

[24] A. Cavallini, Working fluids for mechanical refrigeration - invited paper presented at the 19th international congress of refrigeration, *International Journal of Refrigeration*, Vol. 19, No. 8, pp. 485-496 (1996).

[25] M. Bhatti, A critical look at R-744 and R-134a mobile air conditioning systems, *SAE Paper*, No. 970527 (1997).

[26] S. Fischer, J. Sand, Total Environment Impact (TEWI) calculations for alternative automotive air-conditioning systems, *SAE Paper*, No. 970526 (1997).

[27] H. Gentner, Passenger car air conditioning using carbon dioxide as refrigerant, *Proceedings of the Third IIR-Gustav Lorentzen Conference on Natural Working Fluids*, Oslo, Norway, pp. 303-313 (1998).

[28] ASHRAE, ASHRAE Handbook: Applications, Atlanta, GA: American Society of Heating, Refrigerating and Air-Conditioning Engineers (1998).

[29] E. H. Hunt, D. H. Reid, D. R. Space, F. E. Tilton, Commercial airliner environmental control systems: engineering aspects of cabin air quality, *Proceedings of the Aerospace Medical Association Annual Meeting*, Anaheim (CA) (1995).

[30] Power Optimised Aircraft, Contract Number G4RD-CT-2001-00601 under the European Community 5^{th} Framework Programme for Research - Competitive Sustainable Growth - Key Action: New Perspectives in Aeronautics, *www.poa-project.com* (2002-2005).

[31] L. F. Faleiro, Trends towards a more electrical aircraft, *Liebherr-Aerospace*, Lindenberg (DE), *www.poa-project.com* (2004).

[32] W. J. Vankan, J. Kos, W. F. Lammen, Approximation models for multidisciplinary system design - Application in a design study for power optimised aircraft, *Proceedings of the International Congress on Evolutionary Methods for Design, Optimization and Control with Applications to Industrial Problems EUROGEN 2003*, Barcelona, *www.poa-project.com* (2003).

[33] A. Cavallini, F. Steimle, Natural Working Fluids in Historic Perspective, *Proceedings of the Third IIR-Gustav Lorentzen Conference on Natural Working Fluids*, Oslo, Norway, pp. 37-42 (1998).

[34] A. Cavallini, Properties of CO_2 as refrigerant, *European Seminar: Carbon Dioxide as Refrigerant, Theoretical and Design Aspects*, Milano, Italy (2004).

[35] G. Lorentzen, Revival of carbon dioxide as a refrigerant, *International Journal of Refrigeration*, Vol. 17, No. 5 (1994).

[36] G. Lorentzen, The use of natural refrigerant: a complete solution to the $CFC/HCFC$ predicament, *International Journal of Refrigeration*, Vol. 18, No. 3 (1995).

[37] O. K. Rice, Critical phenomena, in: F.D. Rossini (Editor), Thermodynamics and physics of matter, Princeton University Press, Princeton, New Jersey, pp. 419-499 (E) (1955).

[38] J. Millat, J. H. Dymond, C. A. Nieto de Castro, Transport properties of fluids, Cambridge University Press, Cambridge, United Kingdom (1996).

[39] M. Girault, D. Petit, Identification methods in nonlinear heat conduction. Part I: model reduction, *International Journal of Heat and Mass Transfer*, Vol. 48, pp. 105118 (2005).

[40] L. Cecchinato, M. Corradi, E. Fornasieri, L. Zamboni, Carbon dioxide as refrigerant for tap water heat pumps: a comparison with the traditional solution, *Proceeding of XXI IIR International Congress of Refrigeration*, Washington D.C., USA (2003).

[41] G. E. P. Box, W.G. Hunter, J. S. Hunter, Statistics for experimenters, John Wiley & Sons, New Jork (1978).

[42] Y. Hwang, R. Radermacher, Theoretical evaluation of carbon dioxide refrigeration cycle, *International Journal of HVAC & Research*, Vol. 4, No. 3, pp. 245-264 (1998).

[43] E. S. Gaddis, D. B. Spalding, J. Taborek, Heat Exchanger Theory, in Begell House Inc. (ed.), *Heat Exchanger Design Handbook*, Vol. I, Ch. 1, Hemisphere, New York (1989).

[44] W. M. Kays, A. L. London, Compact Heat Exchangers, McGraw-Hill, New York (1984).

[45] J. P. Chiou, The Effect of Longitudinal Heat Conduction on Crossflow Heat Exchanger, *Transactions of ASME*, *Journal of Heat Transfer*, Vol. 100, pp. 346-351 (1978).

[46] Ch. Ranganayakulu, K. N. Seetharamu, K. V. Sreevatsan, The Effects of Longitudinal Conduction in Compact Plate-Fin and Tube-Fin Heat Exchangers Using a Finite-Element Method, *International Journal of Heat and Mass Transfer*, Vol. 40, No. 6, pp. 1261-1277 (1997).

[47] Ch. Ranganayakulu, K. N. Seetharamu, K. V. Sreevatsan, The Effects of Inlet Fluid Flow Nonuniformity on Thermal Performance and Pressure Drops in Crossflow Plate-Fin Compact Heat Exchangers, *International Journal of Heat and Mass Transfer*, Vol. 40, No. 1, pp. 27-38 (1997).

[48] J. P. Chiou, The Advancement of Compact Heat Exchanger Theory Considering the Effects of Longitudinal Heat Conduction and Flow Nonuniformity, *Symposium on Compact Heat Exchangers - History*, *ASME*, pp. 101-105 (1980).

[49] Ch. Ranganayakulu, K. N. Seetharamu, The Combined Effects of Wall Longitudinal Heat Conduction, Inlet Fluid Flow Nonuniformity and Temperature Nonuniformity in Compact Tube-Fin Heat Exchangers: a Finite Element Method, *International Journal of Heat and Mass Transfer*, Vol. 42, pp. 263-273 (1999).

[50] J. M. Corberán, P. F. De Córdoba, J. Gonzálvez, F. Alias, Semiexplicit Method for Wall Temperature Linked Equations (SEWTLE): a General Finite-Volume Technique for the Calculation of Complex Heat Exchangers, *Numerical Heat Transfer: Part. B*, Vol. 40, pp. 37-59 (2001).

[51] R. Romero-Méndez, M. Sen, K. T. Yang, R. L. McLain, Effect of Tube-To-Tube Conduction on Plate-Fin and Tube Heat Exchanger Performance, *International Journal of Heat and Mass Transfer*, Vol. 40, No. 16, pp. 3909-3916 (1997).

[52] J. L. Lage, Tube-To-Tube Heat Transfer Degradation Effect on Finned-Tube Heat Exchangers, *Numerical Heat Transfer: Part A*, Vol. 39, pp. 321-337 (2001).

[53] S. V. Patankar, Numerical Heat Transfer and Fluid Flow, Hemisphere, New York (1980).

[54] L. J. Segerlind, Applied finite analysis, Wiley, New York (1984).

[55] M. L. Krasnov, G.I. Makarenko, A.I. Kiselev, Calculus of variations, MIR Editions, Moscow (1984).

[56] B. S. V. Prasad, Fin Efficiency and Mechanisms of Heat Exchange Through Fins in Multi-Stream Plate-Fin Heat Exchangers: Formulation, *International Journal of Heat and Mass Transfer*, Vol. 39, No. 2, pp. 419-428 (1996).

[57] J. M. Yin, C. W. Bullard, P. S. Hrnjak, R-744 gas cooler model development and validation, *International Journal of Refrigeration*, Vol. 24, pp. 692-701 (2001).

[58] Y. Chang, C. C. J. Wang, Air side performance of brazed aluminium heat exchangers, *Journal of Enhanced Heat Transfer*, Vol. 3, No. 1, pp. 15-28 (1996).

[59] E. Idelchik, Handbook of Hydraulic Resistance, 3rd Edition, CRC Press (1994).

[60] S. W. Churchill, Friction-factor equation spans all fluid flow regimes, *Chemical Engineering*, Vol. 7, pp. 91-92 (1977).

[61] Y. Chang, C. C. J. Wang, A generalized heat transfer correlation for louver fin geometry, *International Journal of Heat and Mass Transfer*, Vol. 40, No. 3, pp. 533-544 (1997).

[62] J. Pettersen, R. Rieberer, A. Leister, Heat transfer and pressure drop characteristics of supercritical carbon dioxide in microchannel tubes under cooling, *International Institute of Refrigeration Commissions B1,B2,E1 and E2*, Purdue University Press, pp. 99-106 (2000).

[63] R. Rieberer, CO2 properties, *IIR Workshop on CO2 Technology in Refrigeration, Heat Pump and Air Conditioning Systems*, Mainz, Germany (1999).

[64] J. Pettersen, A. Hafner, G. Skaugen, Development of compact heat exchangers for CO_2 air-conditioning systems, *International Journal of Refrigeration*, Vol. 21, No. 3, pp. 180-193 (1998).

[65] J. Millat, J. H. Dymond, C. A. Nieto de Castro, Transport properties of fluids, Cambridge University Press, Cambridge, United Kingdom (1996).

[66] O. K. Rice, Critical phenomena, in: F.D. Rossini (Editor), Thermodynamics and physics of matter, Princeton University Press, Princeton, New Jersey, pp. 419-499 (1955).

[67] S. Kakaç, The effect of temperature-dependent fluid properties on convective heat transfer, in: S. Kakaç, R. K. Shah, W. Aung (Editors), Handbook of single-phase convective heat transfer, Wiley, New York, pp. 18.1-18.56 (1987).

[68] B. S. Petukhov, Heat transfer and friction in turbulent pipe flow with variable physical properties, *Advances in Heat Transfer*, Vol. 6, pp. 503-565 (1960).

[69] S. S. Pitla, D. M. Robinson, E. A. Groll, S. Ramadhyani, Heat transfer from supercritical carbon dioxide in tube flow: a critical review, *International Journal of Heating Ventilating Air-Conditioning and Refrigerating Research*, Vol. 3, No. 4, pp. 281-301 (1998).

[70] E. A. Krasnoshchekov, I. V. Kuraeva, V. S. Protopopov, Local heat transfer of carbon dioxide at supercritical pressure under cooling conditions, *High Temperature (translated from Teplofizika Vysokikh Tempeartur)*, Vol. 7, No. 5, pp. 856-862 (1970).

[71] V. L. Baskov, I. V. Kuraeva, V. S. Protopopov, Heat transfer with the turbulent flow of a liquid at supercritical pressure in tubes under cooling conditions, *High Temperature (translated from Teplofizika Vysokikh Tempeartur)*, Vol. 1, No. 15, pp. 96-102 (1977).

[72] N.E. Petrov, V.N. Popov, Heat transfer and resistance of carbon dioxide being cooled in the supercritical region, *Thermal Engineering (translated from Teploenergetika)*, Vol. 32, No. 3, pp. 16-19 (1985).

[73] J. Pettersen, R. Rieberer, A. Leister, Heat transfer and pressure drop characteristics of supercritical carbon dioxide in microchannel tubes under cooling, *International Institute of Refrigeration, Commissions B1,B2,E1 and E2*, Purdue University Press, pp. 99-106 (2000).

[74] S. V. Pitla, E. A. Groll, S. Ramadhayani, New correlation for the heat transfer coefficient during in-tube cooling of turbulent supercritical carbon dioxide, *International Institute of Refrigeration Commissions B1,B2,E1 and E2*, Purdue University Press, pp. 259-267 (2000).

[75] S. M. Liao, T. S. Zhao, Measurements of heat transfer coefficients from supercritical carbon dioxide flowing in horizontal mini/micro channels, *Journal of Heat Transfer*, Vol. 124, pp. 413-420 (2002).

[76] J. D. Jackson, W. B. Hall, Influences of buoyancy on heat transfer to fluids flowing in vertical tubes under turbulent conditions, Turbulent Forced Convection in Channels and Bundles, Hemisphere, New York (1979).

[77] S. H. Yoon, J. H. Kim, Y. W. Hwang, M. S. Kim, K. Min, Y. Kim, Heat transfer and pressure drop characteristics during the in-tube cooling process of carbon dioxide in the supercritical region, *International Journal of Refrigeration*, Vol. 26, pp. 857-864 (2003).

[78] V. N. Popov, N. E. Petrov, Calculation of heat transfer and flow resistance in the turbulent pipe flow of cooled carbon dioxide in the supercritical region, *High Temperature (translated from Teplofizika Vysokikh Tempeartur)*, Vol. 23, No. 2, pp. 309-316 (1985).

[79] V. N. Popov, E. P. Valueva, Heat transfer and turbulent flow of water at supercritical parameters if state in a vertical tube with significant effect of free convection, *Thermal Engineering (translated from Teploenergetika)*, Vol. 33, pp. 22-29 (1986).

[80] W. B. Hall, Heat transfer near the critical point, *Advances in Heat Transfer*, Vol. 7, pp. 1-83 (1981).

[81] S. B. Pope, Turbulent flows, Cambridge University Press, Cambridge (2000).

[82] H. Schlichting, Boundary layer theory, 4th edition, McGraw-Hill, New York (1960).

[83] R. G. Deissler, C. S. Eian, Analytical and experimental investigation of fully developed turbulent flow of air in a smooth tube with heat transfer with variable fluid properties, NACA TN 2629 (1952).

[84] V. S. Sastry, N. M. Schnurr, An analytical investigation of forced convection heat transfer to fluids near the thermodynamic critical point, *Journal of Heat Transfer*, Vol. 97, No. 2, pp. 226-230 (1975).

[85] K. Goldmann, Heat transfer to supercritical water and other fluids with temperature depedent properties, *Chemical Engineering Progress Symposium*, Vol. 50, No. 11, pp. 105-113 (1954).

[86] C. P. Bellmore, R. L. Reid, Numerical prediction of wall temperatures for near-critical para-hydrogen in turbulent upflow inside vertical tubes, *Journal of Heat Transfer*, Vol. 105, pp. 536-541 (1983).

[87] D. C. Montgomery, G. C. Runger, N. F. Hubele, Engineering statistics, John Wiley & Sons, New Jork (2001).

[88] B. E. Launder, D. B. Spalding, Lectures in Mathematical Models of Turbulence, Academic Press, London (1972).

[89] H. K. Versteeg, W. Malalasekera, An introduction to computational fluid dynamics: the finite volume method, Addison-Wesley, London (1996).

[90] V. Yakhot, S. A. Orszag, Renormalization group analysis of turbulence: I. basic theory, *Journal of Scientific Computing*, Vol. 1, No. 1, pp. 1-51 (1986).

[91] T. J. Craft, A. V. Gerasimov, H. Iacovides, B. E. Launder, Progress in the generalization of wall-function treatments, *International Journal of Heat and Fluid Flow*, Vol. 23, pp. 148-160 (2003).

[92] M. Wolfstein, The velocity and temperature distribution of one-dimensional flow with turbulence augmentation and pressure gradient, *International Journal of Heat and Mass Transfer*, Vol. 12, pp. 301-318 (1969).

[93] H. C. Chen, V. C. Patel, Near-wall turbulence models for complex flows including separation, *AIAA Journal*, Vol. 26, No. 6, pp. 641-648 (1988).

[94] T. Jongen, Simulation and modeling of turbulent incompressible flows, Ph.D. Dissertation, EPF Lausanne, Lausanne, Switzerland (1992).

[95] V. V. Altunin, Thermophysical properties of carbon dioxide, Stardarty, Moscow (1975).

[96] E. W. Lemmon, M. O. McLinden, D. G. Friend, Thermophysical properties of fluid systems, in: P.J. Linstrom, W. G. Mallard (Editors), NIST Chemistry WebBook, National Institute of Standards and Technology (2003).

[97] J. H. Ferziger, M. Peric, Computational methods for fluid dynamics, Springer-Verlag, Berlin (1996).

[98] S. H. Lee, J. R. Howell, Turbulent developing convective heat transfer in a tube for fluids near the critical point, *International Journal of Heat and Mass Transfer*, Vol. 41, No. 10, pp. 1205-1218 (1998).

[99] R. D. Wood, J. M. Smith, Heat transfer in the critical region - temperature and velocity profiles in turbulent flow, *A.I.Ch.E. Journal*, Vol. 10, No. 2, pp. 180-186 (1964).

[100] G. Scalabrin, L. Piazza, M. Condosta, Convective cooling of supercritical carbon dioxide inside tubes: heat transfer analysis through neural network, *International Journal of Heat and Mass Transfer*, Vol. 46, pp. 4413-4425 (2003).

[101] S. Ansumalia, I. V. Karlinb, S. Succi, Kinetic theory of turbulence modeling: smallness parameter, scaling and microscopic derivation of Smagorinsky model, *Physica A*, Vol. 338, pp. 379394 (2004).

[102] D. A. Wolf-Gladrow, Lattice-Gas Cellular Automata and Lattice Boltzmann Models: an Introduction, *Lecture Notes in Mathematics*, Springer, 2003.

[103] S. Chen, G. D. Doolen, Lattice Boltzmann method for fluid flow, *Annual Review of Fluid Mechanics*, Vol. 30, pp. 329-338 (1998).

[104] S. Succi, The Lattice Boltzmann Equation for Fluid Dynamics and Beyond, Oxford University Press (1999).

[105] S. Wolfram, Cellular Automata and Complexity, Addison-Wesley, Reading, MA (1994).

[106] J. von Neumann, The Theory of Self-Reproducing Automata, University of Illinois Press, Urbana (1966).

[107] K. Zuse, Calculating Space, Technical Report Tech. Transl. AZT-70-164-GEMIT, MIT Project MAC (1970).

[108] J. Hardy, Y. Pomeau, O. de Pazzis, Time evolution of a twodimensional model system. I. Invariant states and time correlation functions, *Journal of Mathematical Physics*, Vol. 14, No. 12, pp. 1746-1759 8 (1973).

[109] S. Wolfram, Statistical mechanics of cellular automata, *Review of Modern Physics*, Vol. 55, pp. 601-644 (1983).

[110] S. Wolfram, Computer software in science and mathematics, *Scientific American*, Vol. 251, pp. 188-203 (1984).

[111] S. Wolfram, Cellular automata as models of complexity, *Nature*, Vol. 311, pp. 419-424 (1984).

[112] U. Frisch, B. Hasslacher, Y. Pomeau, Lattice-gas automata for the Navier-Stokes equation, *Physics Review Letters*, Vol. 56, No. 14, pp. 1505-1508 (1986).

[113] S. Wolfram, Cellular Automaton Fluids 1: Basic Theory, *Journal of Statistical Physics*, Vol. 45, No. 3-4, pp. 471-526 (1986).

[114] U. Frisch, D. d'Humiéres, B. Hasslacher, P. Lallemand, Y. Pomeau, J.-P. Rivet, Lattice gas hydrodynamics in two and three dimensions, *Complex Systems*, Vol. 1, pp. 649-707 (1987).

[115] G. McNamara, G. Zanetti, Use of the Boltzmann equation to simulate lattice-gas automata, *Physics Review Letters*, Vol. 61, pp. 2332-2335 (1988).

[116] J. M. V. A. Koelman, A simple lattice Boltzmann scheme for Navier-Stokes fluid flow, *Europhysics Letters*, Vol. 15, No. 6, pp. 603-607 (1991).

[117] Y. H. Qian, D. d'Humiéres, P. Lallemand, Lattice BGK models for Navier-Stokes equation, *Europhysics Letters*, Vol. 17, No. 6, pp. 479-484 (1992).

[118] G. McNamara, B. J. Alder, Analysis of the lattice Boltzmann treatment of hydrodynamics, *Physica A*, Vol. 194, pp. 218-228 (1993).

[119] X. He, L.-S. Luo, Theory of the lattice Boltzmann method: From the Boltzmann equation to the lattice Boltzmann equation, *Physical Review E*, Vol. 56, No. 6, pp. 6811-6817 (1997).

[120] R. Liboff, Kinetic theory: classical, quantum and relativistic description, Wiley, NY (1998).

[121] C. Cercignani, Theory and applications of the Boltzmann equation, Scottish Academic Press, Edinburgh and London, UK (1975).

[122] Y. Sone, Kinetic Theory and Fluid Dynamics, Birkhäuser, Boston, 2002.

[123] J. Kevorkian, J.D. Cole, Multiple scale ans singular perturbation methods, in *Applied Mathematical Sciences 114*, J. E. Marsden, L. Sirovich (Editors), Springer, New York (1996).

[124] G. Uhlenbeck, G. Ford, Lectures in Statistical Mechanics, Providence (1963).

[125] P. Bhatnagar, E. P. Gross, M. K. Krook, A model for collision processes in gases. I. Small amplitude processes in charged and neutral one-component systems, *Physical Review*, Vol. 94, No. 3, pp. 511-525 (1954).

[126] P. Welander, On the temperature jump in a rarefied gas, *Arkiv för Fysik*, Vol. 7, No. 44, pp 507-553 (1954).

[127] T. Abe, Derivation of the Lattice Boltzmann Method by Means of the Discrete Ordinate Method for the Boltzmann Equation, *Journal of Computational Physics*, Vol. 131, pp. 241-246 (1997).

[128] X. Shan, X. He, Discretization of the velocity space in the solution of the Boltzmann equation, *Physical Review Letters*, Vol. 80, pp. 6568 (1998).

[129] G. A. Bird, *Molecular Gas Dynamics and the Direct Simulation of Gas Flows*, Oxford University Press, Oxford (1994).

[130] P. J. Davis, P. Rabinowitz, Methods of Numerical Integration, 2nd ed. Academic, New York (1984).

[131] D. d'Humieres , M. Bouzidi, P. Lallemand, Thirteen-velocity three-dimensional lattice Boltzmann model, *Physical Review E*, Vol. 63, No. 066702-1-7 (2001).

[132] Z. Guo, C. Zheng, B. Shi, Discrete lattice effects on the forcing term in the lattice Boltzmann method, *Physical Review E*, Vol. 65, No. 046308 (2002).

[133] I. Ginzbourg, P. M. Adler, Boundary flow condition analysis for the three-dimensional lattice Boltzmann model, *Journal Physique II France*, Vol. 4, pp. 191-214 (1994).

[134] P. Lallemand, L.-S. Luo, Theory of the lattice Boltzmann method: Dispersion, dissipation, isotropy, Galilean invariance, and stability, *Physical review E*, Vol. 61, No. 6, pp. 6546-6562 (2000).

[135] P. Lallemand, L.-S. Luo, Theory of the lattice Boltzmann method: Acoustic and thermal properties in two and three dimensions, *Physical review E*, Vol. 68, No. 036706 (2003).

[136] D. dHumiéres, I. Ginzburg, M. Krafczyky, P. Lallemand, L.-S. Luo, Multiple-relaxation-time lattice Boltzmann models in three dimensions, *Proceedings of the Royal Society London*, Ser. A 360, pp. 437 (2002).

[137] D. dHumiéres, Generalized lattice Boltzmann equations, in *Rarefied gas dynamics: theory and simulations* (ed. B. D. Shizgal & D. P. Weaver), *Progress in Aeronautics and Astronautics*, Vol. 159, pp. 450-458 (1992).

[138] I. Ginzburg, Introduction of upwind and free boundary into lattice Boltzmann method, In *Discrete modelling and discrete algorithms in continuum mechanics* (ed. Th. Sonar & I. Thomas), pp. 97-110, Berlin (2001).

[139] G. R. McNamara, A. L. Garcia, B. J. Alder, Stabilization of thermal lattice Boltzmann models, *Journal of Statistical Physics*, Vol. 81, pp. 395-408 (1995).

[140] L. Giraud, D. dHumiéres, P. Lallemand, A lattice Boltzmann model for Jeffreys viscoelastic fluid, *Europhysics Letters*, Vol. 42, pp. 625-630 (1998).

[141] R. J. Mason, A Multi-Speed Compressible Lattice-Boltzmann Model, *Journal of Statistical Physics*, Vol. 107, No. 1-2, pp. 385-400 (2002).

[142] L. O. E. Santos, P. C. Facin, P. C. Philippi, Lattice-Boltzmann model based on field mediators for immiscible fluids, *Physical Review E*, Vol. 68, 056302 (2003).

[143] X. He, S. Chen, G. D. Doolen, A novel thermal model for lattice Boltzmann method in incompressible limit, *Journal of Computational Physics*, Vol. 146, pp. 282-300 (1998).

[144] R. S. Maier, R. S. Bernard, D. W. Grunau, Boundary conditions for the lattice Boltzmann method, *Physics of Fluids*, Vol. 8, pp. 1788-1801 (1996).

[145] Q. Zou, X. He, On pressure and velocity boundary conditions for the lattice Boltzmann BGK model, *Physics of Fluids*, Vol. 9, pp. 1591-1598 (1997).

[146] E. B. Arkilic, M. A. Schmidt, K. S. Breuer, Gaseous slip flow in long microchannels, *Journal of Microelectromechanical systems*, Vol. 6, No. 2 (1997).

[147] S. Harris, *An Introduction to the Theory of the Boltzmann Equation*, Holt, Rinehart and Winston, New York (1971).

[148] S. Schaff, P. Chambre, Flow of rarefied gases, in *Fundamentals of Gas Dynamics*, Princeton University Press, Princeton, New York (1958).

[149] C. Y. Lim, C. Shu, X. D. Niu, Y. T. Chew, Application of lattice Boltzmann method to simulate microchannel flows, *Physics of Fluids*, Vol. 14, No. 7, pp. 2299-2308 (2002).

[150] X. Nie, G. D. Doolen, S. Chen, Lattice-Boltzmann Simulations of Fluid Flows in MEMS, *Journal of Statistical Physics*, Vol. 107, No. 1-2, pp. 279-289 (2002).

[151] X. He, Q. Zou, L.-S. Luo, M. Dembo, Analytical solutions of simple flows and analysis of nonslip boundary conditions for the lattice Boltzmann BGK model, *Journal of Statistical Physics*, Vol. 87, No. 1-2, pp. 115-136 (1997).

[152] O. Filippova, D. Hänel, Lattice-Boltzmann simulations of gas-particle flow in filters, *Computers & Fluids*, Vol. 26, pp. 697-712 (1997).

[153] O. Filippova, D. Hänel, Boundary-fitting and local grid refinement for lattice-BGK models, *International Journal of Modern Physics C*, Vol. 9, No. 8, pp. 1271-1279 (1998).

[154] R. Mei, W. Shyy, On the finite difference-based lattice Boltzmann method in curvilinear coordinates, *Journal of Computational Physics*, Vol. 143, No. 2, pp. 426-448 (1998).

[155] E. G. Flekkoy, Lattice bhatnagar-gross-krook models for miscible fluids, *Physical Review E*, Vol. 47, p. 4247 (1993).

[156] X. Shan, G. Doolen, Multicomponent lattice-Boltzmann model with interparticle interaction, *Journal of Statistical Physics*, Vol. 81, p. 379 (1995).

[157] V. Sofonea, R. F. Sekerka, BGK models for diffusion in isothermal binary fluid systems, *Physica A*, Vol. 299, p. 494 (2001).

[158] Z. Guo, T. S. Zhao, Discrete velocity and lattice Boltzmann models for binary mixtures of nonideal fluids, *Physical Review E*, Vol. 68, No. 035302 (2003).

[159] L.-S. Luo, S. S. Girimaji, Theory of the lattice Boltzmann method: Two-fluid model for binary mixtures, *Physical Review E*, Vol. 67, No. 036302 (2003).

[160] A. Xu, Finite-Difference Lattice Boltzmann Methods for binary fluids, Pre-Print, arXiv:cond-mat/0406012, www.arxiv.org (2004).

[161] P. C. Fancin, P. C. Philippi, L.O.E. dos Santos, Non-linear lattice-Boltzmann model for ideal miscible fluids, *Journal of Future Generation Computer Systems*, in press (2004).

[162] K. Xu, BGK-Based Scheme for Multicomponent Flow Calculations, *Journal of Computational Physics*, Vol. 134, No. 122 (1997).

[163] Y.S. Lian, K. Xu, A Gas-Kinetic Scheme for Multimaterial Flows and Its Application in Chemical Reactions, *Journal of Computational Physics*, Vol. 163, No. 349, pp. 349-375 (2000).

[164] L.-S. Luo, Unified theory of lattice Boltzmann models for nonideal gases, *Physical Review Letters*, Vol. 81, No. 8, p. 1618 (1998).

[165] S. Chapman, T. G. Cowling, *The Mathematical Theory of Non-Uniform Gases*, Cambridge University Press, Cambridge (1970).

[166] I. Kolodner, On the Application of the Boltzmann Equations to the Theory of Gas Mixtures, Ph.D. dissertation, New York University (1950).

[167] P. L. Bhatnagar, E. P. Gross, M. Krook, A model for collision processes in gases. I. Small amplitude processes in charged and neutral one-component systems, *Physical Review*, Vol. 94, p. 511 (1954).

[168] E. P. Gross, M. Krook, Model for collision processes in gases: small-amplitude oscillations of charged two-Component systems, *Physical Review*, Vol. 102, p. 593 (1956).

[169] L. Sirovich, Kinetic modelling of gas mixtures, *Physics of Fluids*, Vol. 5, p. 908 (1962).

[170] T. F. Morse, Kinetic model equations for a gas mixture, *Physics of Fluids*, Vol. 7, pp. 2012-2014 (1964).

[171] B.B. Hamel, Ph.D. Dissertation, Princeton University (1963).

[172] B. B. Hamel, Kinetic model of binary mixtures, *Physics of Fluids*, Vol. 8, No. 3, pp. 418-425 (1965).

[173] F. J. McCormack, Construction of linearized kinetic models for gaseous mixtures and molecular gases, *Physics of Fluids*, Vol. 16, pp. 2095-2105 (1973).

[174] V. Garzó, A. Santos, J. J. Brey, A kinetic model for a multicomponent gas, *Physics of Fluids A*, Vol. 1, pp. 380-383 (1989).

[175] P. Andries, K. Aoki, B. Perthame, A Consistent BGK-Type Model for Gas Mixtures, *Journal of Statistical Physics*, Vol. 106, pp. 993-1018 (2002).

[176] X. He, X. Shan, G. D. Doolen, Discrete Boltzmann equation model for nonideal gases, *Physical Review E*, Vol. 57 R13 (1998).

[177] L.-S. Luo, Theory of the lattice Boltzmann method: Lattice Boltzmann models for nonideal gases, *Physical Review E*, Vol. 62, No. 4, pp. 4982-4996 (2000).

[178] J. H. Ferziger, H. G. Kaper, Mathematical Theory of Transport Processes in Gases, North-Holland, Amsterdam (1972).

[179] R. C. Reid, The properties of gases and liquids, McGraw-Hill, New York (1987).

[180] C. Pan, J. F. Prins, C.T. Miller, A high-performance lattice Boltzmann implementation to model flow in porous media, *Computer Physics Communications*, Vol. 158, pp. 89-105 (2004).

[181] N. Satofuka, T. Nishioka, Parallelization of lattice Boltzmann method for incompressible flow computations, *Computational Mechanics*, Vol. 23, pp. 164171 (1999).

[182] V. Kumar, A. Grama, A. Gupta, G. Karypis, Parallel Computing, Benjamin/Cummings, California (1994).

[183] N. MacDonald, E. Minty, T. Harding, S. Brown, Writing Message-Passing Parallel Programs with MPI, Edinburgh Parallel Computing Centre, The University of Edinburgh (2001).

[184] T. Fritz, Connecting components for CO_2 circuits, *SAE Automotive Alternate Refrigerants Systems Symposium* (1999).

[185] D. M. Ashby, G. Buch, Elastomer developments for sealing automotive climate control systems using carbon dioxide, *SAE Automotive Alternate Refrigerants Systems Symposium*, 2002.